ELECTRONIC SUPPLEMENTARY INFORMATION

Mesogenic $[Rh(L)_4](A)$ Complexes Form Mesophases with $Rh^I\cdots Rh^I$-Containing and Triphenylene-Discotic Segregated Columns. Effect of $Rh^I\cdots Rh^I$ Interactions and $A^- = [Au(CN)_2]^-$ on Hole Mobility

Verónica Conejo-Rodríguez,[†] Bertrand Donnio,*[‡] Benoît Heinrich,[‡] Roberto Termine,[&] Attilio Golemme,[&] and Pablo Espinet*[†].

[†]IU CINQUIMA/Química Inorgánica, Facultad de Ciencias, Universidad de Valladolid, E-47071 Valladolid, Spain
[‡]Institut de Physique et Chimie des Matériaux de Strasbourg (IPCMS), UMR 7504 (CNRS-Université de Strasbourg), F-67034 Strasbourg Cedex 2, France.
[&]LASCAMM CR-INSTM, CNR-Nanotec, Dipartimento di Fisica, 87036 Rende, Italy.
E-mail: espinet@qi.uva.es

Table of Contents

GENERAL REMARKS

All reactions were carried out under dry N_2. The solvents were purified according to standard procedures.[1] $[Rh(COD)Cl]_2$,[2] $[Rh(COD)_2](BF_4)$,[3] 4-methylphenylisocyanide ($\mathbf{L^A}$),[4] and 2-(6-(4-isocyanophenoxy)hexyloxy)-3,6,7,10,11-pentakishexyloxytriphenylene ($\mathbf{L^{D1}}$),[5] were prepared according to literature procedures. Only representative examples are described, as the syntheses were similar for the rest of the complexes. Yields, and IR and analytical data are given for all the complexes. The precursor 3,5-dimethoxyaniline and the ligands Xylylisocyanide ($\mathbf{L^X}$) and *p*-metoxiphenilisocyanide ($\mathbf{L^B}$) were purchased from commercial suppliers and used as received.

Infrared spectra were recorded with Perkin–Elmer Frontier (4000–200 cm^{-1}) equipped with an ATR accessory (Attenuated total reflection) for the direct recording of solid samples. Visible absorption spectra of solutions were recorded in a Shimadzu UV-2550 spectrophotometer. Luminescence spectra were recorded with a Perkin-Elmer LS-55 spectrometer. The NMR spectra were recorded with Bruker Avance 400 Ultrashield, and Varian 500/54 Premium Shielded instruments. The ^1H and ^{19}F NMR spectra are referenced to tetramethylsilane (TMS), and $CFCl_3$ respectively.

The elemental analyses were performed with a Carlo Erba 1108 microanalyzer (Vigo University). MALDI-TOF MS was performed using a Bruker Daltonics autoflex speed instrument equipped with nitrogen laser (340 nm). Positive-ion mode spectra were recorded using the reflective mode. The accelerating voltage was 19 kV. The analytical sample was obtained by mixing the dichloromethane solution of the sample (1 mg/mL) and a dichloromethane solution of the matrix (DCTB, 10 mg/mL) in a 1/5 (vol/vol) ratio. The prepared solution of the sample and the matrix (0.5 µL) was loaded on the MALDI plate and allowed to dry at 23ºC before the plate was inserted into the vacuum chamber of the MALDI instrument.

Microscopy studies were carried out on a Leica DMRB microscope equipped with a Mettler FP82HT hot stage and a Mettler FP90 central processor, at a heating rate of 10°C min^{-1}. For differential scanning calorimetry (DSC) a Perkin-Elmer DSC7 instrument was used, which was calibrated with water and indium. The scanning rate was 10 °C min^{-1}, the samples were sealed in aluminium capsules in the air, and the holder atmosphere was dry nitrogen.

Experimental procedure for X-ray Crystallography

A single crystal was attached to a glass fiber and transferred to an Agilent Supernova diffractometer with an Atlas CCD area detector. Data collection was performed with Mo-Kα radiation (λ = 0.71073 Å) or Cu-Kα (λ = 1.54184 Å). Data integration, scaling and empirical absorption correction was carried out using the CrysAlisPro program package.[6] The crystal was kept at 294 K during data collection. Using Olex2,[7] the structure was solved with the olex2.solve[8]

and refined with Shelx program[9]. The non-hydrogen atoms were refined anisotropically and hydrogen atoms were placed at idealized positions and refined using the riding model. Refinement proceeded smoothly to give the residuals shown at the end of the SI section. CCDC 2091366-2091367 contain the supporting crystallographic data for this paper. These data can be obtained free of charge at www.ccdc.cam.ac.uk/conts/retrieving.html [or from the Cambridge Crystallographic Data Centre, 12, Union Road, Cambridge CB2 1EZ, UK; fax: (internat.) +44-1223/336-033; E-mail: deposit@ccdc.cam.ac.uk].

The SWAXS patterns were obtained with a transmission Guinier-like geometry. A linear focalized monochromatic Cu Kα1 beam (λ = 1.5405 Å) was obtained using a sealed-tube generator (600 W) equipped with a bent quartz monochromator. In all cases, the crude powder was filled in Lindemann capillaries of 1 mm diameter and 10 µm wall-thickness. The wide-angle regions were recorded with a curved Inel CPS120 counter gas-filled detector linked to a data acquisition computer (periodicities up to 90 Å). The small-angle regions were also recorded on image plates and scanned with Amersham Typhoon IP with 25 µm resolution (periodicities up to 120 Å).

GIWAXS measurements were conducted at PLS-II 9A U-SAXS beamline of Pohang Accelerator Laboratory (PAL) in Korea. Samples consisted in layers on silicon wafer of thirty to sixty nanometers thickness. The X-rays coming from the vacuum undulator (IVU) were monochromated using Si(111) double crystals and focused on the detector using K-B type mirrors. Patterns were recorded with a Rayonix 2D SX 165 CCD detector. The sample-to-detector distance was about 225 mm for energy of 11.015 keV (1.1256 Å).

SYNTHESIS OF THE COMPOUNDS

a. Synthesis of the ligands

3,5-Dimethoxyphenylformamide (1)

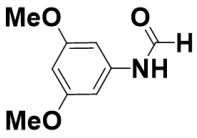

(1)

8 g of 3,5-dimethoxyaniline (0.052 mol) were dissolved in 70 mL of formic acid, refluxed for 7 h, and then stirred overnight at room temperature. The solution was evaporated to dryness and the dark solid residue was purified by column chromatography in $CHCl_3$. The yellow fractions were dried and the solid was recrystallized from CH_2Cl_2/Et_2O to obtain a white solid. This solid was washed with Et_2O (2 × 10 mL) and n-hexane (2 × 5 mL). Yield: 7.5 g (79%).

^{1}H NMR (400.14 MHz, $CDCl_3$ 298 K, Figure ESI1) two conformational isomers: δ 8.67 (bs, 1H, *CHO*), 8.33 (bs, 1H, *CHO*); 8.11 (bs, 1H, *NH*), 7.34 (bs, 1H, *NH´*), 6.76 (bs, 2H, H_1), 6.31-6.19 (m, 4H, $1H_2 + 2H_2' + H_1'$), 3.78-3.75 (m, 12H, 2 × OCH_3).

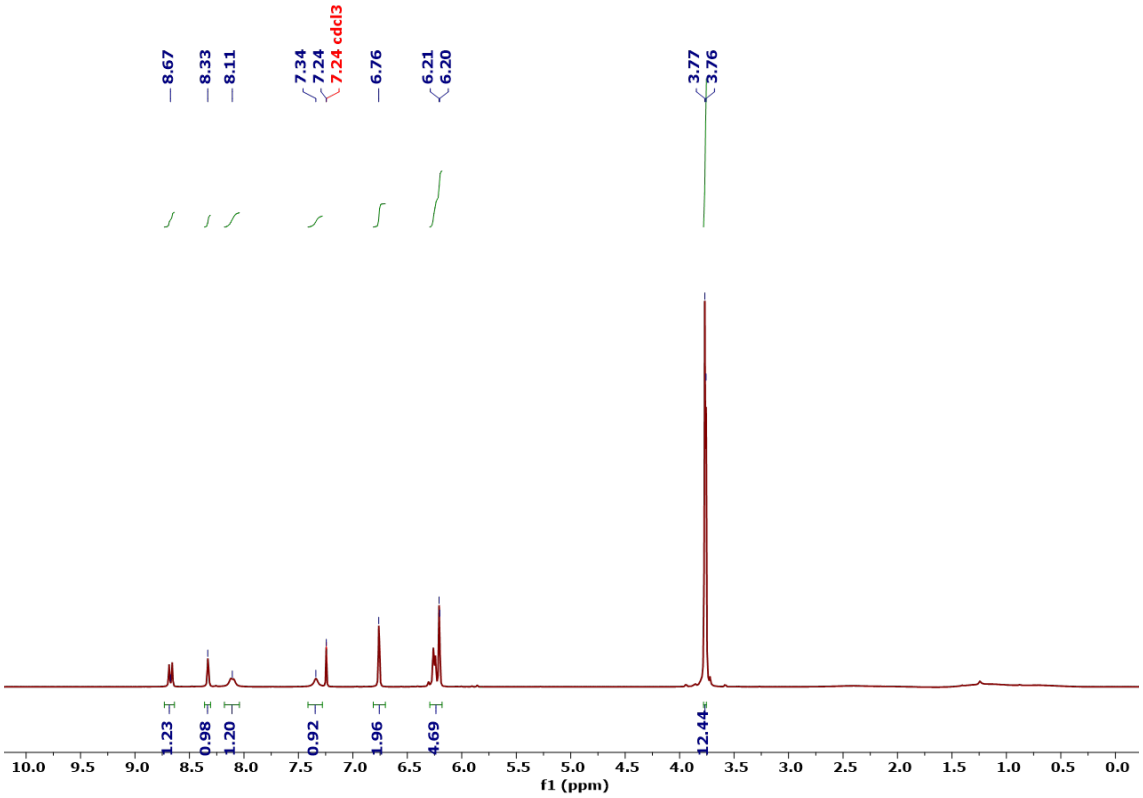

Figure ES1. ^{1}H NMR spectrum of **1** at 298 K in $CDCl_3$

Ligand L^C 3,5-$(OMe)_2C_6H_3(NC)$ (2)

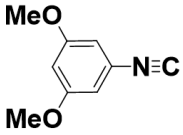

L^C (2)

A solution 3,5-Dimetoxylphenylformamide (**1**) (4 g, 22 mmol) and triethylamine (8.5 mL, 60 mmol) in dry dichloromethane (60 mL), under nitrogen atmosphere, was cooled down in an ice bath at 0 ºC and a solution of bistrichloromethyl carbonate (triphosgene; 2.4 g, 8.1 mmol) in dry dichloromethane (15 mL) was added dropwise under stirring. The mixture was stirred at room temperature for 2 h and some white solid precipitated. Water and CH_2Cl_2 were added until complete dissolution of the precipitate. The organic phase was separated and this orange solution was dried by $MgSO_4$ anhydrous and evaporated to dryness. The resulting product was purified by column chromatography (silica gel, (n-hexane/ether 3:1).) to obtain a crystalline white solid. Yield: 2.5 g (69%).

^{1}H NMR (499.72 MHz, $CDCl_3$ 298 K, Figure ESI2): δ 6.51 (d, J= 2.3Hz, 2H, H_o), 6.47 (t, J = 2.3 Hz, 1H, H_p); 3.78 (s, 6H, 2x OCH_3).^{13}C{^{1}H} NMR (125.67 MHz, $CDCl_3$ 298 K, Figure ESI3): δ 163.54(1C, Rh-CN), 161.01 (2C, C_{Ph}-O), 127.68 (1C, C_{Ph}-N), 104.75 (2C, C_{Ph}–H_o), 102.08 (2C, C_{Ph}–H_p), 55.63 (2C, -OCH_3).

IR (ATR, cm^{-1}): 2134 (ν_{CN}).

Anal. Calcd. for $C_9H_9NO_2$: C, 65.84; H, 6.14; N, 8.53; found C, 66.05; H, 5.99; N, 8.45.

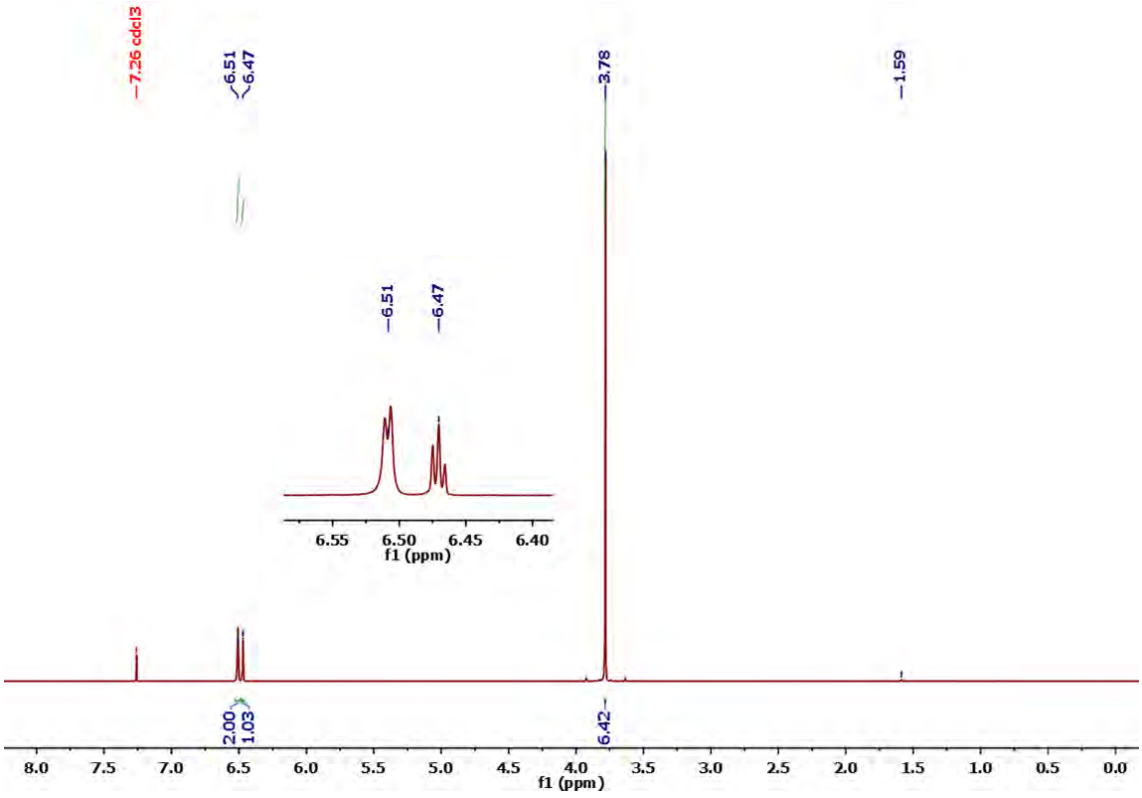

Figure ESI2. ^{1}H NMR spectrum of **L^C (2)** at 298 K in $CDCl_3$

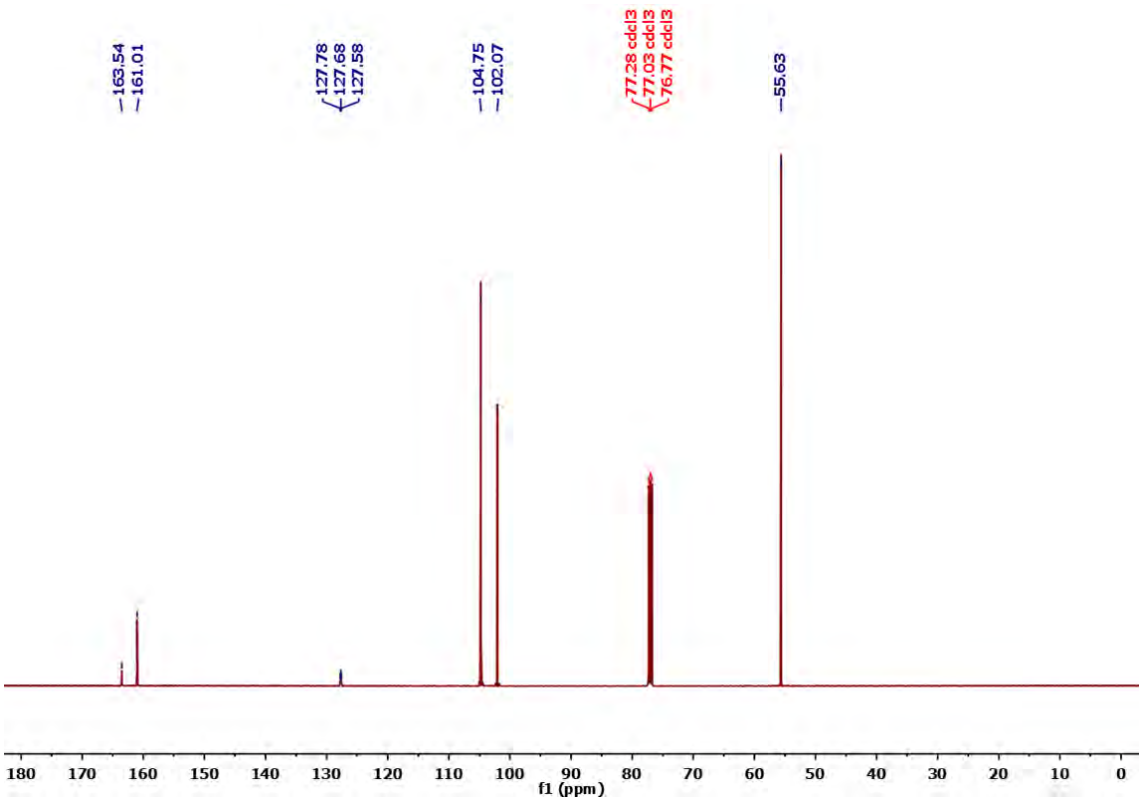

Figure ESI3. $^{13}C\{^{1}H\}$ NMR spectrum of **L^{C} (2)** at 298 K in $CDCl_3$

Preparation of 5-((6-bromohexyl)oxy)-1,3-dimethyl-2-nitrobenzene (3)

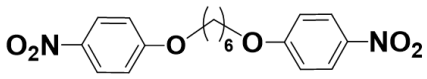

Byproduct (3´)

K_2CO_3 (3.9 g, 28.1 mmol) was added to a solution of 3,5-dimethyl-4-nitrophenol (3.5 g, 21 mmol) and 1,6-dibromohexane (3.6 g, 23 mmol) in butanone (100 mL) under nitrogen. After refluxing for 48 h, the solvent was evaporated to dryness and a yellow residue was obtained. Then water (200 mL) was added, and the organic product was extracted from the stirred mixture with dichloromethane (2 × 50 mL), and dried with $MgSO_4$. The dry solution was concentrated to a small volume. Addition of diethyl ether and cooling in the freezer overnight at -22 ºC afforded a yellow-greenish precipitate which was filtered off, washed with diethyl ether and identified as **Byproduct (3')**.

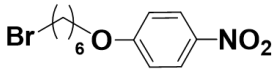

(3)

The combined yellow solution plus the washing diethyl ether solutions, were vacuum evaporated to dryness, and the resulting yellow residue was extracted in n-hexane and crystallized upon cooling the solution at -22 ºC overnight. Yellow crystals of **3** were obtained (4.74 g, 68 % yield).

^{1}H NMR (499.72 MHz, $CDCl_3$ 298 K, Figure ESI4): δ 6.59 (s, 2H, Ar-*H*), 3.96 (t, J = 6.4 Hz, 2H, O-CH_2), 3.42 (t, J = 6.7 Hz, 2H, Br-CH_2), 2.33 (s, 6H, 2 × CH_3 *Xylyl*)), 1.89 (q, 2H, O-CH_2-CH_2), 1.79 (q, 2H, Br-CH_2-CH_2), 1.50 (m, 4H, O-CH_2-(CH_2)n + Br-CH_2-(CH_2)n).

^{13}C{^{1}H} NMR (125.67 MHz, $CDCl_3$ 298 K, Figure ESI5): δ 159.58 (OC_{Ph}), 145.37 (NC_{Ph}), 132.40 (C_{Ph}), 114.35 (H-C_{Ph}), 68.00 (O-*CH_2*), 33.71 (Br-*CH_2*-), 32.60 (O-*CH_2-CH_2*), 28.90 (Br-*CH_2-CH_2*), 27.03 (O-*CH_2-CH_2-CH_2*), 25.20 (Br-*CH_2-CH_2-CH_2*), 18.41 (*CH_3 Xylyl*).

MS (ESI-TOF): m/z calc. for $[M+Na]^+$ (M = $C_{14}H_{20}BrNNaO_3$): 352.0519; found: 352.0526. *Anal.* Calcd. (%) for $C_{14}H_{20}BrNO_3$: C, 50.92; H, 6.10; N, 4.24; found C, 51.02; H, 6.10; N, 4.18.

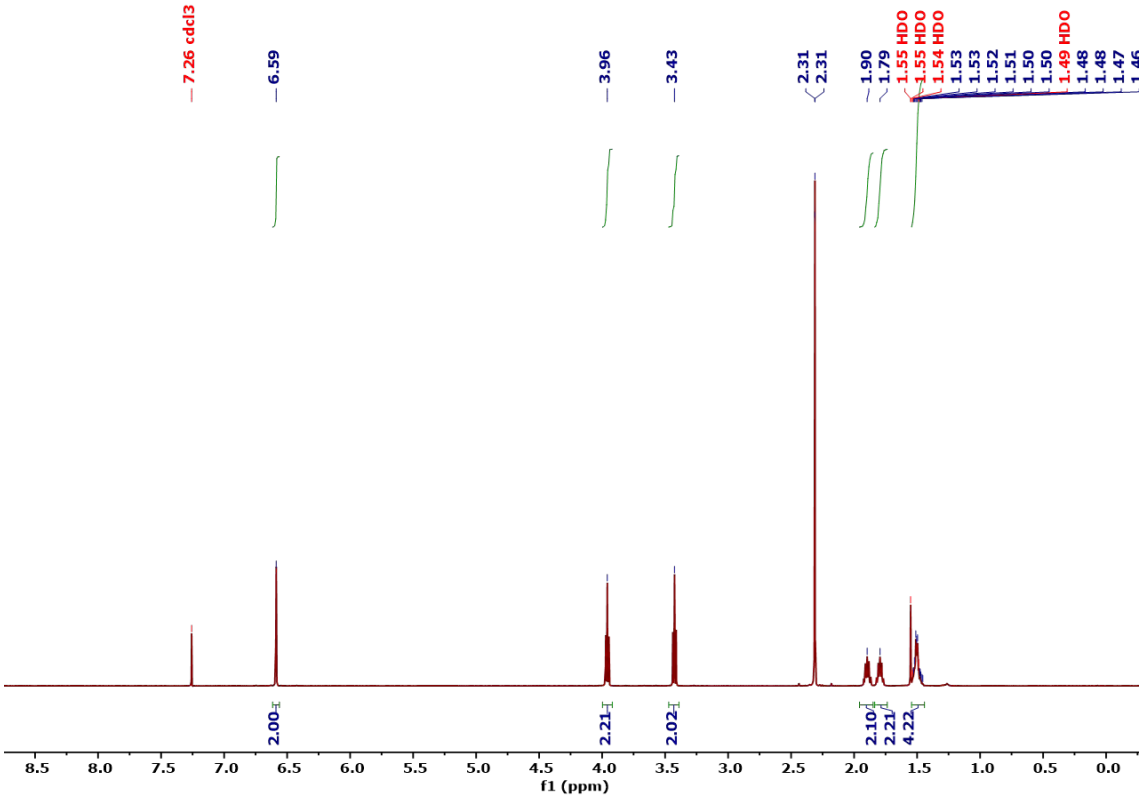

Figure ESI4. ^{1}H NMR spectrum of **3** at 298 K in $CDCl_3$

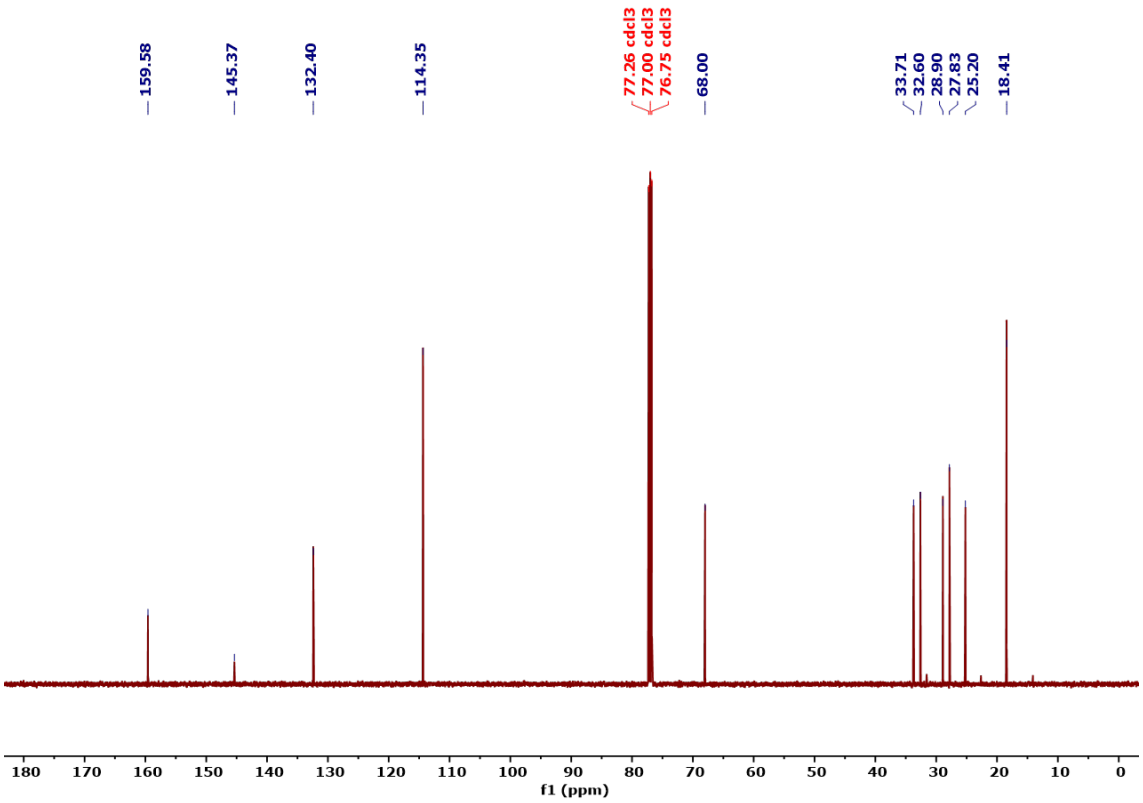

Figure ESI5. $^{13}C\{^{1}H\}$ NMR spectrum of **3** at 298 K in $CDCl_3$

Synthesis of 2-(6-(3,5-dimethyl-4-nitrofenoxy)hexyloxy)-3,6,7,10,11 pentakis(dodecyloxy)triphenylene (4) **figura cambiada**

(4)

To a solution of monohydroxy-3,6,7,10,11-pentakis(dodecyloxy)triphenylene (1.35 g, 1.16 mmol) and 5-((6-bromohexyl)oxy)-1,3-dimethyl-2-nitrobenzene (3.1 g, 9.4 mmol) in dry 2-butanone (40 mL), under nitrogen, was added K_2CO_3 (1.0 g, 6.9 mmol). The mixture was stirred at 100 ºC for 24 h. Then water (50 mL) was added and the mixture was extracted with dichloromethane (2 × 50 mL). The combined organic layers were dried over $MgSO_4$ and the solvent was evaporated under vacuum. The crude product was purified by column chromatography (silica gel, hexane/dichloromethane 3:1 v/v to 2:1 as eluent) to give yellow **4**. Yield: 1.25 g, 77 %.

^{1}H NMR (499.72 MHz, $CDCl_3$ 298 K, Figure ESI6): δ 7.84 (s, 6H, Ar-*H*), 6.59 (s, 2H, Ar-*H*). 4.26-4.21 (m, 12H, O-CH_2), 3.98 (t, J = 6.4 Hz, 2H, O-CH_2), 2.30 (s, 6H, 2 × CH_3 Xylyl), 2.02-1.82 (m, 14H, O-CH_2-*CH_2*), 1.72-1.54 (m, 14H, O-CH_2-CH_2-*CH_2*), 1.46-1.23 (m, 80H, $(CH_2)_n$), 0.90-0.86 (m, 15H, CH_3).

$^{13}C\{^{1}H\}$ NMR (125.67 MHz, $CDCl_3$ 298 K, Figure ESI7): δ 159.65 (OC_{Ph}), 149.06, 149.04, 149.00, 148.96, 148.95, 148.82 (O-C_{TriPh}), 132.39 (CH_3-C_{Ph}), 123.72, 123.69, 123.65, 123.57, 123.56, 123.55 (C_{TriPh}), 114.34 (H-C_{Ph}), 110.00 (N-C_{Ph}), 107.09, 107.03, 107.01, 107.00, 106.99, 106.92 (H-C_{TriPh}), 69.84, 69.76, 69.72, 69.69, 69.60, 69.49, 68.13 (O-CH_2), 31.93, 29.73, 29.71, 29.68, 29.55, 29.53, 29.49, 29.47, 29.38, 29.12, 26.21, 25.95, 25.84, 22.69 (-CH_2-), 18.42 (-CH_3 *Xylyl*), 14.11 (-CH_3).

MS (MALDI-TOF): m/z calc.for [M] (M = $C_{92}H_{151}NO_9$): 1411.1383; found: 1414.1378.

Anal. Calcd. (%) for $C_{92}H_{151}NO_9$: C, 78.08; H, 10.75; N, 0.99; found C, 78.39; H, 10.96; N, 0.99.

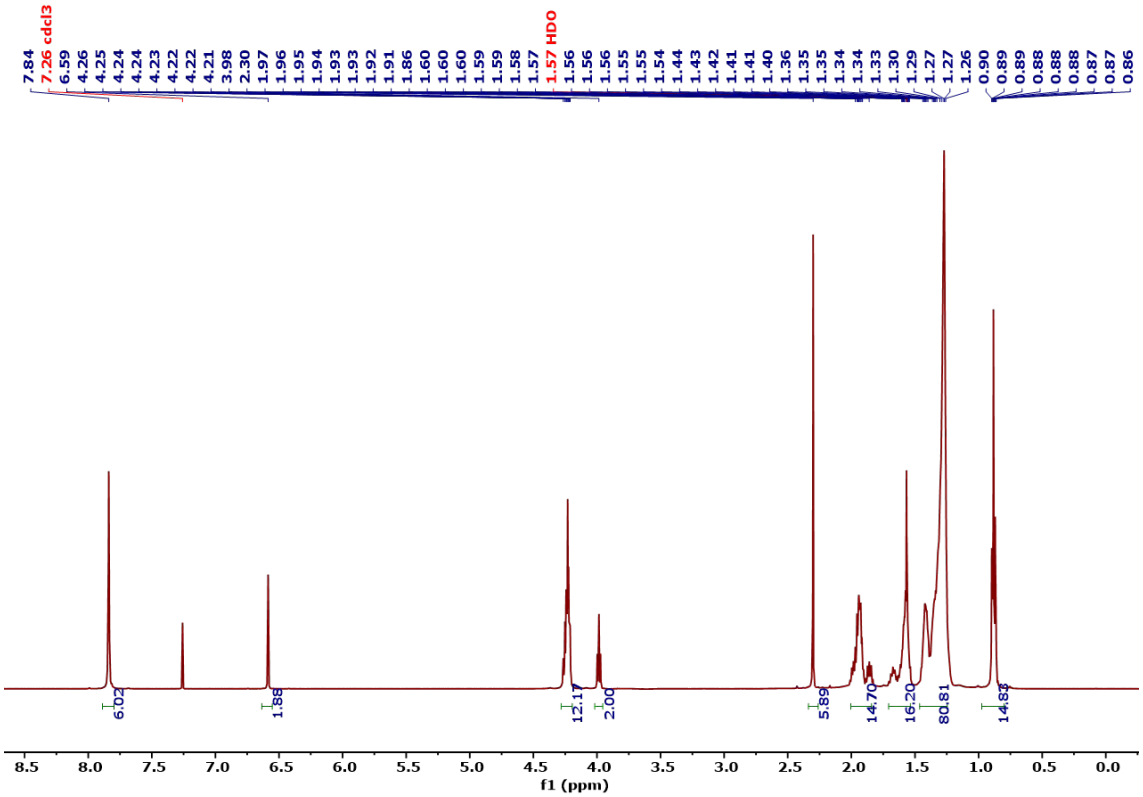

Figure ESI6. ^{1}H NMR spectrum of **4** at 298 K in $CDCl_3$

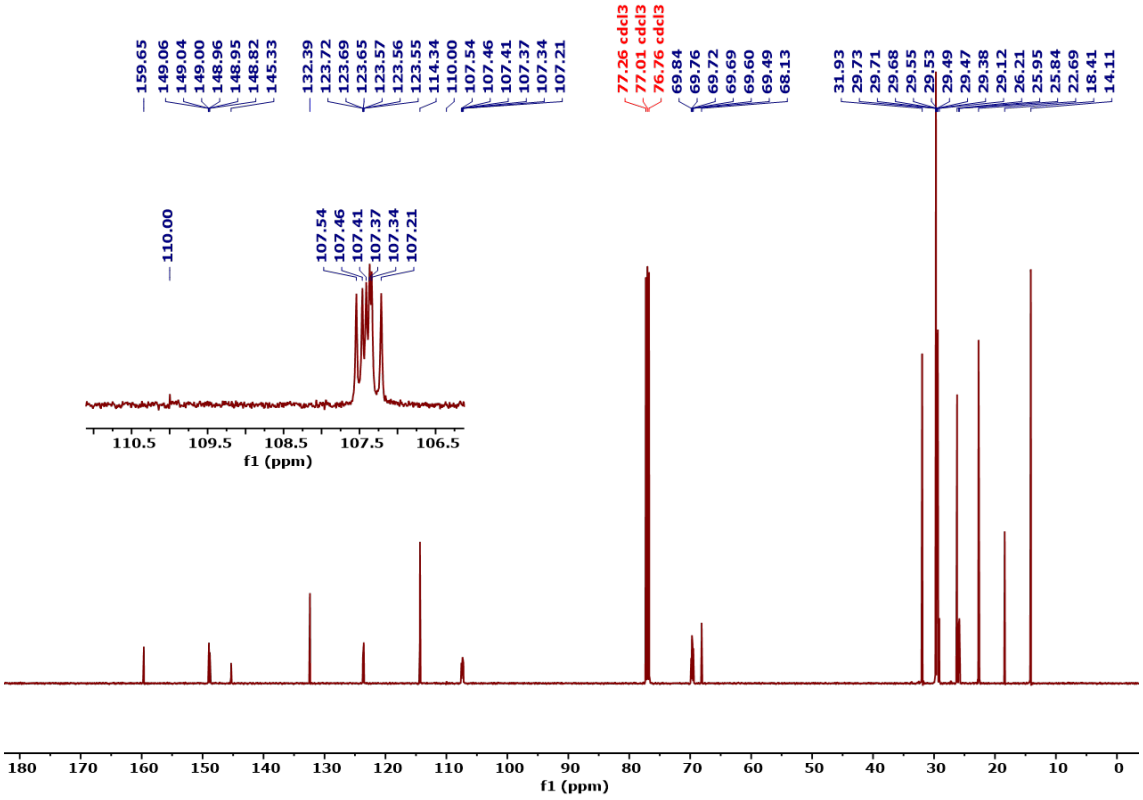

Figure ESI7. $^{13}C\{^{1}H\}$ NMR spectrum of **4** at 298 K in $CDCl_3$

Synthesis of 2-(6-(3,5-Dimethyl-4-formylaminofenoxy)hexyloxy)-3,6,7,10,11-pentakis(dodecyloxy)triphenylene. (5) figura cambiada

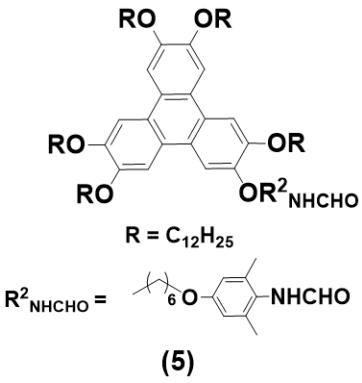

(5)

To a mixture of 2-(6-(3,5-dimethyl-4-nitrofenoxy)hexyloxy)-3,6,7,10,11 pentakis(dodecyloxy)triphenylene (1.2 g, 0.86 mmol) in toluene (60 mL) and formic acid (40 mL), powder tin (0.76 g) was added. The mixture was refluxed for 4 h. After cooling to room temperature, water (200 mL) was added and the mixture was extracted with toluene (2 × 40 mL). The combined organic layers were dried over $MgSO_4$ and the solvent was evaporated under vacuum to give **5** as a white solid (1.17 g, 96 % yield).

^{1}H NMR (499.72 MHz, CD_2Cl_2 298 K, Figure ESI8): two conformational isomers: δ 8.33 (s, 1H, CHO), 7.97 (s, 1H, CHO), 7.85 (s, 6H, Ar-*H*), 6.66 (bs, 1H, NH), 6.64 (s, 2H, Ar-*H*), 4.27-4.22 (m, 12H, O-CH_2), 3.98 (t, J = 6.5 Hz, 4H, O-CH_2), 2.55 (s, 3H, CH_3, Xylyl), 2.19 (s, 3H, CH_3, Xylyl), 2.01-1.83 (m, 14H, O-CH_2-*CH_2*), 1.72-1.54 (m, 14H, O-CH_2-CH_2-*CH_2*), 1.49-1.23 (m, 80H, $(CH_2)_n$), 0.95-0.85 (m, 15H, CH_3).

$^{13}C\{^{1}H\}$ RMN (125.67 MHz, CD_2Cl_2 298 K, Figure ESI9): δ 164.71 (CHO), 159.46 (OC_{Ph}), 149.07, 149.05, 149.03, 149.02, 148.98, 148.95, (O-C_{TriPh}), 137.32 (CH_3-C_{Ph}), 136.80 (CH_3-C_{Ph}), 125.90 (N-C_{Ph}), 125.43 (N-C_{Ph}), 123.42, 123.40, 123.37, 123.36, 123.34, 123.33 (C_{TriPh}), 113.99 (H-C_{Ph}), 113.71 (H-C_{Ph}), 107.09, 107.07, 107.04, 107.01, 106.96, 106.94 (H-C_{TriPh}), 69.59, 69.57, 69.53, 69.51, 69.49, 69.48, 69.38, 67.92, 67.87 (O-CH_2), 31.92, 29.73, 29.70, 29.67, 29.52, 29.51, 29.48, 29.46, 29.44, 29.37, 29.29, 26.20, 25.96, 25.85, 22.68 (-CH_2-), 18.72, 18.46 (-CH_3 *Xylyl*), 13.87 (-CH_3).

IR (ATR, neat, cm^{-1}): 3252 (ν_{NH}), 1656 ($\nu_{C=O}$).

MS (MALDI-TOF): m/z calc. for [M] (M = $C_{93}H_{153}NO_8$): 1412.1591; found: 1412.1591.

Anal. Calcd. (%) for $C_{93}H_{153}NO_8$: C, 79.04; H, 10.91; N, 0.99; found C, 78.84; H, 11.18; N, 0.90.

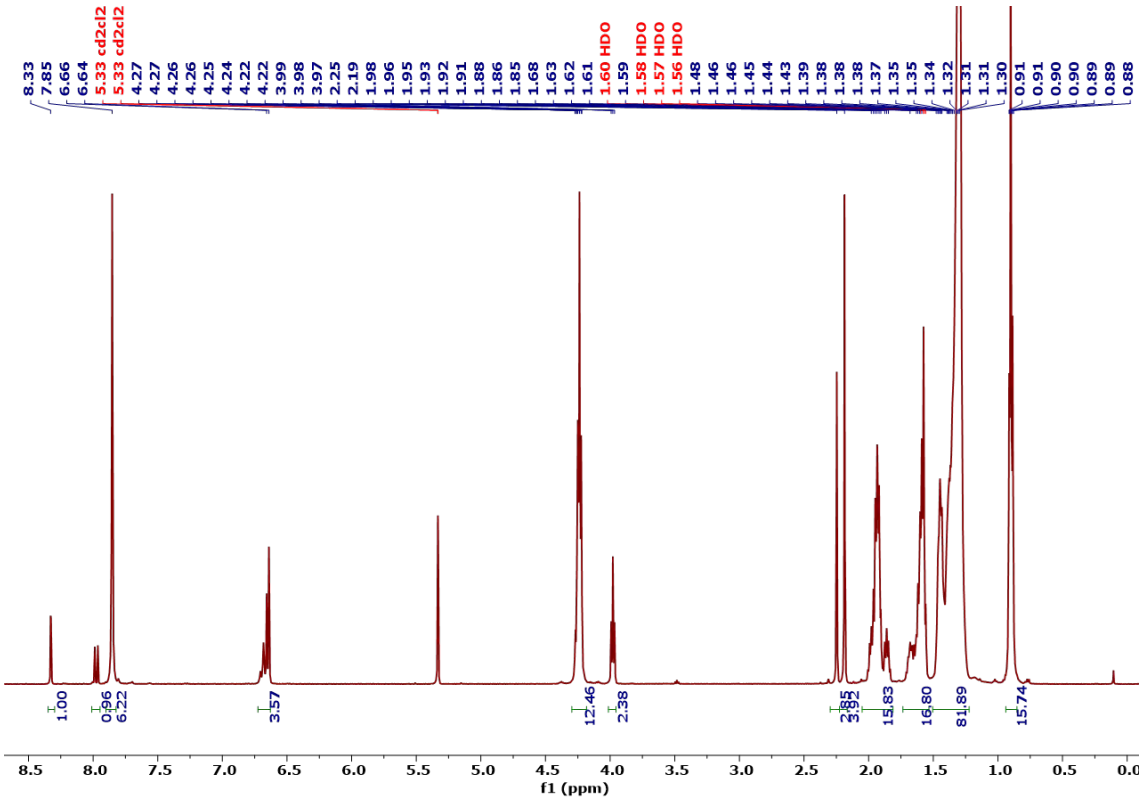

Figure ESI8. ^{1}H NMR spectrum of **5** at 298 K in CD_2Cl_2

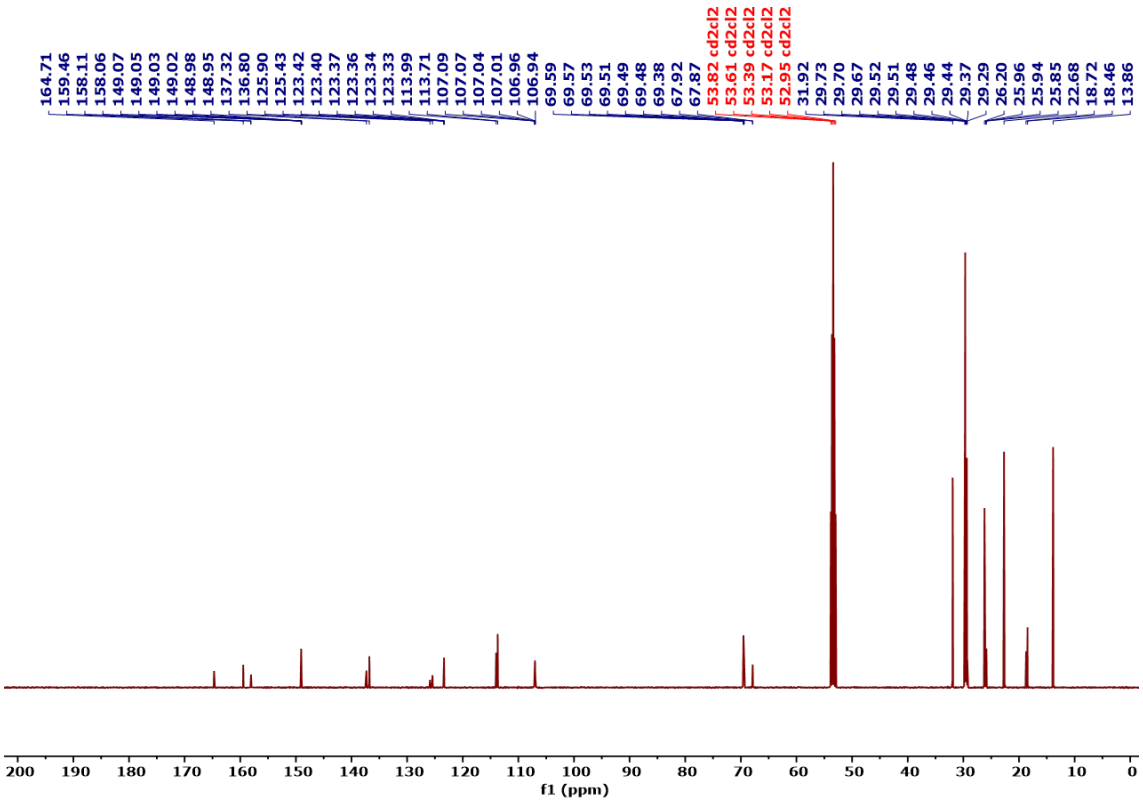

Figure ESI9. $^{13}C\{^{1}H\}$ NMR spectrum of **5** at 298 K in CD_2Cl_2

Ligand L^{D2}: 2-(6-(3,5-Dimethyl-4-isocyanofenoxi)hexyloxy)-3,6,7,10,11-pentakis (dodecyl) oxytriphenylene, $TPh(OC_{12}H_{25})_5(O(CH_2)_6C_6H_2Me_2(NC)$-*p* (6) figura cambiada

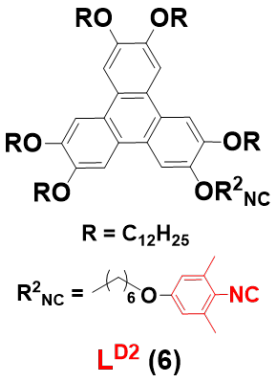

To a solution of 2-(6-(3,5-dimethyl-4-formylaminofenoxy)hexyloxy)-3,6,7,10,11-pentakis(dodecyloxy)triphenylene (1.17 g, 0.83 mmol) and triethylamine (0.32 mL, 2.28 mmol) in dry dichloromethane (50 mL), under nitrogen atmosphere, was added dropwise a solution of bistrichloromethyl carbonate (triphosgene; 0.091 g, 0.31 mmol) in dry dichloromethane (10 mL). The mixture was stirred at room temperature for 1 h and the solvent was pumped off. The resulting residue was purified by column chromatography (silica gel, dichloromethane/hexane 1:1.5 to 1:1) giving **6** as a white solid (0.86 g, 74% yield).

^{1}H NMR (499.72 MHz, CD_2Cl_2 298 K, Figure ESI10): δ 7.85 (s, 6H, Ar-*H*), 6.63 (s, 2H, Ar-*H*). 4.27-4.22 (m, 12H, O-CH_2), 3.98 (t, J = 6.5 Hz, 2H, O-CH_2), 2.37 (s, 6H, (2 × CH_3 Xylyl)), 2.01-1.83 (m, 14H, O-CH_2-*CH_2*), 1.72-1.54 (m, 14H, O-CH_2-CH_2-*CH_2*), 1.50-1.25 (m, 80H, $(CH_2)_n$) 0.95-0.87 (m, 15H, CH_3).

^{13}C{^{1}H} NMR (125.67 MHz, CD_2Cl_2 298 K, Figure ESI11): δ 166.77 (CN), 158.73 (OC_{Ph}), 149.08, 149.07, 149.05, 149.04, 149.02, 148.93 (O-C_{TriPh}), 136.31 (CH_3-C_{Ph}), 123.43, 123.40, 123.39, 123.38, 123.35 123.33 (C_{TriPh}), 119.56 (N-C_{Ph}), 113.40 (H-C_{Ph}), 107.09, 107.03, 107.01, 107.00, 106.99, 106.92 (H-C_{TriPh}), 69.58, 69.56, 69.54, 69.52, 69.46, 69.36, 68.05 (O-*CH_2*), 31.93, 29.73, 29.71, 29.68, 29.53, 29.51, 29.42, 29.38, 29.16, 26.21, 25.96, 25.81, 22.69 (-*CH_2*-), 18.88 (-*CH_3 Xylyl*), 13.87 (-*CH_3*).

IR (ATR, neat, cm^{-1}): 2112 (ν_{NC}).

MS (MALDI-TOF): m/z calc.for [M] (M = $C_{93}H_{152}NO_7$): 1396.1597; found: 1394.2 [M-2H]. For this compound the MALDI-TOF MS did not afford a concordant exact mass, probably because the compound is not stable in the experimental volatilization conditions.

Anal. Calcd. (%) for $C_{93}H_{152}NO_7$: C, 80.00; H, 10.97; N, 1.00; found C, 80.12; H, 11.29; N, 0.97.

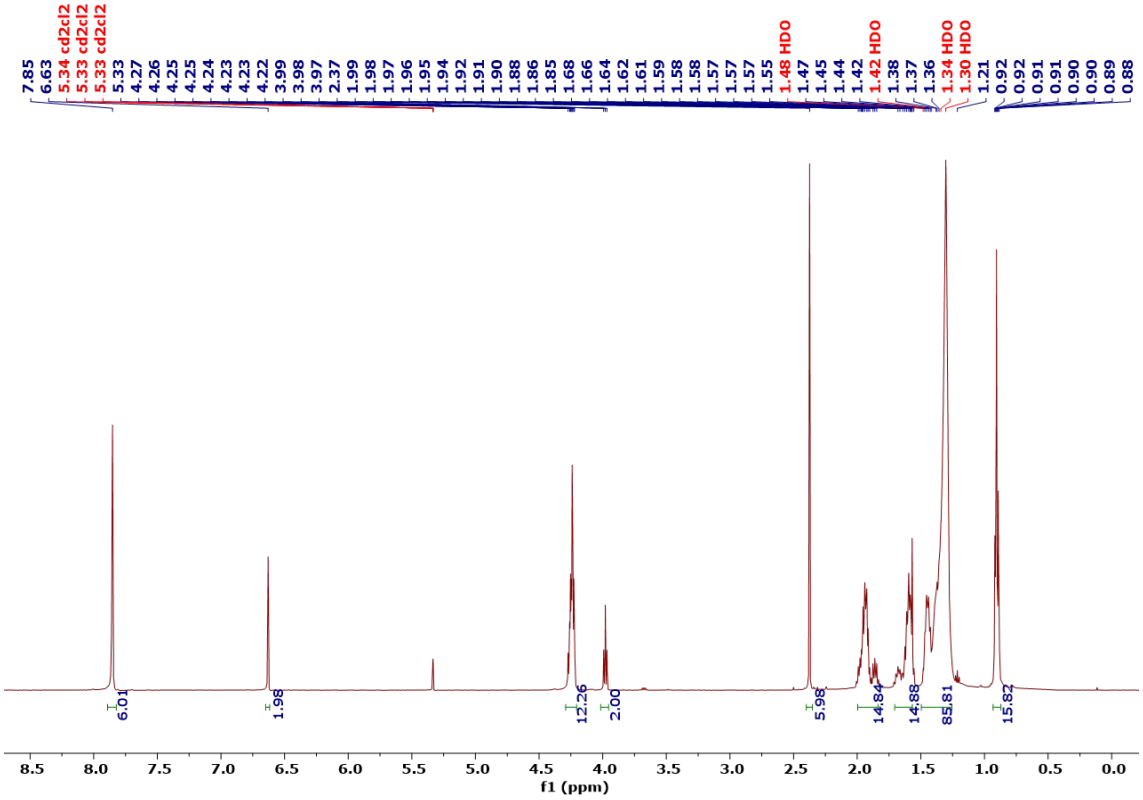

Figure ESI10. ^{1}H NMR spectrum of L^{D2} **(6)** at 298 K in CD_2Cl_2

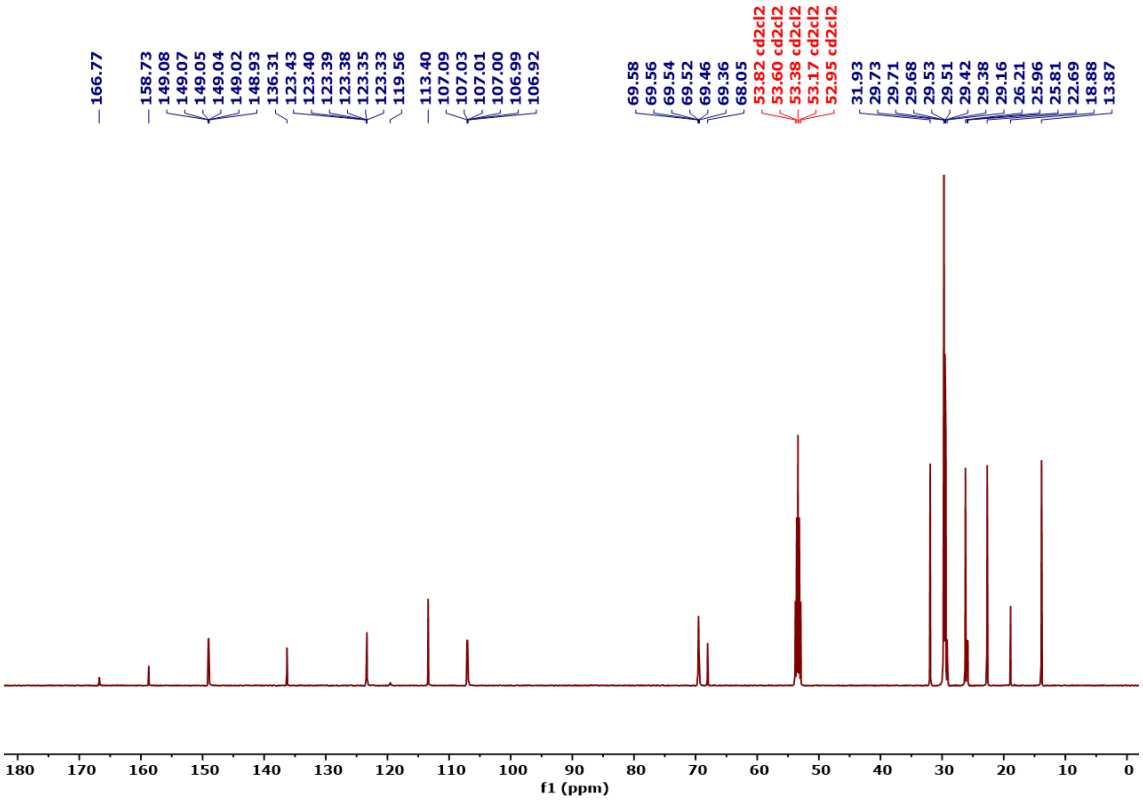

Figure ESI11. $^{13}C\{^{1}H\}$ NMR spectrum of L^{D2} **(6)** at 298 K in CD_2Cl_2

^{1}H comments

Ligands:

The ^{1}H NMR spectra are very similar for all the *p*-substituted isocyanides. In ligands $\mathbf{L^A}$, $\mathbf{L^B}$ and $\mathbf{L^{D1}}$ they show the expected AA´XX´ spin system for the aryl protons of the isocyanide group. An AB_2 spin system is observed for $\mathbf{L^X}$, and a singlet for $\mathbf{L^{D2}}$. In the case of the *m*-substituted ligand (L^C) a triplet for the *ortho*- and a doublet for the *para*-H atoms, and a broad singlet for the two methoxy groups, are observed. The aryl protons of the triphenylene core display a singlet. For the methylene groups, a multiplet and a triplet are observed in the range 4.2–3.9 ppm, corresponding to the first methylene group of the alkyloxy moieties. The remaining chain hydrogen atoms appear overlapped in the range 1.9–1.3 ppm. Singlets for the Me/MeO groups are also observed.

Complexes:

In the ^{1}H NMR spectra of the complexes, the aromatic protons *ortho* to the isocyanide group show a slight deshielding upon coordination to Rh^I, as reported for other related compounds.[10] The OCH_2 protons appear at *ca.* 4 ppm, and the rest of the alkyl protons are seen in the 1.94−0.88 ppm range.

TABLE ESI1 and IR comments

Table ESI1. IR ν(C≡N) isocyanide bands (cm^{-1}) for free and coordinated isocyanide ligands.

L / $\nu_{C\equiv N}$ free	$\nu_{C\equiv N}$ coordinated		
	$[Rh(L)_4](Cl)$	$[Rh(L)_4](BF_4)$	$[Rh(L)_4]$ $[Au(CN)_2]$
$\mathbf{L^A}$ / 2125	2141	2150	2142
$\mathbf{L^B}$ / 2123	2139	2140	2151
$\mathbf{L^C}$ / 2134	2151	2158	2152
$\mathbf{L^X}$ / 2109	2129*	2129**	2133**
$\mathbf{L^{D1}}$ / 2120	2160	2156	2157
$\mathbf{L^{D2}}$ / 2112	2134	2139	2139

ATR measurements.
*Data from reference **Error! Bookmark not defined.** of main text.
Data from reference **Error! Bookmark not defined. of main text.

The IR spectra of the free ligands show a broad band corresponding to ν(C≡N) in the range 2112-2135 cm^{-1}.The solid state IR spectra of all the complexes exhibit stretching ν(C≡N) isocyanide absorptions at higher wavenumbers than in the corresponding free ligands: 40–36 cm^{-1} higher for the Rh^I complexes without methyl groups in *ortho* position and 27–22 cm^{-1} higher for the Rh^I complexes of $\mathbf{L^X}$ and $\mathbf{L^{D2}}$, with methyl groups in *ortho* position (Table 1). All these bands appear in the complexes in the range 2129-2160 cm^{-1} and are broad. For this reason, they are likely overlapping the weaker $\nu(C\equiv N)_{cyanide}$ absorptions in the $[Rh(\mathbf{L})_4][Au(CN)_2]$ complexes (ν(C≡N) for $K[Au(CN)_2]$ appears at 2150 cm^{-1}). In the absence of independent observation, the similarity of all band positions for all the $[Rh(\mathbf{L})_4](A)$ complexes might be consistent with a common cation and suggesting that the $[Au(CN)_2]^-$ moiety is not involved in formation of Rh···Au···Rh interactions in the solids. Other observations discussed later suggest the same.

b. Synthesis of the complexes

For the synthesis of $[Rh(L)_4](A)$ complexes (L = L^A-L^{D2}; A = Cl, BF_4, $[Au(CN)_2]$) the same or very similar procedures were used. Therefore, a general description is given and the characterization data for each type of complex are provided.

i) General procedure for synthesizing [Rh(L)]Cl with arylisocyanide ligands L^A-L^C

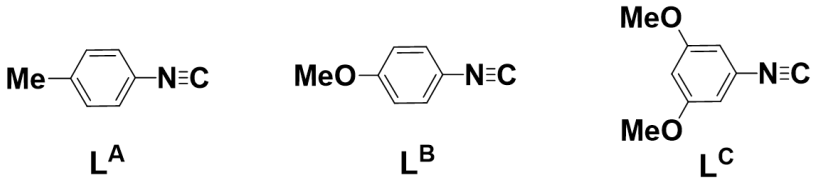

L^A L^B L^C

To a solution of $(\mu\text{-}Cl)_2[Rh(COD)]_2$ in dry dichloromethane a slight excess of the corresponding arylisocyanide (8.2 to 8.5 moles per mol of Rh dimer) was slowly added, and the mixture was stirred at room temperature for 1 hour. Afterwards, the mixture was concentrated to a small volume, Et_2O was added, and the solution was cooled down to -22 ºC overnight. The precipitate was filtered, washed with Et_2O (3 × 5 mL) and vacuum dried.

All the complexes have low solubility in common solvents and decompose after long periods of time in solution. For these reasons $^{13}C\{^1H\}$ NMR spectrum could not be recorded.

$[Rh(L^A)_4]Cl$ (7) (L^A = *p*-$MeC_6H_4(NC)$)

Reagents: $[Rh(\mu\text{-}Cl)(COD)]_2$ (50 mg, 0.101 mmol) in CH_2Cl_2 (20 mL), *p*-$MeC_6H_4(NC)$ (97 mg, 0.83 mmol) in CH_2Cl_2. A dark green solid was obtained: 108 mg (88%).

^1H NMR (499.73 MHz, CD_2Cl_2, 298 K, Figure ESI12) δ 7.40 (m, 8H, H_o), 7.29 (m, 8H, H_m), 2.42 (s, 12H, *p*-*Me*$C_6H_4(NC)$.

IR (ATR, neat, cm^{-1}): 2141 ($\nu_{C\equiv N}$).

MS (MALDI-TOF): m/z Calcd. for $[M^+–(Cl)^-]$ ($M^+ = C_{32}H_{28}N_4Rh$): 571.1364; found: 571.1392.

Anal. Calcd. for $C_{32}H_{28}ClN_4Rh$: C, 63.32; H, 4.65; N, 9.23; found: C, 62.98; H, 4.51; N, 8.83.

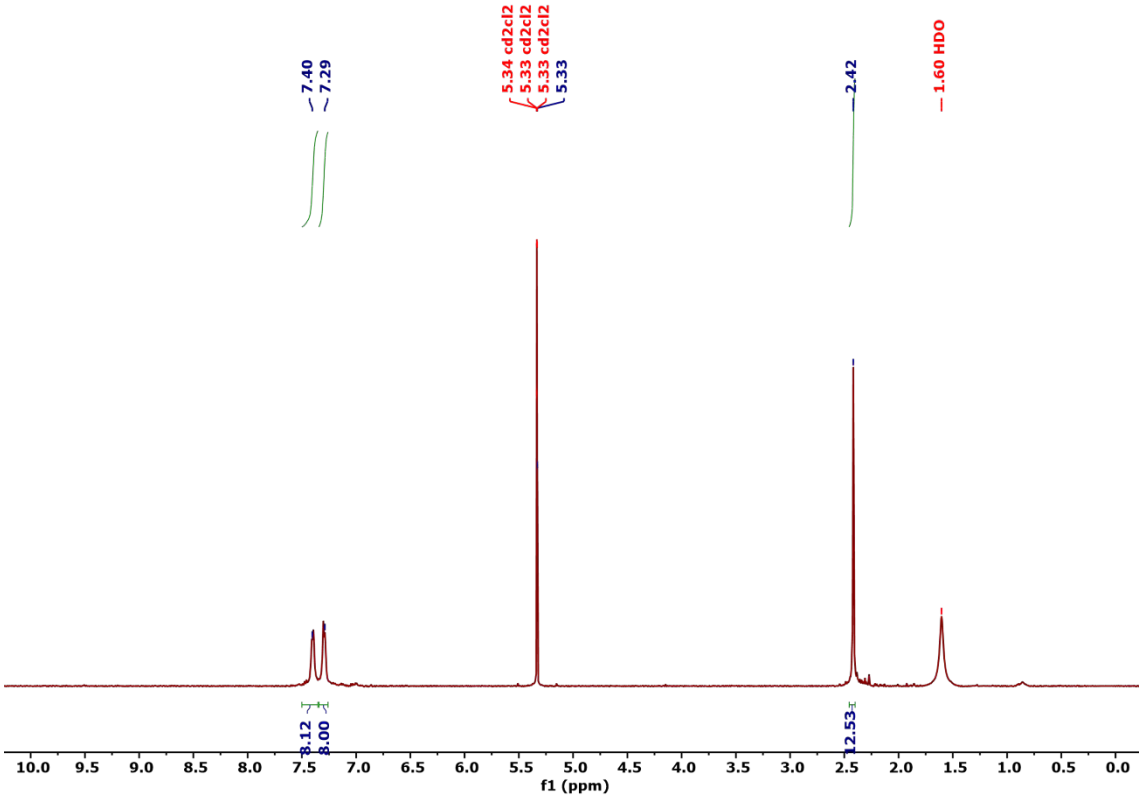

Figure ESI12. ^{1}H NMR spectrum of **7** at 298 K in CD_2Cl_2

[Rh(L^{B})$_4$]Cl (8) (L^{B} = *p*-MeOC$_6$H$_4$(NC))

Reagents: [Rh(μ-Cl)(COD)]$_2$ (50 mg, 0.101 mmol) in CH_2Cl_2 (20 mL), *p*-MeOC$_6$H$_4$(NC) (115 mg, 0.862 mmol) in CH_2Cl_2. A dark green solid was obtained: 111 mg (82%).

^{1}H NMR (499.72 MHz, $CDCl_3$, 298 K, Figure ESI13) δ 7.43 (m, 8H, H$_o$), 6.93 (m, 8H, H$_m$), 3.84 (s, 12H, *p*-*Me*OC$_6$H$_4$(NC)).

IR (ATR, neat, cm^{-1}): 2139 ($\nu_{C\equiv N}$).

MS (MALDI-TOF): *m/z*: Calcd. for [M^{+}–(Cl)$^{-}$] (M^{+} = $C_{32}H_{28}N_4O_4Rh$): 635.1160; found: 635.1169

Anal. Calcd. for $C_{32}H_{28}ClN_4O_4Rh$: C, 57.28; H, 4.21; N, 8.35; found: C, 56.92; H, 3.93; N, 7.98.

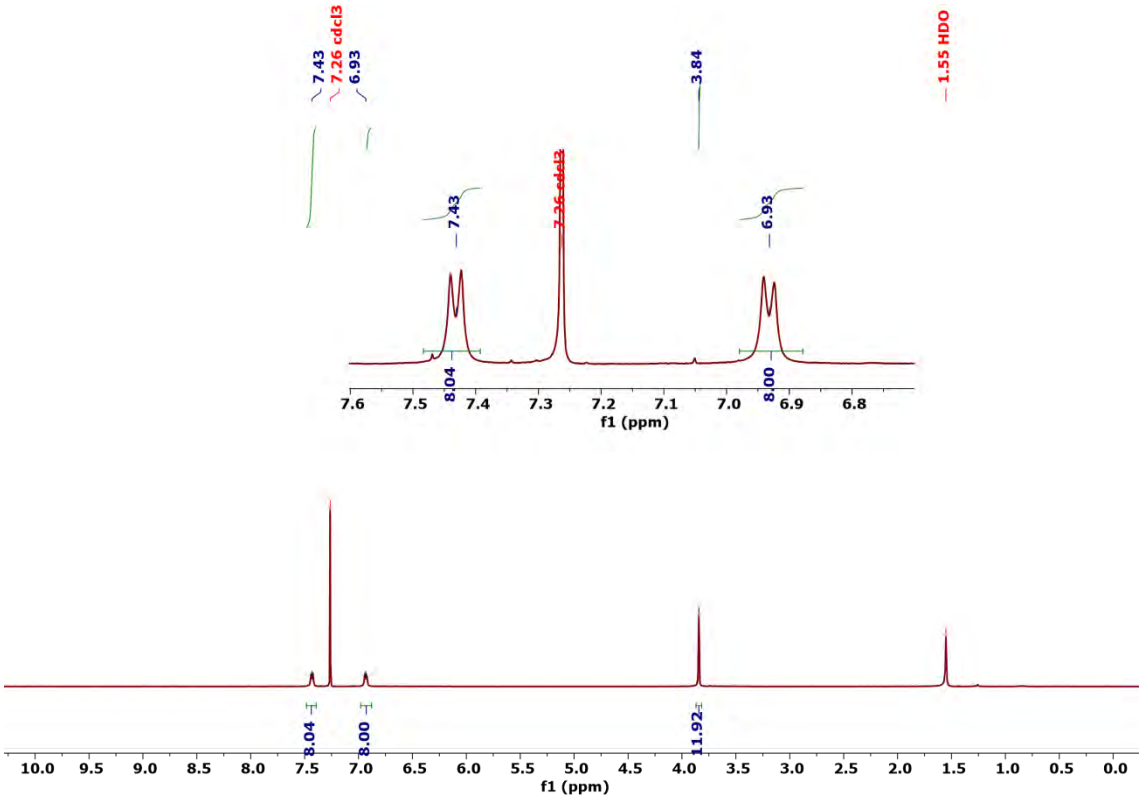

Figure ESI13. ^{1}H NMR spectrum of **8** at 298 K in $CDCl_3$

[Rh(L^{C})$_4$]Cl (9) (L^{C} = 3,5-(OMe)$_2$C$_6$H$_3$(NC))

Reagents: (μ-Cl)$_2$[Rh(COD)]$_2$ (60 mg, 0.122 mmol) in CH_2Cl_2 (20 mL), 3,5-(OMe)$_2$C$_6$H$_3$(NC), (164 mg, 0.998 mmol) in CH_2Cl_2. An intense blue solid was obtained: 156 mg (81%).

Single crystals of [Rh(L^{C})$_4$]Cl were obtained by slow diffusion of hexane into a solution of the complex CH_2Cl_2. All crystallographic data are summarized in the section of X-ray refinement.

^{1}H NMR (499.72 MHz, $CDCl_3$ 298 K, Figure ESI14): δ 6.65 (d, J= 2.2 Hz, 8H, *H$_o$*), 6.51 (t, J = 2.2 Hz, 4H, *H$_p$*); 3.79 (s, 24H, *OCH$_3$*).

IR (ATR, neat, cm^{-1}): 2151 ($\nu_{C\equiv N}$).

MS (MALDI-TOF): m/z Calcd. for [M^{+}–(Cl)$^{-}$] (M^{+} = $C_{36}H_{36}N_4O_8Rh$): 755.1583; found: 755.1585.

Anal. Calcd. for $C_{36}H_{36}ClN_4O_8Rh$: C, 54.66; H, 4.59; N, 7.08; found: C, 54.39; H, 4.57; N, 6.85.

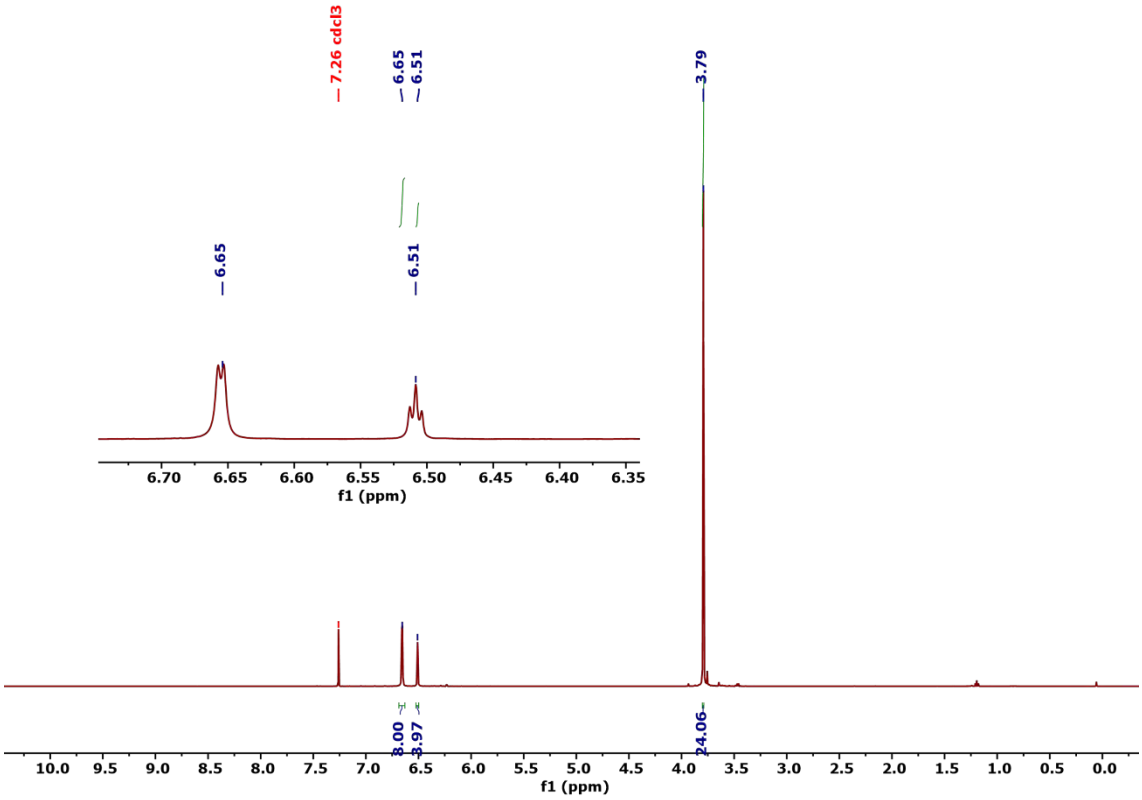

Figure ESI14. ^{1}H NMR spectra of **9** at 298 K in $CDCl_3$

ii) General procedure for the synthesis of $[Rh(L_n)](BF_4)$ with arylisocyanide ligands L^A-L^C.

4.1 moles of the corresponding arylisocyanide per Rh atom were slowly added in dry dichloromethane to a solution of $[Rh(COD)_2](BF_4)$ in dry dichloromethane and the mixture was stirred at room temperature for 1 hour. Afterwards, it was concentrated by evaporation at reduced pressure and then Et_2O was added and cooled at -22 ºC overnight. The precipitate was filtered, washed with Et_2O (3 × 5 mL) and vacuum dried.

$[Rh(L^A)_4](BF_4)$ (11)

Reagents: $[Rh(COD)_2](BF_4)$ (60 mg, 0.148 mmol) in CH_2Cl_2 (20 mL), *p-Me*$C_6H_4(NC)$ (0.099 g, 0.606 mmol) in CH_2Cl_2 (15 mL). A green solid was obtained: 67 mg (69%).

Single crystals of $[Rh(L^A)_4](BF_4)$ were obtained by slow diffusion of hexane into a solution of the complex in acetone. All crystallographic data are summarized in the section of X-ray refinement.

^{1}H NMR (400.15 MHz, $CDCl_3$, 298 K, Figure ESI15) δ 7.39 (m, 8H, H_o), 7.25 (m, 8H, H_m), 2.39 (s, 12H, *p*-$MeC_6H_4(NC)$).

^{19}F NMR (376.47 MHz, $CDCl_3$, 298 K, Figure ESI16) δ –153.75 (s, 4F, $^{10}BF_4^-$) –153.81 (s, 4F, $^{11}BF_4^-$)

IR (ATR, neat, cm^{-1}): 2150 ($\nu_{C\equiv N}$), 1030 (ν^{10}_{BF4}-), 1012 (ν^{11}_{BF4}-).

MS (MALDI-TOF): m/z Calcd. for $[M^+–(BF_4)^-]$ ($M^+ = C_{32}H_{28}N_4Rh$): 571.1364; found: 571.1344.

Anal. Calcd. for $C_{32}H_{28}BF_4N_4Rh$: C, 58.38; H, 4.29; N, 8.51; found: C, 58.13; H, 4.09; N, 8.32.

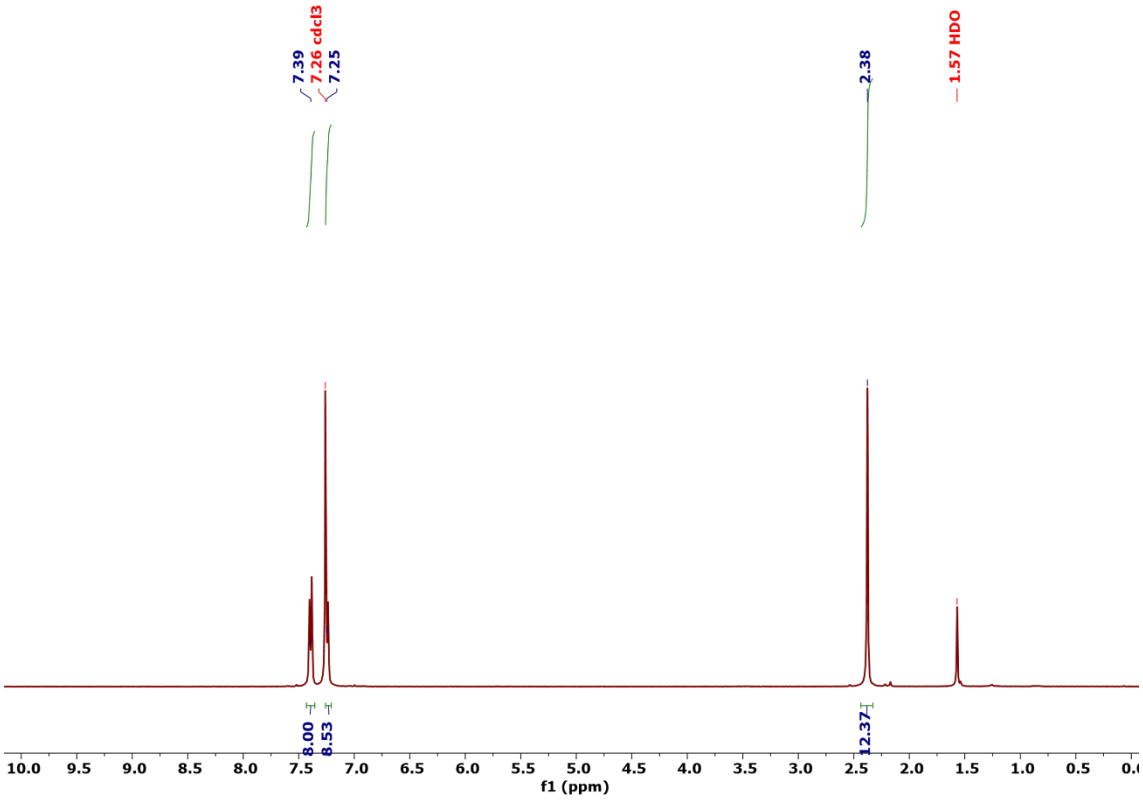

Figure ESI15. ^{1}H NMR spectrum of **11** at 298 K in $CDCl_3$.

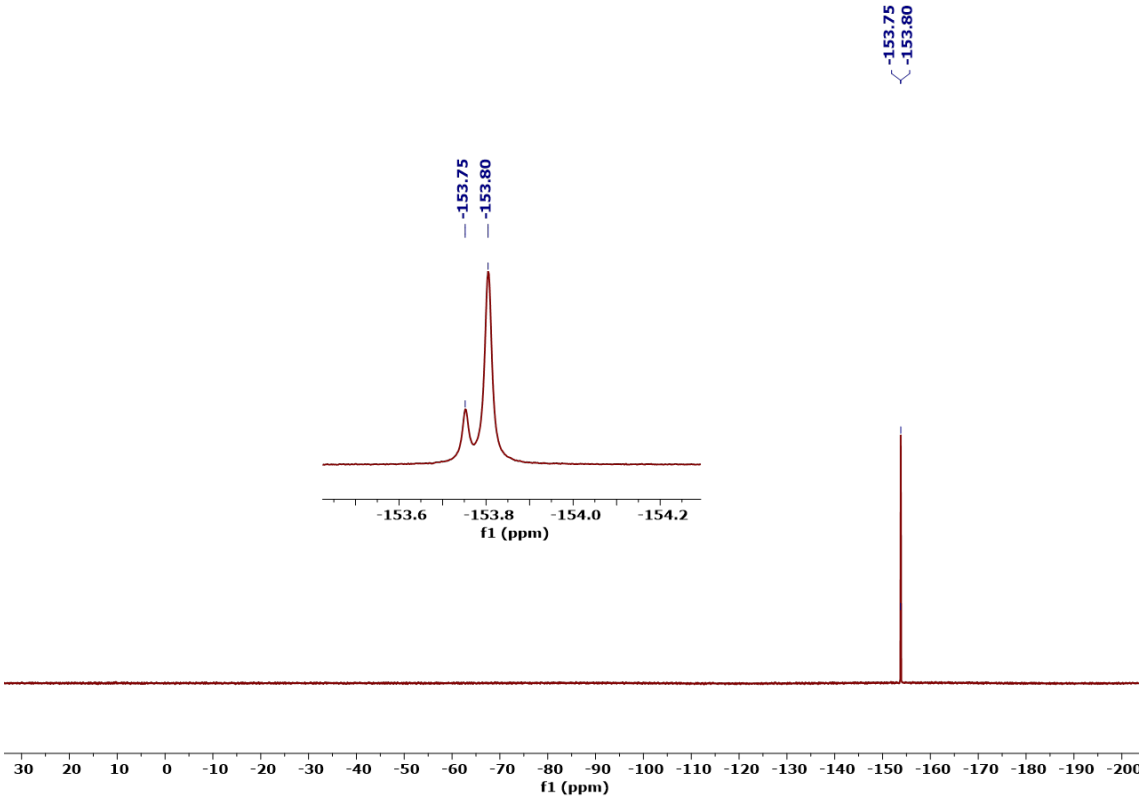

Figure ESI16. ^{19}F NMR spectra of **11** at 298 K in $CDCl_3$.

[Rh(L^B)$_4$](BF$_4$) (12)

Reagents: [Rh(COD)$_2$](BF$_4$) (94 mg, 0.23 mmol) in CH_2Cl_2 (20 mL), CNC_6H_4OMe-*p* (124 mg, 0.93mmol) in CH_2Cl_2 (15 mL). A color change of the solution was observed, from red to greenish-brown. A greenish-brown solid was obtained: 150 mg (90 %).

^{1}H NMR (499.72 MHz, $CDCl_3$ 298 K, Figure ESI17): δ 7.39 (m, 8H, H_o), 6.90 (m, 8H, H_m); 3.83 (s, 12H, OCH_3).

^{19}F NMR (470.15 MHz, $CDCl_3$ 298 K, Figure ESI18): δ –152.96 (s_{broad}, $^{10}BF_4$ and $^{11}BF_4$).

IR (ATR, neat, cm^{-1}): 2140 ($\nu_{C\equiv N}$), 1015 (ν^{10}_{BF4}-), 1000 (ν^{11}_{BF4}-).

MS (MALDI-TOF): *m/z*: Calcd. for [M^+-BF_4^-] (M^+ = $C_{32}H_{28}N_4O_4Rh^+$): 635.1160; found: 635.1169.

Anal. Calcd. for $C_{32}H_{28}BF_4N_4O_4Rh$: C, 53.21; H, 3.91; N, 7.76; found C, 53.32; H, 3.88; N, 7.48.

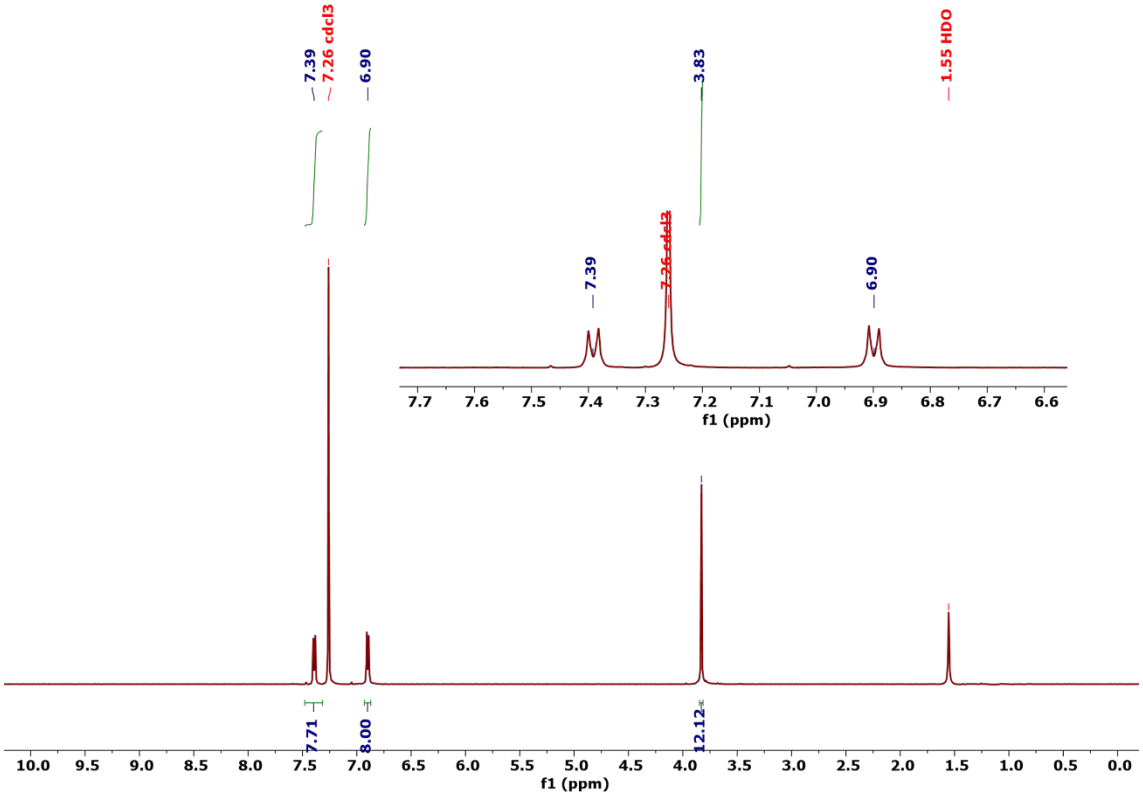

Figure ESI17. ^{1}H NMR spectrum of **12** at 298 K in $CDCl_3$

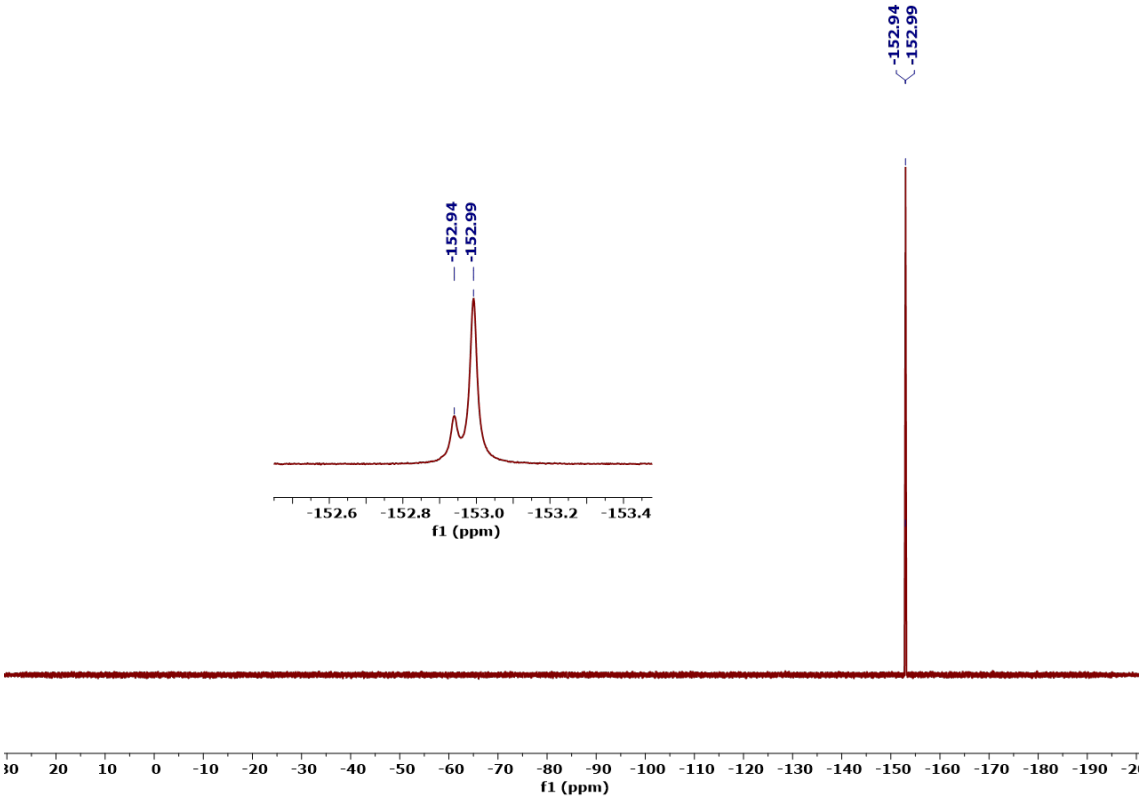

Figure ESI18. ^{19}F NMR spectrum of **12** at 298 K in $CDCl_3$

[Rh(L^C)$_4$](BF$_4$) (13)

Reagents: [Rh(COD)$_2$](BF$_4$) (60 mg, 0.148 mmol) in CH_2Cl_2 (20 mL), 3,5-(OMe)$_2$C$_6$H$_3$(NC) (0.099 g, 0.606 mmol) in CH_2Cl_2. A color change of the solution was observed, from red to dark green. A dark green solid was obtained: 110 mg (89%).

^1H NMR (499.72 MHz, acetone-d_6 298 K, Figure ESI19): δ 6.90 (d, J= 2.2 Hz, 8H, H_o), 6.73 (t, J = 2.2 Hz, 4H, H_p); 3.86 (s, 24H, OCH_3).

^{19}F NMR (470.17 MHz, acetone-d_6, 298 K, Figure ESI20): δ –151,89 (a, 4F, BF_4^-).

IR (ATR, neat, cm^{-1}): 2158 ($\nu_{C\equiv N}$), 1051 (ν^{10}_{BF4}-), 1032 (ν^{11}_{BF4}-).

MS (MALDI-TOF): m/z Calcd. for [M$^+$–(BF$_4$)$^-$]$^+$ (M$^+$ = $C_{36}H_{36}N_4O_8Rh$): 755.1583; found: 755.1591.

Anal. Calcd. for $C_{36}H_{36}BF_4N_4O_8Rh$: C, 51.33; H, 4.31; N, 6.65; found: C, 51.24; H, 4.12; N, 6.51.

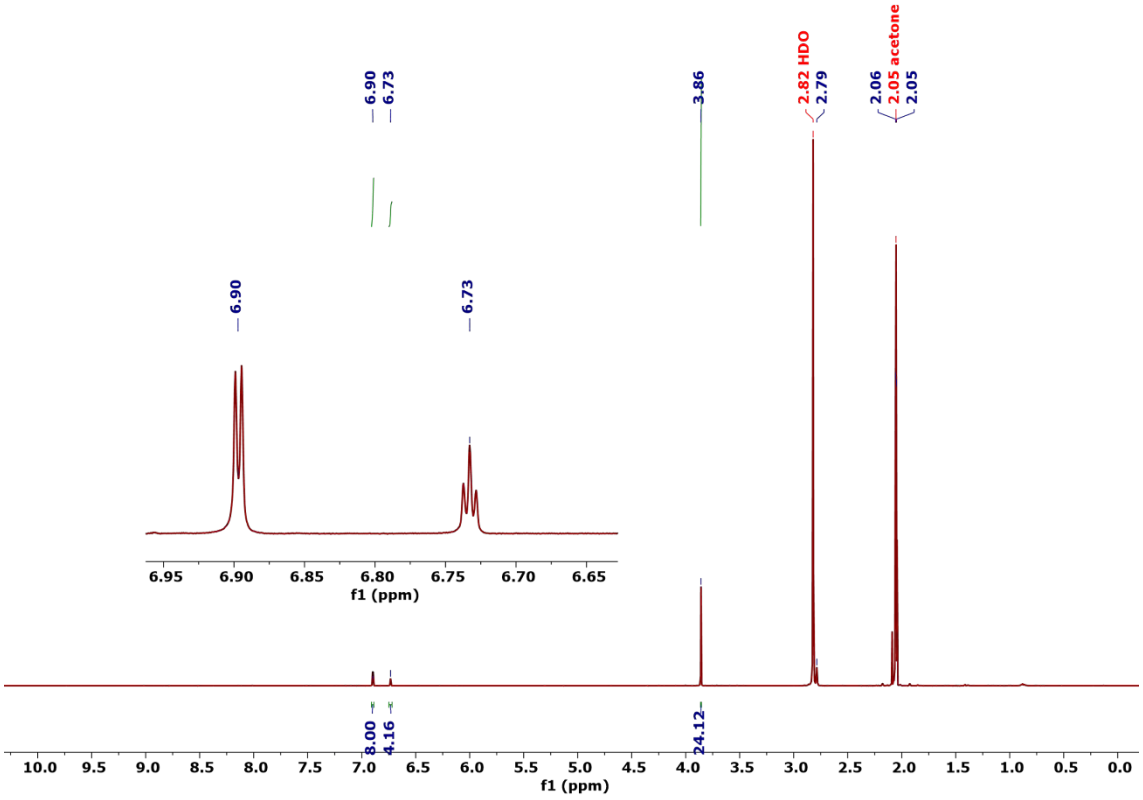

Figure ESI19. ^{1}H NMR spectrum of **13** at 298 K in acetone-d_6

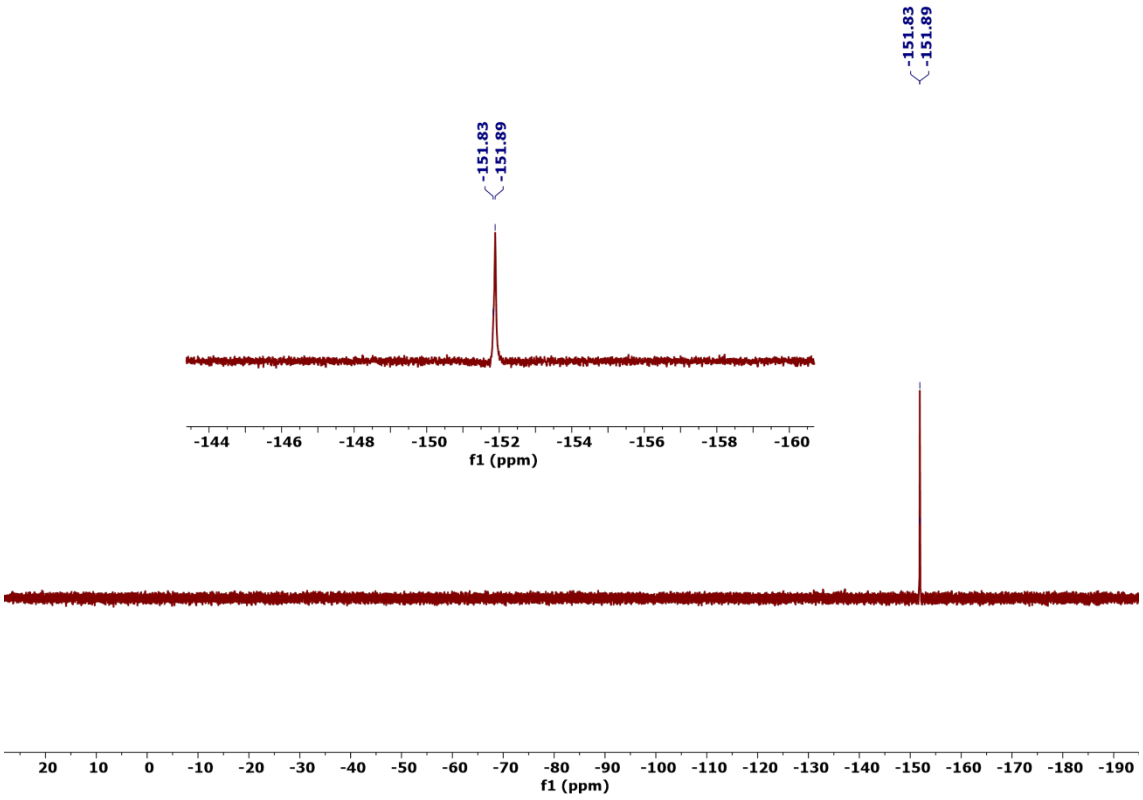

Figure ESI20. ^{19}F NMR spectrum of **13** at 298 K in acetone-d_6

iii) General procedure for the synthesis of [Rh(L)][Au(CN)$_2$] with arylisocyanides L^A-L^C

Potassium dicyanoaurate (I) (1.2 equivalents are used in the reaction) was dissolved in acetone, and a solution of the corresponding a [Rh(L)$_4$](BF$_4$) complex in dichloromethane ws added drop by drop. The mixture was stirred for 3 hours at 40 ºC. In the case of L^A or L^B, the product was extracted with dichloromethane and recrystallized; in the case of L^C, the solvent was evaporated to dryness, washed with water, dried, and recrystallized from dichloromethane.

[Rh(L^A)$_4$][Au(CN)$_2$] (16)

Reagents: [Rh(L^A)$_4$](BF$_4$)(20 mg, 0.030 mmol) in CH_2Cl_2 (40 mL), K[Au(CN)$_2$] (10 mg, 0.033 mmol) in acetone/H_2O (5 mL/3 mL). A green solid was obtained: 20 mg (30%).

^{1}H RMN (499.73 MHz, acetone-*d*$_6$, 298 K, Figure ESI21): δ 7.63 (m, 8H, H$_o$), 7.40 (m, 8H, H$_m$), 2.42 (s, 12H, CNC$_6$H$_4$*Me-p*).

IR (ATR): 2142 cm^{-1} ($\nu_{C\equiv N}$ isocyanide).

MS (MALDI-TOF): m/z Calcd. for [M$^+$–(Au(CN)$_2^-$] (M$^+$ = $C_{32}H_{28}N_4Rh$): 571.1364; found: 571.1385.

Anal. Calcd. for $C_{34}H_{28}AuN_6Rh$: C, 49.77; H, 3.44; N, 10.24; found: C, 49.54; H, 3.22; N, 10.05.

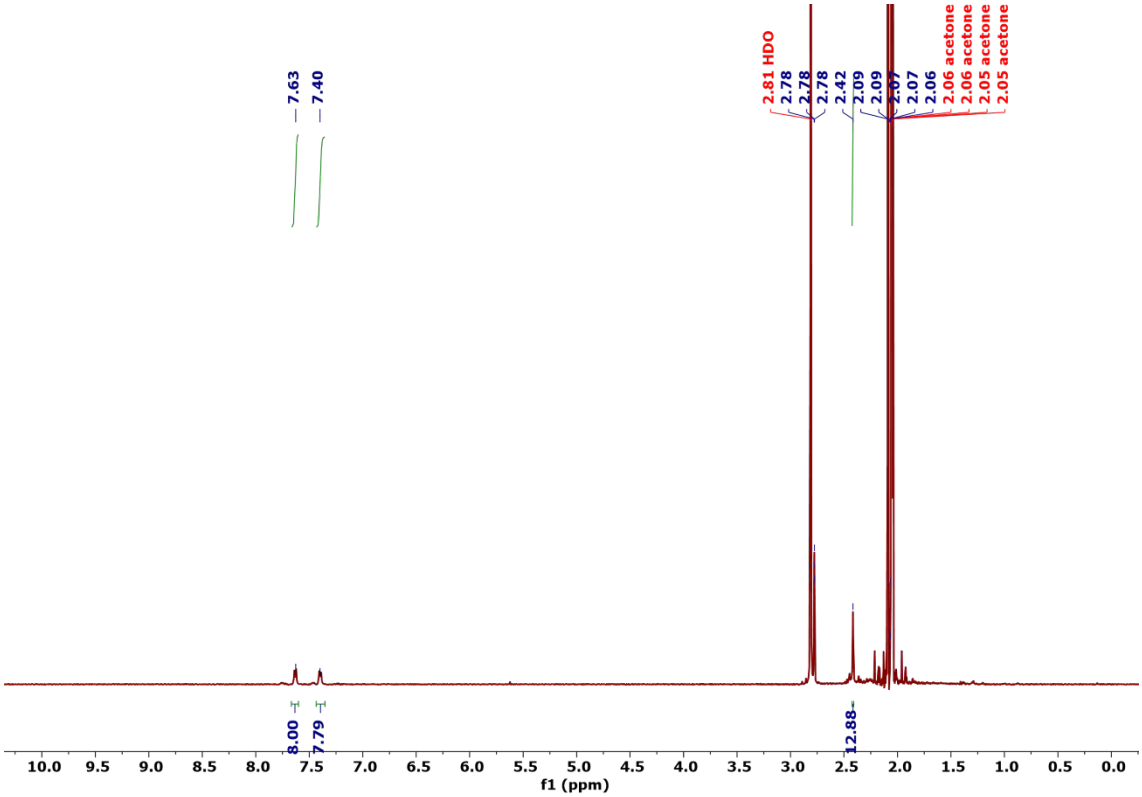

Figure ESI21. ^{1}H NMR spectrum of **16** at 298 K in acetone-*d*$_6$

$[Rh(L^B)_4][Au(CN)_2]$ (17)

Reagents: $[Rh(L^B)_4](BF_4)$ (20 mg, 0.028 mmol) in CH_2Cl_2 (40 mL), $K[Au(CN)_2]$ (9 mg, 0.031 mmol) in acetone (5 mL). A blue-greenish solid was obtained: 24 mg (98%).

^{1}H RMN (499.73 MHz, acetone-d_6, 298 K, Figure ESI22): δ 7.69 (m, 8H, H_o), 7.10 (m, 8H, H_m), 3.89 (s, 12H, CNC_6H_4OMe-*p*).

IR (ATR): 2151 cm^{-1} ($\nu_{C\equiv N}$ isocyanide).

MS (MALDI-TOF): *m/z*: Calcd. for $[M^+–(Au(CN)_2^-]$ ($M^+ = C_{32}H_{28}N_4O_4Rh$): 635.1160; found: 635.1183.

Anal. Calcd. for $C_{34}H_{28}AuN_6O_4Rh \cdot 1\ CH_2Cl_2$: C, 43.36; H, 3.12; N, 8.67; found: C, 43.70; H, 2.93; N, 8.49.

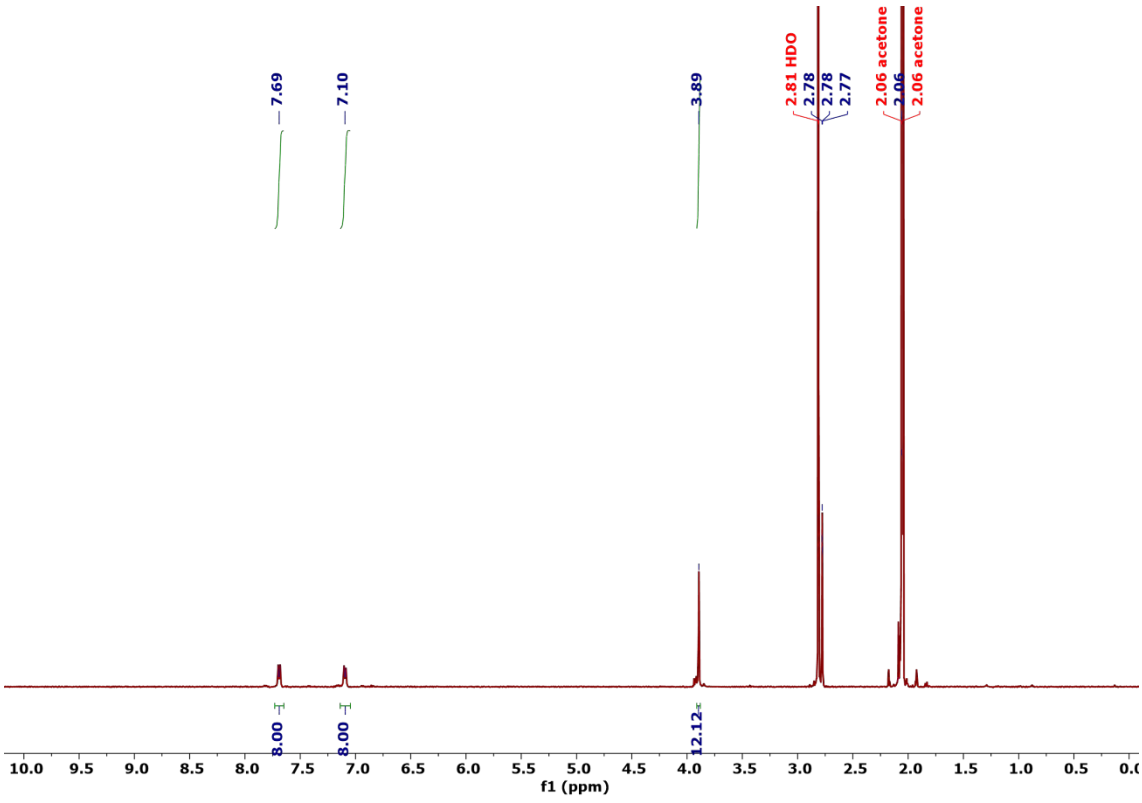

Figure ESI22. ^{1}H NMR spectrum of **17** at 298 K in acetone-d_6

[Rh(L^{C})$_4$][Au(CN)$_2$] (18)

Reagents: [Rh(L^{C})$_4$](BF$_4$) (20 mg, 0.024 mmol) in CH_2Cl_2 (40 mL), K[Au(CN)$_2$] (0.026 mmol) in acetone (5 mL). A dark green solid was obtained: 21 mg (87%).

^{1}H RMN (499.73 MHz, CD_2Cl_2, 298 K, Figure ESI23): δ 6.75 (m, 8H, H_o), 6.59 (m, 4H, H_p), 3.81 (s, 24H, O*CH$_3$*).

IR (ATR): 2132 cm^{-1} ($\nu_{C\equiv N}$ isocyanide).

MS (MALDI-TOF): m/z Calcd. for [M$^+$–(Au(CN)$_2$)$^-$]$^+$ (M$^+$ = $C_{36}H_{36}N_4O_8Rh$): 755.1583; found: 755.1604.

Anal. Calcd. for $C_{38}H_{36}AuN_6O_8Rh$: C, 57.22; H, 4.80; N, 7.41; found: C, 56.94; H, 4.62; N, 7.28.

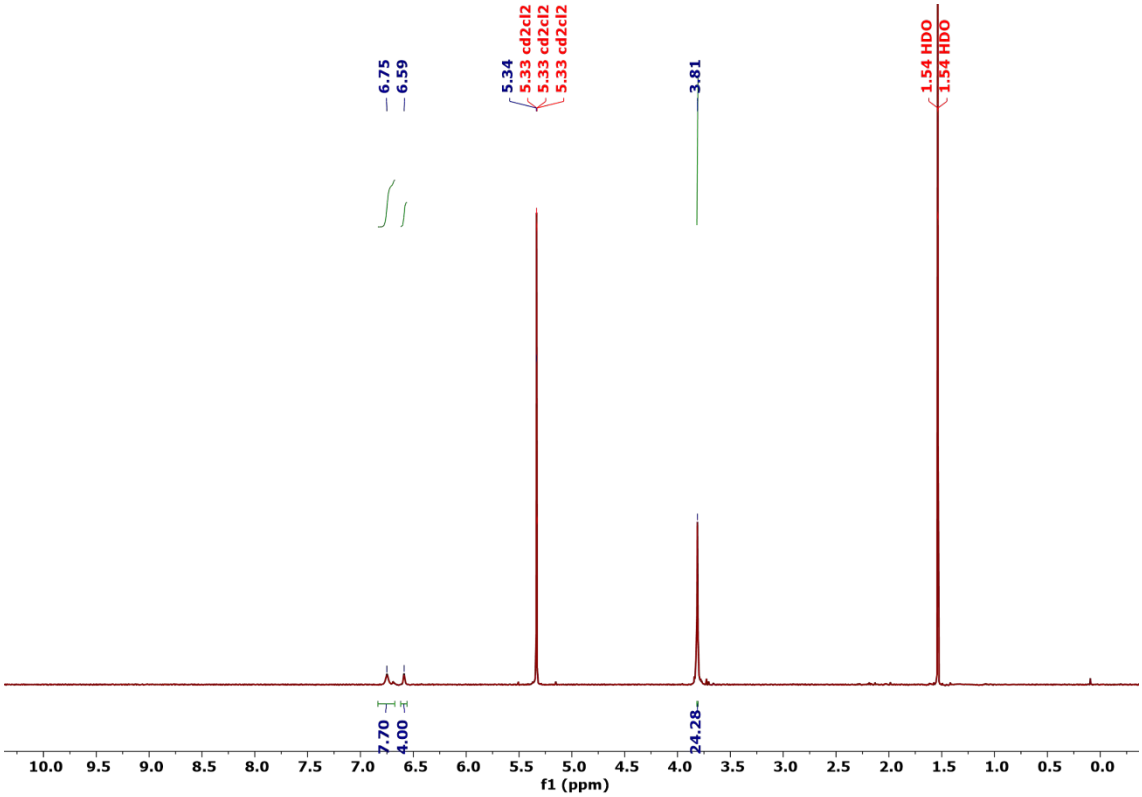

Figure ESI23. ^{1}H NMR spectrum of **18** at 298 K in CD_2Cl_2

[Rh(L^{D1})$_4$]Cl (10)

A solution of $\mathbf{L^{D1}}$ ligand (85 mg, 0.062 mmol) in 10 mL dry CH_2Cl_2 was slowly added into a solution of (μ-Cl)$_2$[RhCOD)]$_2$ in 20 mL of dry CH_2Cl_2 and the mixture was stirred for 1 h. at room temperature. Afterwards, the solution was concentrated by evaporation under reduced pressure, and CH_3CN was added and cooled down at –22 ºC 1 overnight. The green solid was filtered, washed with CH_3CN (3 × 5 mL), and dried in vacuum. A dark green solid was obtained: 80 mg (92%).

^{1}H NMR (499.72 MHz, CD_2Cl_2 298 K, Figure ESI24): δ 7.84 (s, 24H, Ar-*H*), 7.41 (d, J = 8.11Hz, 8H, Ar-*H*). 6.95 (d, J = 8.11, 8H, Ar-*H*). 4.26-4.21 (m, 48H, O-CH_2), 4.04 (t, J = 6.2 Hz, 8H, O-CH_2) 1.97-1.85 (m, 56H, O-CH_2-*CH_2*), 1.72-1.61 (m, 56H, O-CH_2-CH_2-*CH_2*), 1.48-1.25 (m, 320H, $(CH_2)_n$), 0.90-0.86 (m, 60H, CH_3).

^{13}C{^{1}H} NMR (125.67 MHz, CD_2Cl_2 298 K, Figure ESI25): δ (CN not observed), 160.58 (O*C$_{Ph}$*), 149.12, 149.06, 148.98, 148.88 (O-*C$_{TriPh}$*), 128.08 (H-*C$_{Ph}$*), 123.51, 123.46, 123.40, 123.30, 123.27, 123.21 (*C$_{TriPh}$*), 118.43 (N-*C$_{Ph}$*), 115.43 (H-*C$_{Ph}$*), 107.23, 107.09, 107.07, 106.99, 106.93, 106.90 (H-*C$_{TriPh}$*), 69.66, 69.58, 69.52, 69.47, 69.42, 69.35, 68.66 (O-*CH_2*), 31.91, 29.71, 29.69, 29.66, 29.51, 29.44, 29.36, 29.06, 26.20, 25.98, 25.81, 22.67 (-*CH_2*-), 13.86 (-*CH_3*).

IR (ATR, neat, cm^{-1}): 2160 ($\nu_{NC\text{-}Rh}$).

MS (MALDI-TOF): m/z calc. for [(M^+/2-(Cl^-))] (M^+/2 = $C_{182}H_{294}N_2O_{14}Rh$): 2837.1472; found 2837.1435.

Anal. Calcd. (%) for $C_{364}H_{588}ClN_4O_{28}Rh$: C, 77.97; H, 10.57; N, 1.00; found C, 77.91; H, 10.50; N, 1.02.

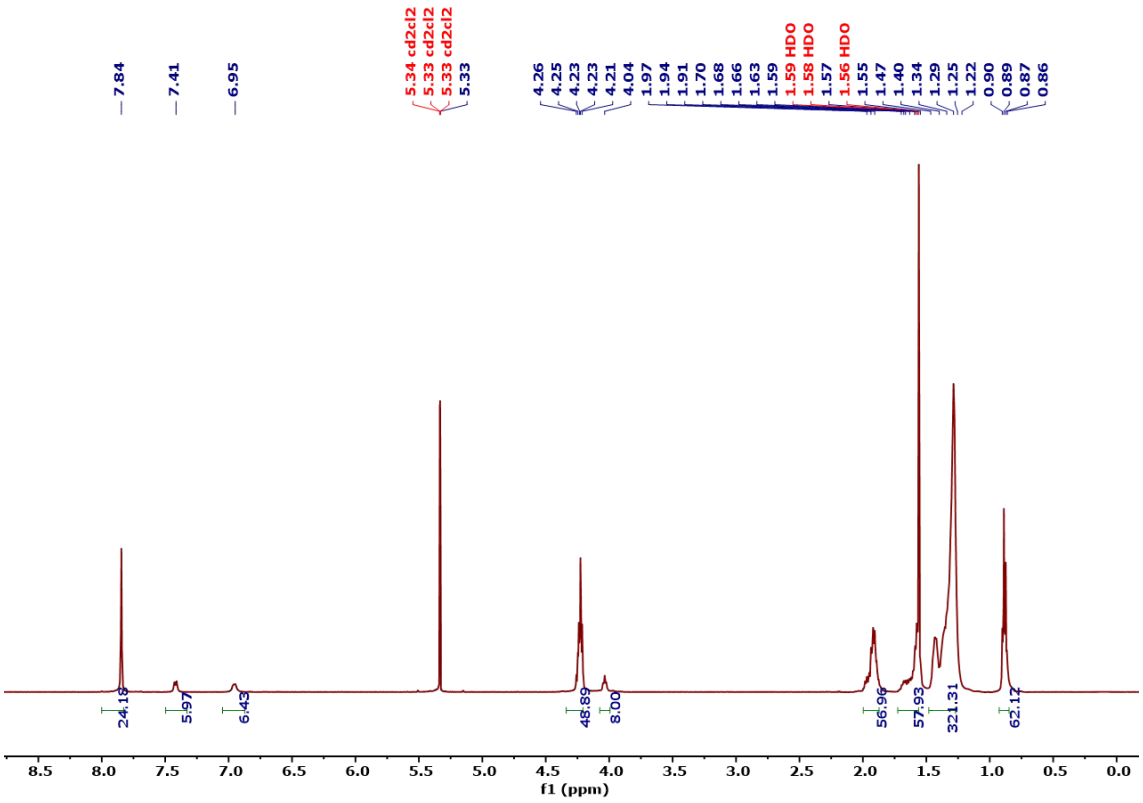

Figure ESI24. ^{1}H NMR spectrum of **10** at 298 K in CD_2Cl_2

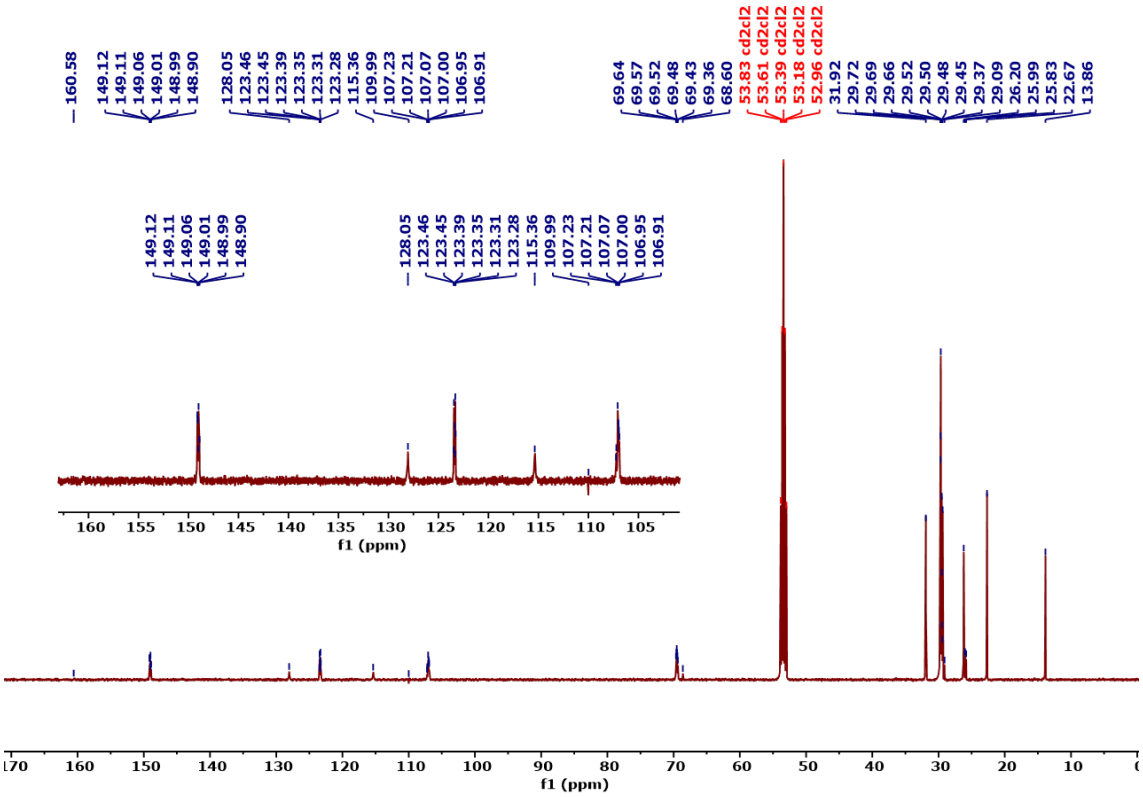

Figure ESI25. ^{13}C{^{1}H} NMR spectra of **10** at 298 K in CD_2Cl_2

v) General Synthesis for complexes $[Rh(L^{D})_4](BF_4)$

The corresponding isocyanotriphenylene ligand (molar ratio 4:1) in dry dichloromethane was added slowly to a stirred solution of $[Rh(COD)_2](BF_4)$ in dry dichloromethane and the mixture was stirred at room temperature for 1h. Then the solution was concentrated by evaporation under reduced pressure to a small volume, and MeCN (5 mL) was added and the mixture was cooled at –22 ºC overnight. The precipitate formed was filtered and washed with MeCN (3 × 5 mL) and cool acetone (1 × 3 mL) to remove the free COD. Finally, the solid was vacuum dried.

$[Rh(L^{D1})_4](BF_4)$ (14)

Reagents: $[Rh(COD)_2](BF_4)$ (10 mg, 0.025 mmol) in CH_2Cl_2 (20 mL), **L^{D1} (9)** (135 mg, 0.098 mmol) in CH_2Cl_2 (5 mL), A color change of the solution was observed (from red to brown-greenish). A green solid was obtained: 120 mg (86%).

^1H NMR (499.72 MHz, CD_2Cl_2 298 K, Figure ESI26): δ 7.85 (s, 24H, Ar-*H*), 7.43 (d, J = 8.11Hz, 8H, Ar-*H*). 6.97 (d, J = 8.11, 8H, Ar-*H*). 4.26-4.22 (m, 48H, O-CH_2), 4.05 (t, J = 6.2 Hz, 8H, O-CH_2) 2.01-1.85 (m, 56H, O-CH_2-*CH_2*), 1.71-1.55 (m, 56H, O-CH_2-CH_2-*CH_2*), 1.47-1.26 (m, 320H, $(CH_2)_n$), 0.89-0.84 (m, 60H, CH_3).

$^{13}C\{^1H\}$ NMR (125.67 MHz, CD_2Cl_2 298 K, Figure ESI27): δ (CN not observed), 160.62 (OC_{Ph}), 149.12, 149.06, 148.98, 148.88 (O-C_{TriPh}), 128.08 (H-C_{Ph}), 123.51, 123.46, 123.40, 123.30, 123.27, 123.21 (C_{TriPh}), 118.43 (N-C_{Ph}), 115.43 (H-C_{Ph}), 107.23, 107.09, 107.07, 106.99, 106.93, 106.90 (H-C_{TriPh}), 69.66, 69.58, 69.52, 69.47, 69.42, 69.35, 68.66 (O-*CH_2*), 31.91, 29.71, 29.69, 29.66, 29.51, 29.44, 29.36, 29.06, 26.20, 25.98, 25.81, 22.67 (-*CH_2*-), 13.86 (-*CH_3*).

^{19}F NMR (470.15 MHz, CD_2Cl_2; 298 K, Figure ESI28): δ -153.48 (B^{13}), -153.54 (B^{11}).

IR (ATR, neat, cm^{-1}): 2156 ($\nu_{C\equiv N}$).

MS (MALDI-TOF): m/z calc.for $[(M^+-(BF_4^-)]$ (M^+ = $C_{364}H_{588}N_4O_{28}Rh$): 5568.3794; found: 5568.3774

Anal. Calcd. (%) for $C_{364}H_{588}BF_4N_4O_{28}Rh$: C, 77.27; H, 10.47; N, 0.99; found: C, 76.91; H, 10.28; N, 1.02.

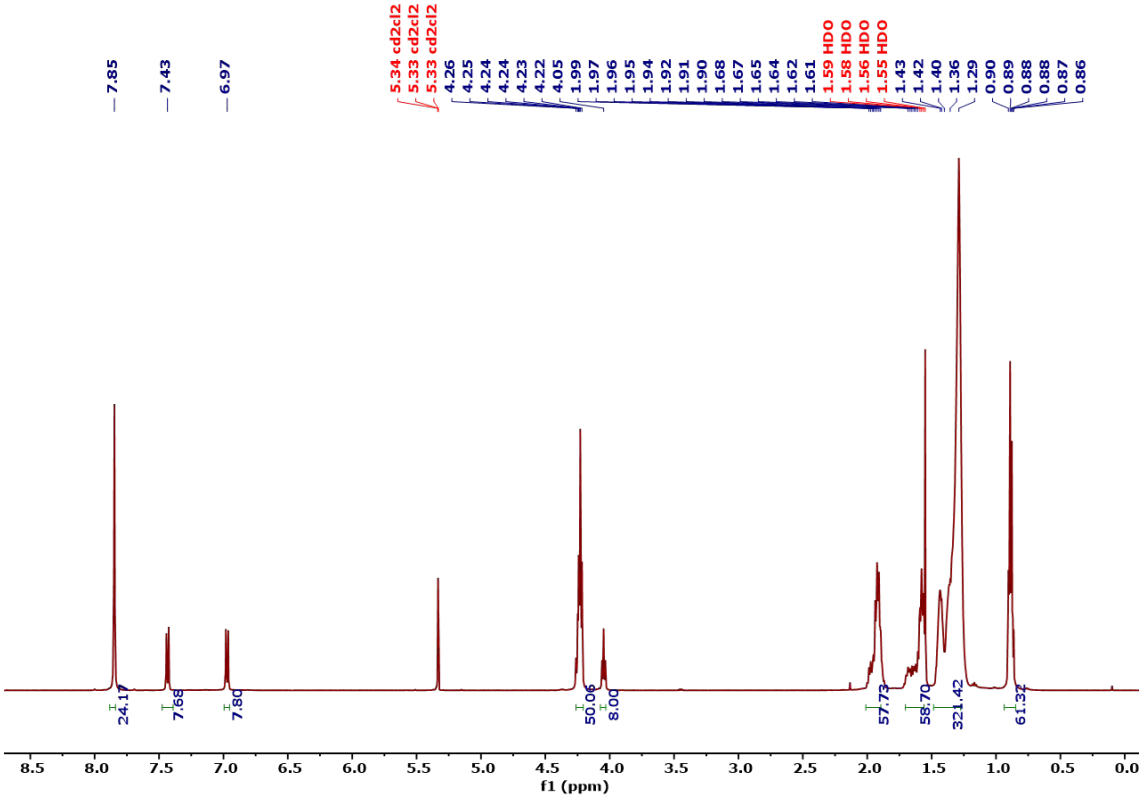

Figure ESI26. ^{1}H NMR spectrum of **14** at 298 K in CD_2Cl_2

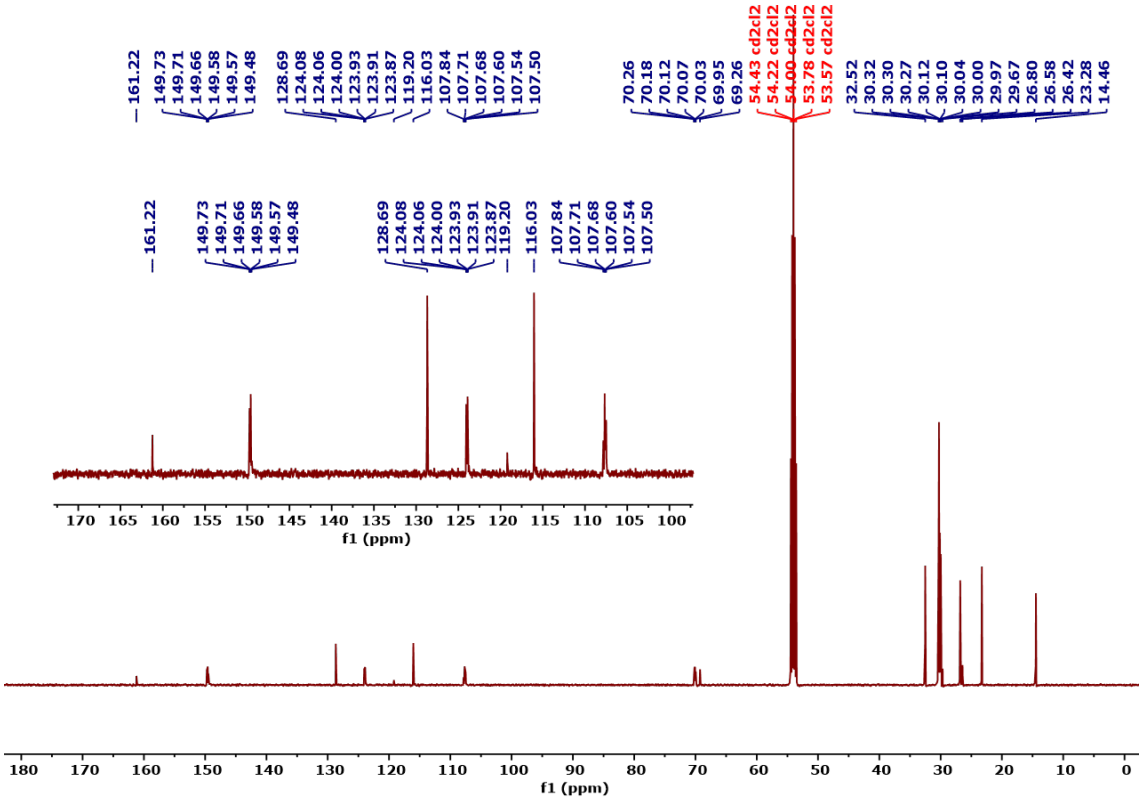

Figure ESI27. $^{13}C\{^{1}H\}$ NMR spectrum of **14** at 298 K in CD_2Cl_2

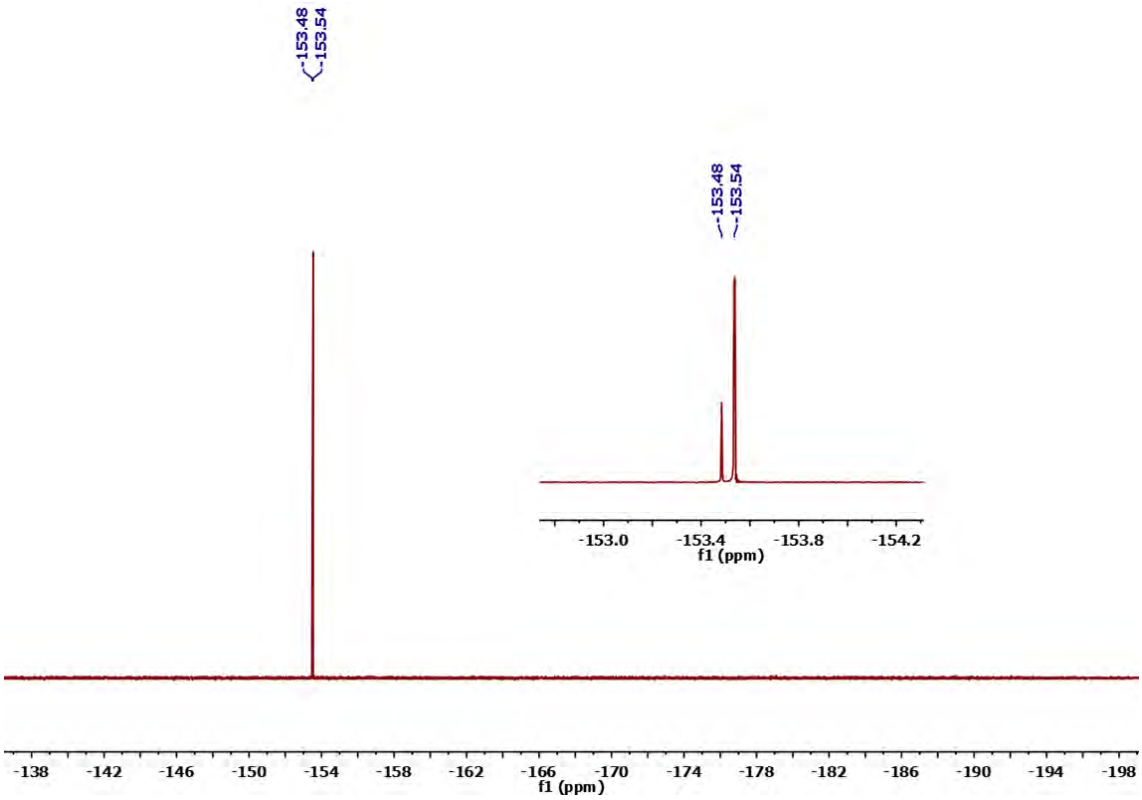

Figure ESI28. ^{19}F NMR spectrum of **14** at 298 K in CD_2Cl_2

[Rh(L^{D2})$_4$](BF$_4$) (15)

Reagents: [Rh(COD)$_2$](BF$_4$) (7.2 mg, 0.018 mmol) in CH_2Cl_2 (20 mL), $\mathbf{L^{D2}}$ (100 mg, 0.072 mmol) in CH_2Cl_2 (5 mL). A color change of the solution was observed (from red to yellow-greenish). A red solid was obtained: 120 mg (86%).

^{1}H NMR (499.72 MHz, CD_2Cl_2 298 K, Figure ESI29): δ 7.85 (s, 24H, Ar-*H*), 6.70 (s, 8H, Ar-*H*). 4.37-4.17 (m, 48H, O-CH_2), 4.00 (t, J = 6.2 Hz, 8H, O-CH_2), 2.41 (s, 24H, 4 x (2 × CH_3, Xylyl), 2.14-1.87 (m, 56H, O-CH_2-*CH_2*), 1.69-1.55 (m, 56H, O-CH_2-CH_2-*CH_2*), 1.47-1.25 (m, 320H, $(CH_2)_n$), 0.91-0.87 (m, 60H, CH_3).

^{13}C{^{1}H} NMR (125.67 MHz, CD_2Cl_2 298 K, Figure ESI30): δ (CN not observed), 159.90 (OC_{Ph}), 149.12, 149.11, 149.06, 149.00, 148.99, 148.90 (O-C_{TriPh}), 137.02 (CH_3-C_{Ph}), 123.46, 123.40, 123.34, 123.32, 123.31, 123.28, (C_{TriPh}), 118.79 (N-C_{Ph}), 114.02 (H-C_{Ph}), 107.21, 107.08, 107.00, 106.95, 106,94, 106.91 (H-C_{TriPh}), 69.64, 69.58, 69.52, 69.48, 69.44, 69.37, 68.40 (O-*CH_2*), 31.93, 29.73, 29.70, 29.67, 29.53, 29,51, 29.45, 29.38, 29.12, 26.21, 25.99, 25.84, 22.68 (-*CH_2*-), 18.82 (-*CH_3, Xylyl),* 13.87 (-*CH_3*).

^{19}F NMR (470.15 MHz, CD_2Cl_2; 298 K, Figure ESI31): δ -153.43 (B^{13}), -153.48 (B^{11}).

IR (ATR, neat, cm^{-1}): 2140 ($\nu_{C\equiv N}$).

MS (MALDI-TOF): m/z calcd. for (M^+-BF_4^-) (M^+ = $C_{372}H_{604}N_4O_{28}Rh$: 5679.5012; found: 5679.4967.

Anal. Calcd. (%) for $C_{372}H_{604}BF_4N_4O_{28}Rh$: C, 77.43; H, 10.55; N, 0.97; found: C, 77.24; H, 10.69; N, 0.91.

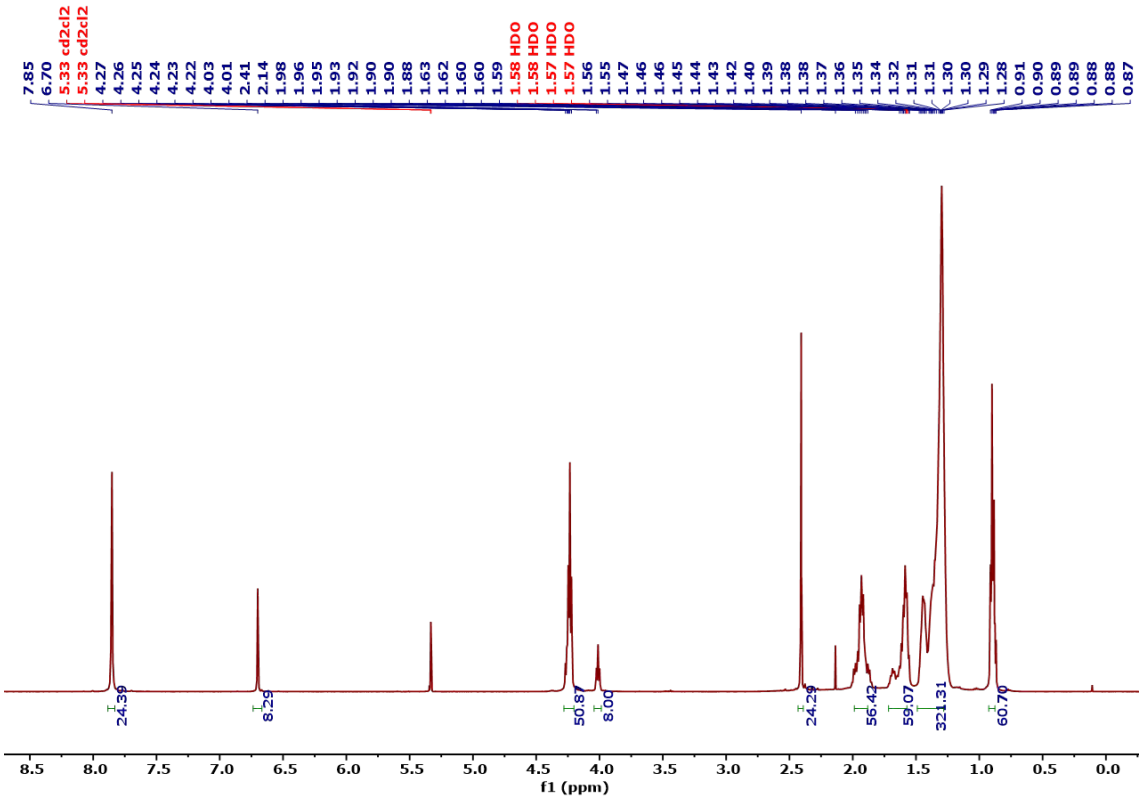

Figure ESI29. ^{1}H NMR spectrum of **15** at 298 K in CD_2Cl_2

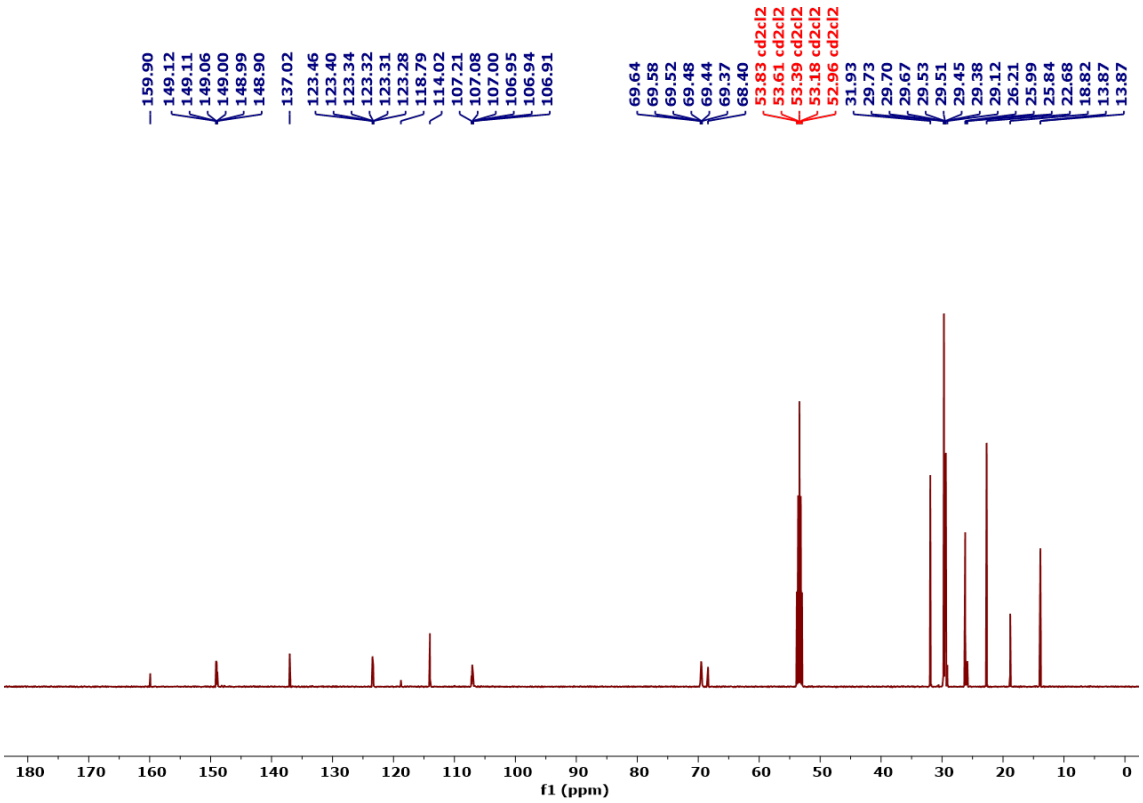

Figure ESI30. $^{13}C\{^{1}H\}$ NMR spectrum of **15** at 298 K in CD_2Cl_2

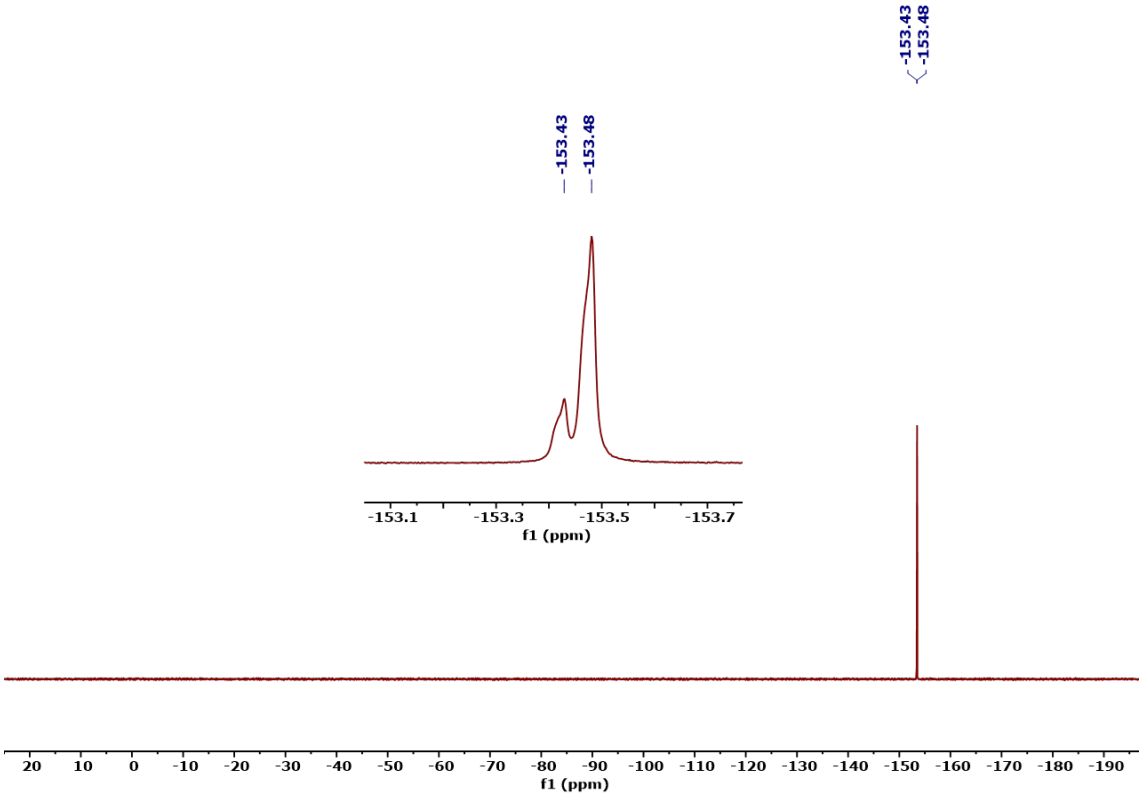

Figure ESI31. ^{19}F NMR spectrum of **15** at 298 K in CD_2Cl_2

vi) General Synthesis for complexes $[Rh(L^D)][Au(CN)_2]$

$[Rh(L^{D1})_4][Au(CN)_2]$ (19)

A $K[Au(CN)_2]$ (3.9 mg, 0.026 mmol) solution in acetone (3 mL) was added dropwise into a solution of $[Rh(L^{D1})_4](BF_4)$ (**14**) (70 mg, 0.012 mmol) in CH_2Cl_2 (40 mL). This mixture was stirred for 2 h at rt. Then, it was evaporated and the blue-greenish residue was washed with water (3 × 5 mL) and a cool mixture of CH_3CN-acetone (3:1). Finally, the dark green solid was vacuum dried. Yield 60 mg (83%).

^1H NMR (499.72 MHz, CD_2Cl_2 298 K, Figure ESI32): δ 7.85 (s, 24H, Ar-*H*), 7.46 (d, J = 8.11Hz, 8H, Ar-*H*). 6.96 (d, J = 8.11, 8H, Ar-*H*). 4.26-4.21 (m, 48H, O-CH_2), 4.04 (t, J = 6.2 Hz, 8H, O-CH_2) 2.00-1.84 (m, 56H, O-CH_2-*CH_2*), 1.71-1.55 (m, 56H, O-CH_2-CH_2-*CH_2*), 1.48-1.27 (m, 320H, $(CH_2)_n$), 0.93-0.82 (m, 60H, CH_3).
$^{13}C\{^1H\}$ NMR (125.67 MHz, CD_2Cl_2 298 K, Figure ESI33): δ (CN not observed), 160.48 (OC_{Ph}), 149.11, 149.05, 148.99, 148.90 (O-C_{TriPh}), 128.11 (H-C_{Ph}), 123.44, 123.42, 123.39, 123.36, 123.31, 123.28 (C_{TriPh}), 118.87 (N-C_{Ph}), 115.33 (H-C_{Ph}), 107.20, 107.07, 106.99, 106.96, 106.92, 106.85 (H-C_{TriPh}), 69.64, 69.57, 69.52, 69.48, 69.44, 69.36, 68.61 (O-*CH_2*), 31.92, 29.72, 29.69, 29.66, 29.51, 29.49, 29.37, 29.09, 26.20, 25.99, 25.83, 22.67 (-*CH_2*-), 13.86 (-*CH_3*).

IR (ATR, neat, cm^{-1}): 2157 ($\nu_{N\equiv C\text{-}Rh}$).
MS (MALDI-TOF): m/z calc.for $((M^+ + H) - [Au(CN)_2^-])$ ($M^+ = C_{364}H_{588}N_4O_{28}Rh$): 5570.39; found: 5571.90; m/z calc.for $((M^+/2) - [Au(CN)_2^-])$ ($M^+/2 = C_{182}H_{294}N_2O_{14}Rh$): 2837.1472; found: 2837.1434.
Anal. Calcd. (%) for $C_{366}H_{588}AuN_6O_{28}Rh$: C, 75.52; H, 10.18; N, 1.44; found C, 75.38; H, 9.57; N, 1.39.

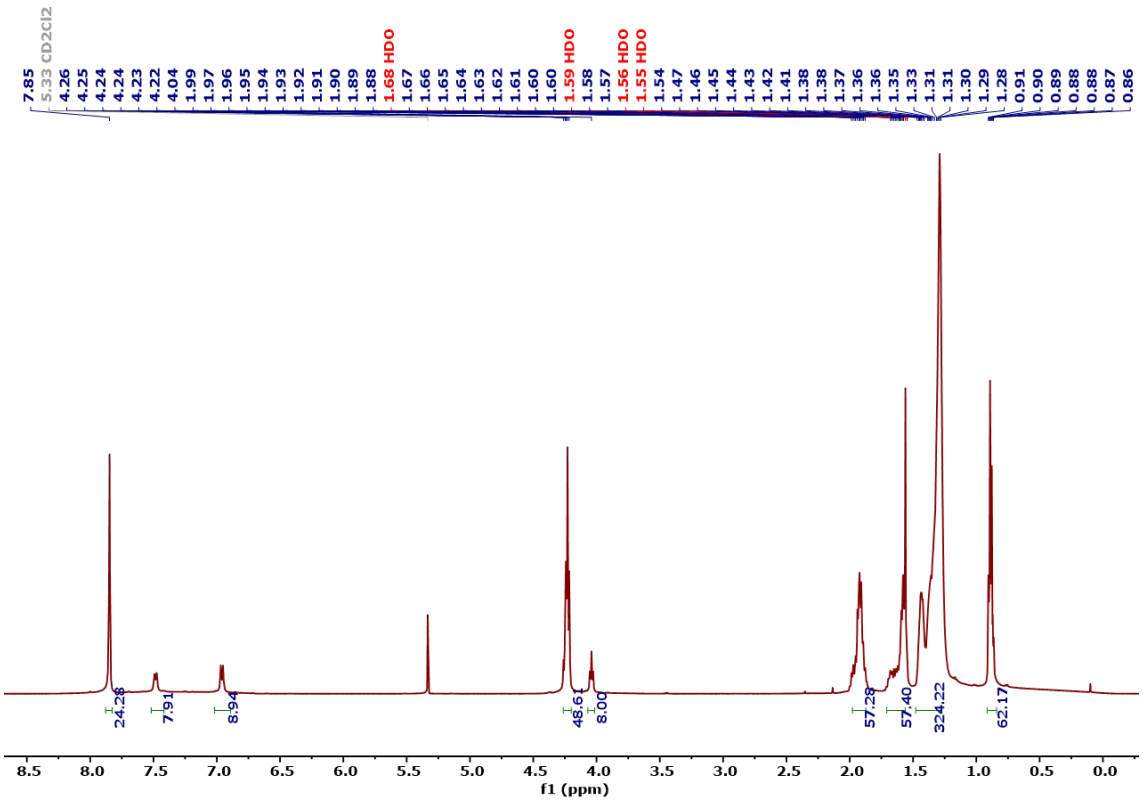

Figure ESI32. ^{1}H NMR spectrum of **19** at 298 K in CD_2Cl_2

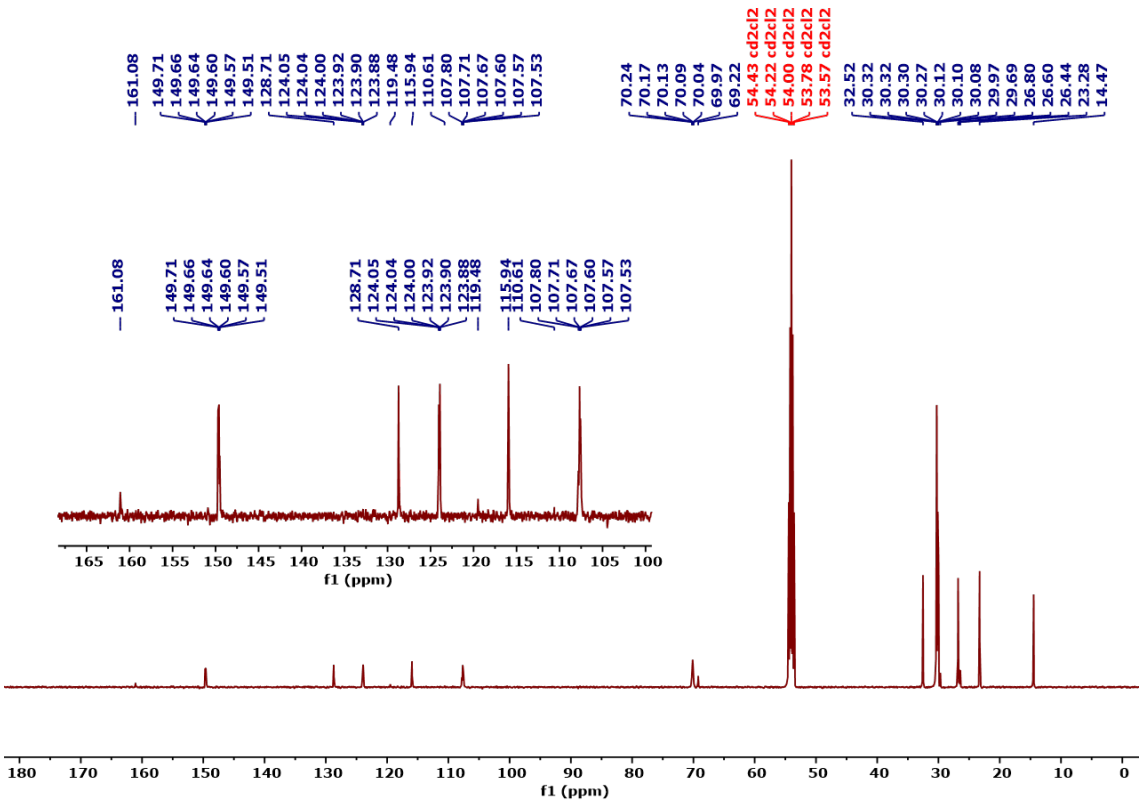

Figure ESI33. $^{13}C\{^{1}H\}$ NMR spectrum of **19** at 298 K in CD_2Cl_2

[Rh(L^{D2})$_4$][Au(CN)$_2$] (20)

A K[Au(CN)$_2$] (3.3 mg, 0.026 mmol) solution in acetone (3 mL) was added dropwise into a solution of [Rh(L^{D2})$_4$]BF$_4$ (**15**) (60 mg, 0.010 mmol) in CH_2Cl_2 (40 mL). This mixture was stirred for 3 h at 35 ºC. Then, it was evaporated and the blue-greenish residue was washed with water (3 × 5 mL) and with a cool mixture of MeCN-acetone (3:1). Finally, the red solid was vacuum dried. Yield 48 mg (78%).

^{1}H NMR (499.72 MHz, CD_2Cl_2 298 K, Figure ESI34): δ 7.85 (s, 24H, Ar-*H*), 6.69 (bs, 8H, Ar-*H*). 4.26-4.22 (m, 48H, O-CH_2), 4.00 (t, J = 6.2 Hz, 8H, O-CH_2), 2.41 (s, 24H, 4 x (2 × -CH_3, Xylyl)), 1.99-1.86 (m, 56H, O-CH_2-*CH_2*), 1.70-1.55 (m, 56H, O-CH_2-CH_2-*CH_2*), 1.47-1.29 (m, 320H, $(CH_2)_n$), 0.91-0.86 (m, 60H, CH_3).

^{13}C{^{1}H} NMR (125.67 MHz, CD_2Cl_2 298 K, Figure ESI35): δ (CN not observed), 159.84 (OC_{Ph}), 149.11, 149.10, 149.06, 149.01, 148.99, 148.90 (O-C_{TriPh}), 137.05 (CH_3-C_{Ph}), 123.45, 123.40, 123.31, 123.28 (C_{TriPh}), 118.84 (N-C_{Ph}), 113.98 (H-C_{Ph}), 107.20, 107.18, 107.08, 107.00, 106.95, 106.91 (H-C_{TriPh}), 69.64, 69.58, 69.52, 69.44, 69.37, 68.38 (O-*CH_2*), 31.92, 29.72, 29.70, 29.50, 29.44, 29.37, 26.20, 26.16, 25.99, 25.84, 22.68, 18.86 (-*CH_2*-), 18.86 (Ph-*CH_3*) 13.87, 13.86 (-*CH_3*).

IR (ATR, neat, cm^{-1}): 2139 ($\nu_{N\equiv C\text{-}Rh}$).

MS (MALDI-TOF): m/z calc.for (M^+-[Au(CN)$_2^-$]) (M^+ = $C_{372}H_{604}N_4O_{28}Rh$): 5679.5012; found: 5679.5060.

Anal. Calcd. (%) for $C_{374}H_{604}AuN_6O_{28}Rh$: C, 75.72; H, 10.26; N, 1.42; found C, 75.40; H, 10.16; N, 1.48.

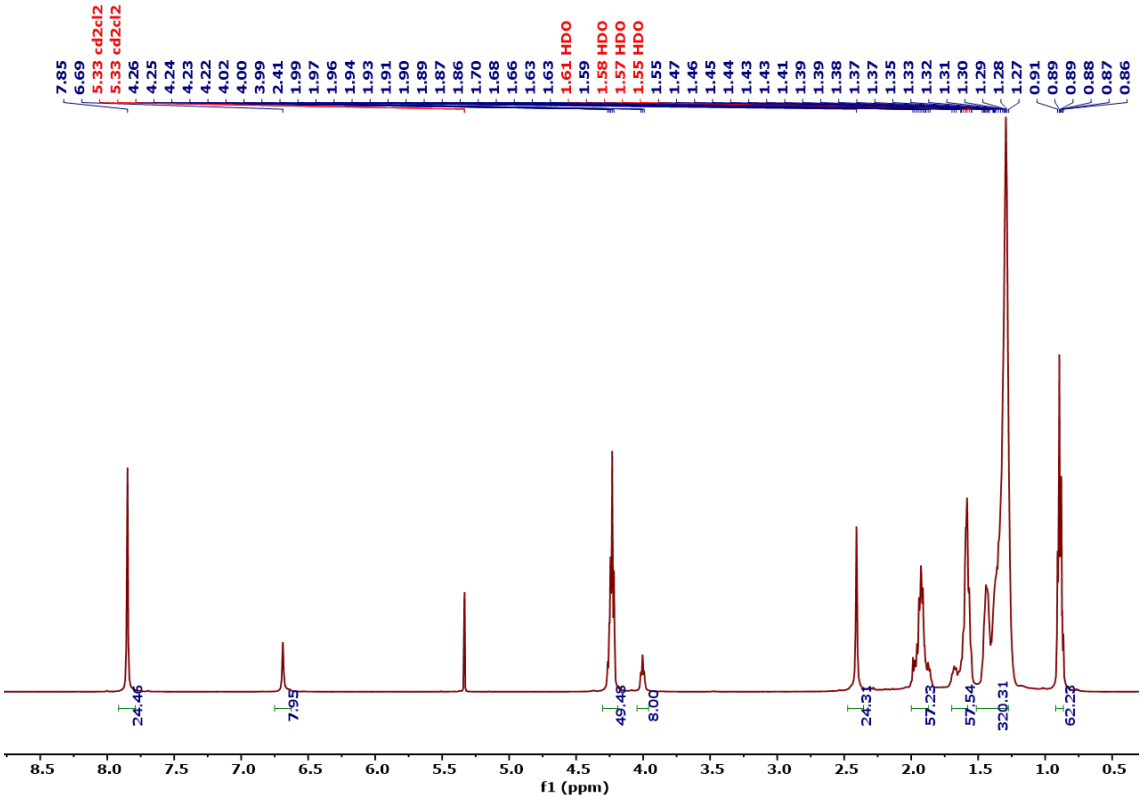

Figure ESI34. ^{1}H NMR spectrum of **20** at 298 K in CD_2Cl_2.

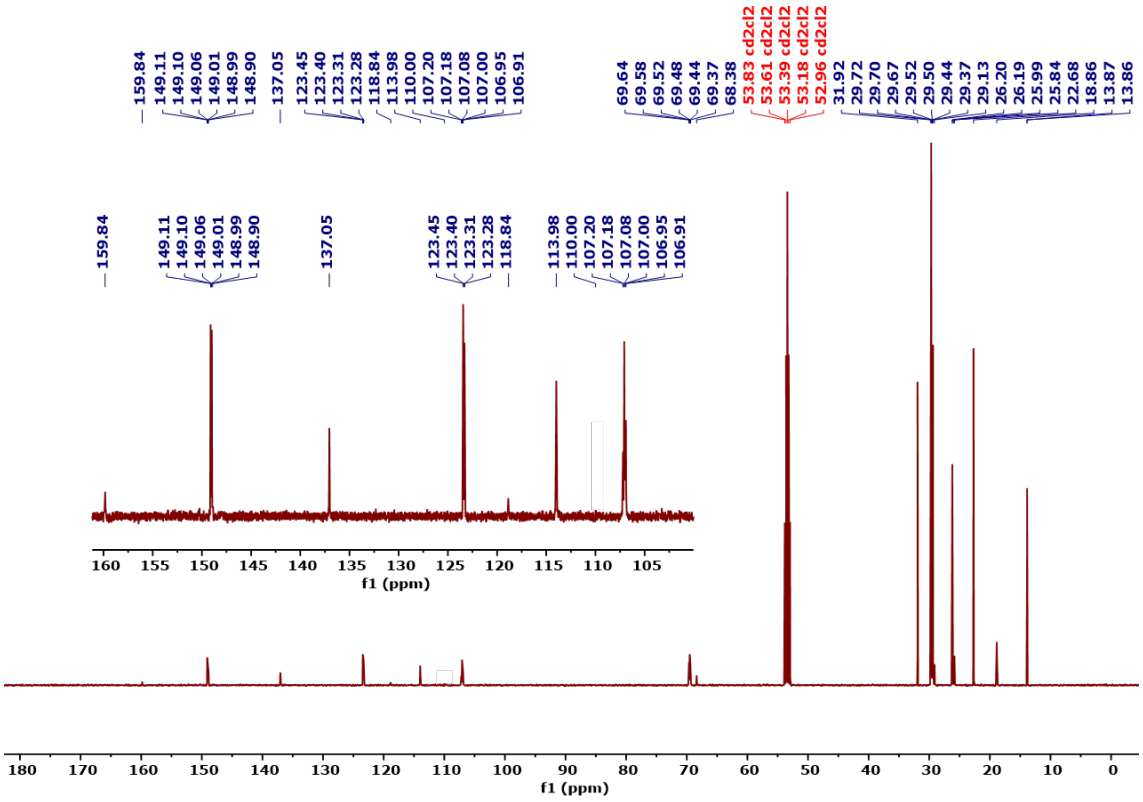

Figure ESI35. $^{13}C\{^{1}H\}$ NMR spectrum of **20** at 298 K in CD_2Cl_2

UV-VISIBLE DATA

Table ESI2: UV-visible data for the free isocyanides and the isocyanide rhodium complexes, in dichloromethane solution at 298 K

Compd.	UV-Vis (CH_2Cl_2)/nm ($\varepsilon/M^{-1}\,cm^{-1}$)
6 (L^{D2})	279.5 ($20.3\cdot10^4$), 308 ($5.03\cdot10^4$), 346 ($7.00\cdot10^3$)
9[b]	227.5 ($6.33\cdot10^4$), 256.5 ($3.60\cdot10^4$), 331.5 ($4.15\cdot10^4$), 407 ($5.22\cdot10^3$), 457 ($6.20\cdot10^2$)
10[a]	279.5 ($30.5\cdot10^4$), 346 ($5.60\cdot10^4$), 405 ($5.80\cdot10^3$), 460 ($7.00\cdot10^2$)
11[b]	250.5 ($7.15\cdot10^4$), 337 ($5.51\cdot10^4$), 408 ($7.40\cdot10^3$), 460 ($1.18\cdot10^3$)
12[a]	260 ($8.32\cdot10^4$), 347.5 ($6.10\cdot10^4$), 405 ($9.20\cdot10^3$), 460 ($2.00\cdot10^3$)
13[b]	227.5 ($6.81\cdot10^4$), 257 ($4.63\cdot10^4$), 334 ($4.92\cdot10^4$), 411 ($6.72\cdot10^3$), 465 ($7.80\cdot10^2$)
14[a]	272 ($34.8\cdot10^4$), 346.5 ($6.75\cdot10^4$), 406 ($6.80\cdot10^3$), 462 ($9.00\cdot10^2$)
15[a]	280 ($37.4\cdot10^4$), 309 ($13.5\cdot10^4$), 348 ($8.13\cdot10^4$), 406 ($9.10\cdot10^3$), 462 ($1.60\cdot10^2$)
16[b]	226.5 ($5.90\cdot10^4$), 260 ($3.73\cdot10^4$), 334.5 ($2.84\cdot10^4$), 412 ($3.46\cdot10^3$)
17[a]	269 ($15.7\cdot10^4$), 340 ($4.71\cdot10^4$), 402.5 ($6.60\cdot10^3$)
18[b]	227 ($6.88\cdot10^4$), 260 ($4.90\cdot10^4$), 334 ($4.01\cdot10^4$), 412 ($4.80\cdot10^3$)
19[a]	279 ($33.5\cdot10^4$), 309 ($9.91\cdot10^4$), 345 ($5.14\cdot10^4$), 407 ($4.30\cdot10^3$)
20[a]	280 ($36.2\cdot10^4$), 309 ($13.0\cdot10^4$), 348 ($7.70\cdot10^4$), 406 ($5.50\cdot10^3$)
	[a]Spectra recorded at 10^{-5} M. [b]Spectra recorded at 5×10^{-5} M.

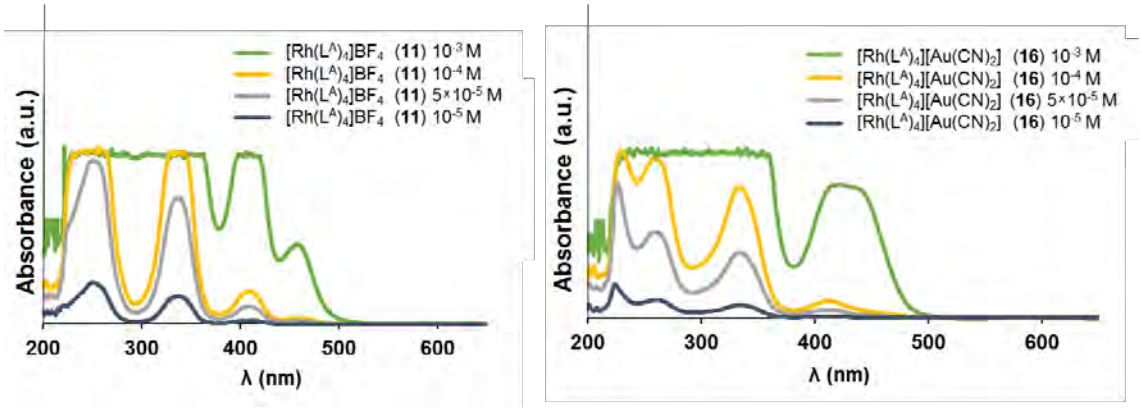

Figure ESI36. UV-Visible spectra of the complexes **11** and **16** in dichloromethane solutions at different molarities and 298 K.

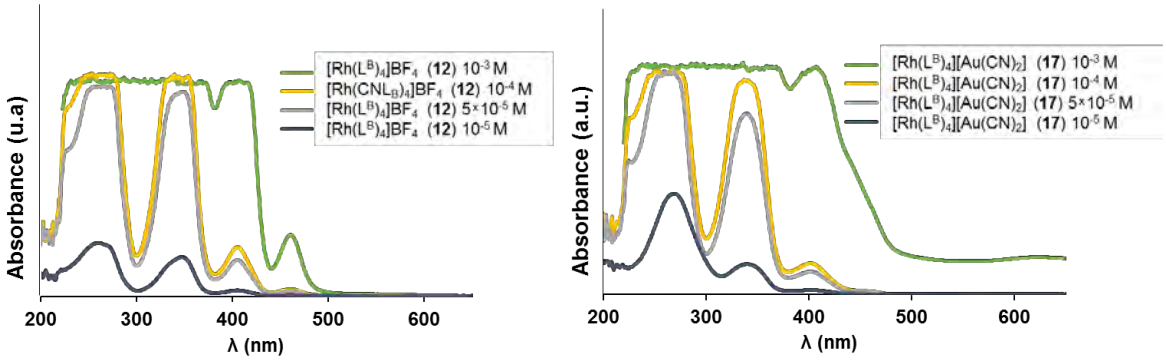

Figure ESI37. UV-Visible spectra of the complexes **12** and **17** in dichloromethane solutions at different molarities and 298 K.

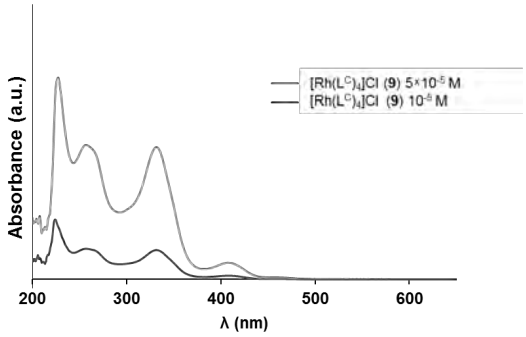

Figure ESI38. UV-Visible spectra of the complex **9** in dichloromethane solutions at different molarities and 298 K.

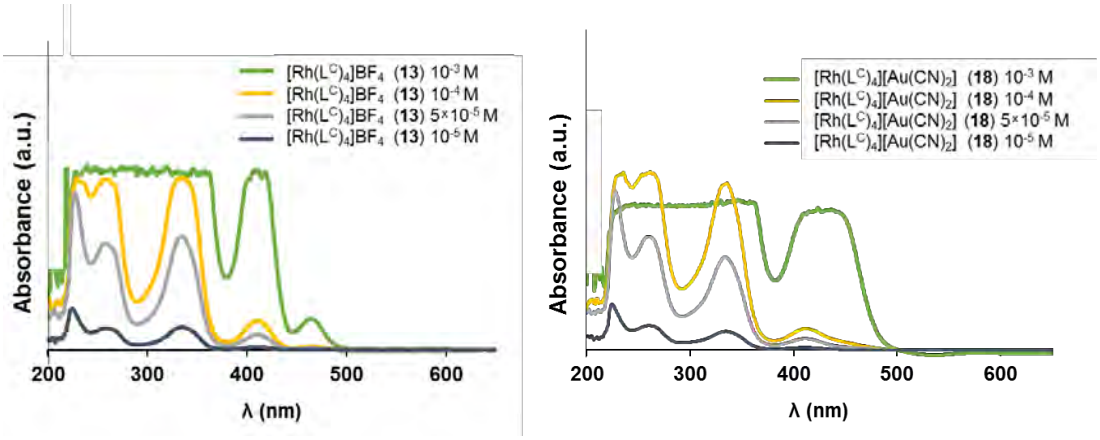

Figure ESI39. UV-Visible spectra of the complexes **13** and **18** in dichloromethane solutions at different molarities and 298 K.

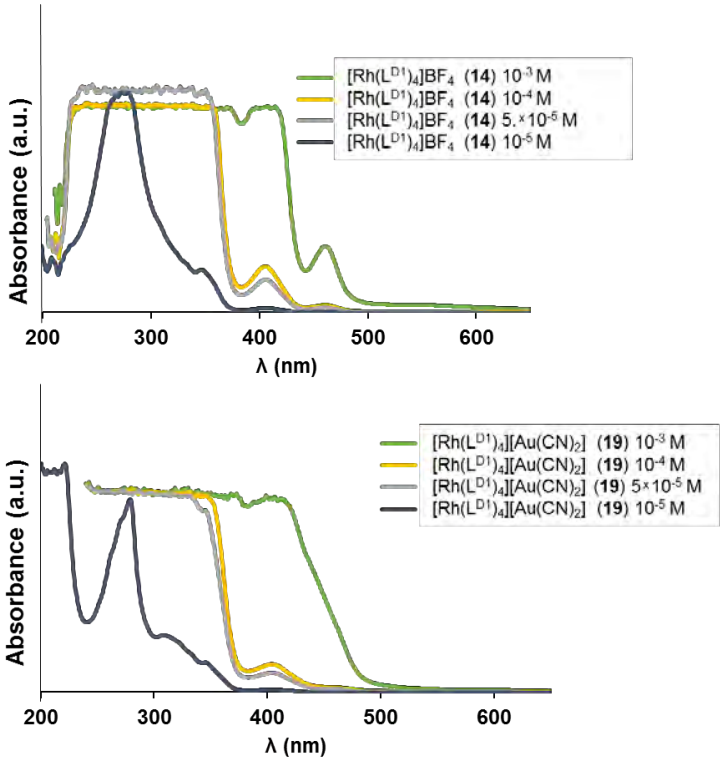

Figure ESI40. UV-Visible spectra of the complexes **14** and **19** in dichloromethane solutions at different molarities and 298 K.

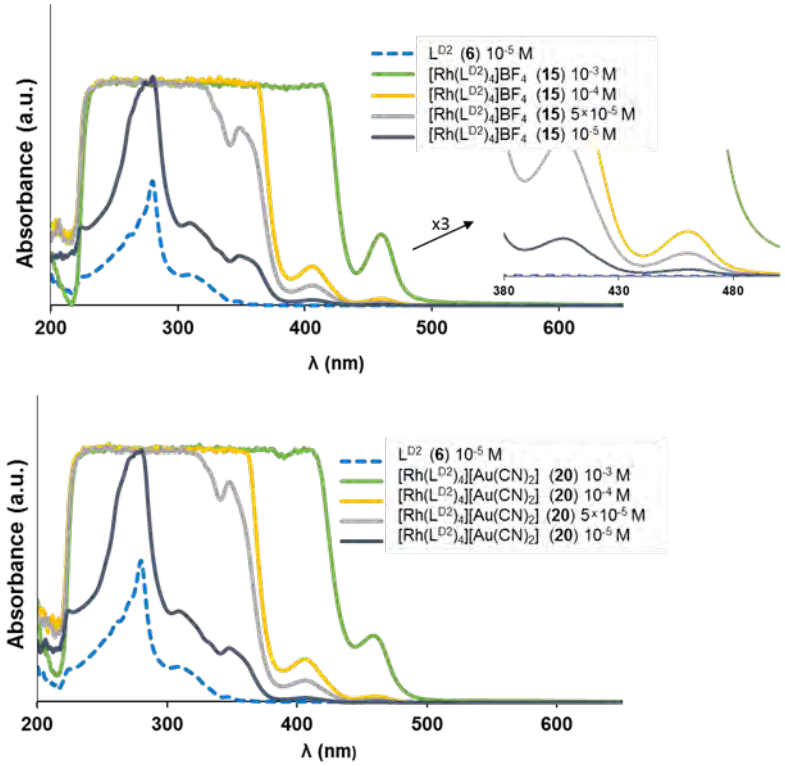

Figure ESI41. UV-Visible spectra of the ligand **6** and the complexes **15** and **20** in dichloromethane solutions at different molarities and 298 K. *The top picture shows a magnified region for observing the existence of curves around 465 nm at lower concentration of 5 x 10^{-5} M for complex **15**

REFINEMENT DATA OF THE X-RAY STRUCTURES

a) In Single crystal

Table ESI3: Crystal data and structure refinements for complexes (**9**) and (**11**).

	[Rh{3,5-$(OMe)_2C_6H_3(NC)$}$_4$]Cl (**9**)	[Rh(*p*-$MeC_6H_4(NC)$)$_4$]BF_4 (**11**)
Empirical formula	$C_{36}H_{36}ClN_4O_8Rh$	$C_{32}H_{28}BN_4F_4Rh$
Formula weight	791.05	658.30
Temperature/K	294	180.00(14)
Crystal system	monoclinic	monoclinic
Space group	$P2_1/n$	C2/c
a/Å	3.8977(4)	14.6259(3)
b/Å	26.059(3)	16.8572(3)
c/Å	21.706(3)	27.9530(5)
α/°	90	90
β/°	94.320(10)	94.306(2)
γ/°	90	90
Volume/Å^3	2198.4(4)	6872.4(2)
Z	2	8
ρ_{calc}g/cm^3	1.195	1.272
μ/mm^{-1}	0.495	0.543
F(000)	812.0	2672.0
Crystal size/mm^3	0.433 × 0.108 × 0.073	0.422 × 0.353 × 0.225
Radiation	MoKα (λ = 0.71073)	MoKα (λ = 0.71073)
2θ range for data collection/°	7.3 to 59.23	6.736 to 59.41
Index ranges	$-4 \le h \le 4$, $-30 \le k \le 32$, $-15 \le l \le 28$	$-20 \le h \le 18$, $-19 \le k \le 21$, $-28 \le l \le 38$
Reflections collected	8766	23228
Independent reflections	4988 [R_{int} = 0.0759, R_{sigma} = 0.1339]	8391 [R_{int} = 0.0244, R_{sigma} = 0.0295]
Data/restraints/parameters	4988/0/236	8391/0/428
Goodness-of-fit on F^2	1.019	1.219
Final R indexes [I>=2σ (I)]	R_1 = 0.0814, wR_2 = 0.2163	R_1 = 0.0966, wR_2 = 0.2604
Final R indexes [all data]	R_1 = 0.1508, wR_2 = 0.2840	R_1 = 0.1090, wR_2 = 0.2665
Largest diff. peak/hole/eÅ^{-3}	1.26/-0.64	0.81/-1.02

b) In Mesophase

Table ESI4. Mesomorphic, Structural, and Geometrical Parameters for complexes $[Rh(L^{Di})_4]A$ (i = 1,2)

A (anion) Sample type / T (°C)[a]	Phase[b]	2D lattice parameters[c] Cell parameters[d]	V_{mol} (Å³)[e] ρ (g/cm³) N_{mol},[f]	h_π(Å)[g] h_{mol}(Å)	$Z_{col,RhA}$[h] h_{RhA} (Å) $N_{RhA,c}$	$Z_{col,Tph}$[i] h_{Tph} (Å) $N_{Tph,c}$	⟨ψ$_{Tph}$⟩ (°)[j] $dh_{Tph,c}$ (Å)
$[Rh(L^{D1})_4](A)$							
A = Cl Film / 20	Col_o	*a* = 97.8; *b* = 53.3; γ = 97° *A* = 5170 Å² (*Z* = 2); *a*/*b* = 1.83	9260 1.00	3.56 3.58	2 3.58	8 3.58	~0
A = Cl Bulk / 20	Col_r	*a* = 84.2(6); *b* = 62.0(7); γ = 90° *A* = 5230 Å² (*Z* = 2); *a*/*b* = 1.36	9260 1.00	3.55 3.54	2 3.54	8 3.54	~0
A = Cl Bulk / 80	Col_r	*a* = 84.1(4); *b* = 61.8(4); γ = 90° *A* = 5203 Å² (*Z* = 2); *a*/*b* = 1.36	9493 0.98	3.6 3.65	2 3.65	8 3.65	~0
A = BF_4 Film / 20	Col_o	*a* = 98.5; *b* = 57.9; γ = 93° *A* = 5695 Å² (*Z* = 2); *a*/*b* = 1.70	9282 1.01	3.55 3.26	2 3.26	10 4.07	29
A = BF_4 Bulk / 20	Col_r	*a* = 84.1(2); *b* = 61.8; γ = 90° *A* = 5199 Å² (*Z* = 2); *a*/*b* = 1.36	9282 1.01	3.54 3.57	2 3.57	8 3.57	~0
A = BF_4 Bulk / 80	Col_r + Orth	*a* = 83.9(6); *b* = 61.4(9); γ = 90° *A* = 5163 Å² (*Z* = 2); *a*/*b* = 1.36 *a* = 93.4; *b* = 62.4(5); γ = 90° *A* = 5833 Å² (*Z* = 2); *a*/*b* = 1.50 *c* = 48.4(4); *V* = 282500 Å²	9515 0.99 9515 0.99 29.7	3.55 3.69 3.55 3.26	2 3.69 2 3.26 14.8	8 3.69 10 4.08 11.9	16 0 5.5
A = BF_4 Bulk / 120	Orth	*a* = 90.8(8); *b* = 63.3; γ = 90° *A* = 5753 Å² (*Z* = 2); *a*/*b* = 1.44 *c* = 48.3(7); *V* = 278300 Å²	9671 0.97 28.8	3.60 3.36	2 3.36 14.4	10 4.20 11.5	0 6.5
A = $Au(CN)_2$ Film / 20	Col_o	*a* = 96.6; *b* = 55.0; γ = 96° *A* = 5284 Å² (*Z* = 2); *a*/*b* = 1.76	9316 1.00	3.50 3.53	2 3.53	8 3.53	~0
A = $Au(CN)_2$ Bulk / 20	Col_r	*a* = 86.1(5); *b* = 63.2(9) γ = 90° *A* = 5452 Å² (*Z* = 2); *a*/*b* = 1.36	9316 1.04	3.54 3.42	2 3.42	undefin ed	undefined
A = $Au(CN)_2$ Bulk / 80	Col_{r1} + Col_{r2}	*a* = 85.5(5); *b* = 62.9(7); γ = 90° *A* = 5387 Å² (*Z* = 2); *a*/*b* = 1.36 *a* = 89.7(7); *b* = 64.9(6); γ = 90° *A* = 5832 Å² (*Z* = 2); *a*/*b* = 1.38	9550 1.01 9550 1.01	3.57 3.55 3.57 3.27	2 3.55 2 3.27	8 3.55 10 4.09	~0 29
A = $Au(CN)_2$ Bulk / 120	Col_{r2}	*a* = 88.6(8); *b* = 64.9; γ = 90° *A* = 5755 Å² (*Z* = 2); *a*/*b* = 1.37	9706 0.99	3.58 3.37	2 3.37	10 4.22	32
$[Rh(L^{D2})_4](A)$							
A = BF_4 Film / 20	Col_o	*a* = 81.3; *b* = 60.9; γ = 96° *A* = 4930 Å² (Z = 2); *a*/*b* = 1.33	9492 1.01	3.55 3.85	2 3.85	8 3.85	23
A = BF_4 Bulk / 70	Col_o	*a* = 84.7(7); *b* = 69.5(4); γ = 93.5(8)° *A* = 5883 Å² (Z = 2); *a*/*b* = 1.22	9691 0.99	3.60 3.29	2 3.29	10 4.12	29
A = $Au(CN)_2$ Film / 20	Col_o	*a* = 75.1; *b* = 49.6; γ = 96° *A* = 3705 Å² (Z = 2); *a*/*b* = 1.51	9527 1.03	3.56 5.14	2 5.14	6 3.86	22
A = $Au(CN)_2$ Bulk / 80	Col_o	*a* = 83.7(6); *b* = 69.5(2); γ = 93.9(4)° *A* = 5810 Å² (Z = 2); *a*/*b* = 1.21	9767 1.01	3.56 3.36	2 3.36	10 4.20	32

[a]T: temperature of the measurement; [b]Col_o, Col_r, Col_{r1}, Col_{r2}: oblique and rectangular columnar structures; Orth: orthorhombic structure; [c]*a*, *b*, γ, *A* = *a*×*b*×sinγ, *Z*, *a*/*b*: lattice parameters, lattice area, number of molecular elementary motif per lattice and lattice parameter ratio; [d]*c*, *V*: lattice parameter and cell volume of Orth mesophase; [e]V_{mol}, ρ: molecular volume and density; [f]N_{mol}: number of molecules per cell (Orth mesophase); [g]h_π: average distance between stacked triphenylene (TPh) rings from position of scattering maximum in pattern; $h_{mol} = (Z \times V_{mol})/A$: molecular slice thickness; [h]$Z_{col,RhA}$, $h_{RhA} = (Z_{col,RhA}/Z) \times h_{mol}$: number of piles per lattice and molecular slice thicknesses for rhodium complexes and counter-ions (RhA); $N_{RhA,c} = c/h_{RhA}$: number of RhA units per pile and unit cell (Orth phase); [i]$Z_{col,Tph}$, $h_{Tph} = (Z_{col,TPh}/4Z) \times h_{mol}$ number of columns per lattice and molecular slice thicknesses for Tph; $N_{Tph,c} = c/h_{Tph}$: number of Tph units per column and unit cell; [j]$\langle\psi_{Tph}\rangle = \text{acos}(h_\pi/h_{Tph,col})$: mean out of plane tilt angles of piled Tph units; $dh_{Tph,c} = c - N_{Tph,c} \times h_\pi$: interruption zone thickness of segmented Tph columns (Orth phase). ***For the meaning of "RhA units" and "TPh units" see Figure 11.***

Table ESI 5: Table of indexation of mesophases of **Rh(L^{D1})$_4$** and **Rh(L^{D2})$_4$** salt series

q_{exp} (Å^{-1})	d_{exp} (Å)	I [x(Å)]	*hk*	q_{cal} (Å^{-1})	d_{cal} (Å)	Mesophase parameters
Compound **Rh(L^{D1})$_4$Cl** (20°C)						
0.1256	50.03	VS	11	0.1257	49.97	Col_r
0.1490	42.16	S	20	0.1491	42.13	a = 84.2(6) Å
0.2024	31.05	M	02	0.2025	31.04	b = 62.0(7) Å
0.2517	24.96	S	22	0.2515	24.99	A = 5230 Å^2
0.2983	21.06	M	40	0.2983	21.07	(Z = 2)
0.3127	20.09	M	13	0.3127	20.09	
0.3601	17.45	VW	42	0.3605	17.43	
0.3770	16.67	VW	33	0.3772	16.66	
0.3863	16.27	W	51	0.3863	16.26	
0.4051	15.51	W	04	0.4049	15.52	
1.43	4.4	VS [13]	h_{ch}+h_{ion}			
1.769	3.55	W [28]	h_{π}			
Compound **Rh(L^{D1})$_4$Cl** (80°C)						
0.1260	49.87	VS	11	0.1261	49.83	Col_r
0.1493	42.09	S	20	0.1494	42.07	a = 84.1(4) Å
0.2032	30.93	M	02	0.2032	30.92	b = 61.8(4) Å
0.2522	24.91	M	22	0.2522	24.91	A = 5203 Å^2
0.2988	21.03	M	40	0.2987	21.04	(Z = 2)
0.3138	20.02	M	13	0.3138	20.02	
0.3872	16.23	VW	51	0.3870	16.24	
0.4059	15.48	VW	04	0.4064	15.46	
1.40	4.5	VS [12]	h_{ch}+h_{ion}			
1.745	3.60	M [20]	h_{π}			
Compound **Rh(L^{D1})$_4$BF$_4$** (20°C)						
0.1260	49.85	VS	11	0.1262	49.80	Col_r

0.1494	42.07	S	20	0.1494	42.06	a = 84.1(2) Å
0.2033	30.90	M	02	0.2033	30.90	b = 61.8(0) Å
0.2525	24.88	M	22	0.2523	24.90	A = 5199 Å^2
0.2989	21.02	M	40	0.2988	21.03	(Z = 2)
0.3140	20.01	M	13	0.3140	20.01	
0.3872	16.23	VW	51	0.3871	16.23	
0.4059	15.48	VW	04	0.4067	15.45	
1.43	4.4	VS [13]	$h_{ch}+h_{ion}$			
1.776	3.54	M [20]	h_{π}			

q_{exp} (Å^{-1})	d_{exp} (Å)	I [x(Å)]	*hk*	q_{cal} (Å^{-1})	d_{cal} (Å)	Mesophase parameters
Compound **Rh(L^{D1})$_4$BF$_4$** (80^{o}C)						
0.1209	51.95	VS	110	0.1210	51.91	Col_r
0.1269	49.52	VS	11	0.1267	49.61	a = 83.9(6) Å
0.1348	46.63	S	200	0.1345	46.70	b = 61.4(9) Å
0.1497	41.98	S	20	0.1497	41.98	A = 5163 Å^2
0.2012	31.23	M	020	0.2012	31.23	(Z = 2)
0.2040	30.80	M	02	0.2044	30.75	
0.2432	25.84	W	220	0.2421	25.96	Orth
0.2536	24.78	M	22	0.2533	24.80	a = 93.4(0) Å
0.2575	24.40	W	002	0.2594	24.22	b = 62.4(5) Å
0.2692	23.34	M	400	0.2691	23.35	c = 48.4(4) Å
0.2861	21.96	W	112	0.2863	21.95	$A = a \times b$ = 5833 Å^2
0.2943	21.35	W	202	0.2922	21.50	
0.2992	21.00	W	40	0.2993	20.99	(Z = 2)
0.3085	20.36	M	130	0.3092	20.32	V = 282500 Å^3
0.3156	19.91	W	13	0.3155	19.91	
0.3363	18.68	W	420	0.3360	18.70	
0.3505	17.93	W	510	0.3511	17.90	
0.3627	17.32	W	42	0.3625	17.34	
		W	330	0.3631	17.30	
0.3795	16.56	VW	33	0.3800	16.54	
0.3883	16.18	VW	51	0.3879	16.20	
0.4026	15.61	VW	040	0.4024	15.61	
			600	0.4036	15.57	
1.40	4.5	VS [12]	h_{ch}+h_{ion}			
1.768	3.55	W [27]	h_{π}			
q_{exp} (Å^{-1})	d_{exp} (Å)	I [x(Å)]	*hk*	q_{cal} (Å^{-1})	d_{cal} (Å)	Mesophase parameters

Compound **Rh(L^{D1})$_4$BF$_4$** (120°C)						
0.1211	51.90	VS	110	0.1210	51.94	Orth
0.1379	45.57	S	200	0.1383	45.44	a = 90.8(8) Å
0.1980	31.73	VW	020	0.1985	31.65	b = 63.3(0) Å
0.2303	27.28	VW	310	0.2299	27.33	c = 48.3(7) Å
0.2423	25.93	W	220	0.2419	25.97	$A = a \times b$ = 5753 Å^2
0.2596	24.21	M	002	0.2598	24.18	
0.2766	22.72	M	400	0.2765	22.72	(Z = 2)
0.2877	21.84	VW	112	0.2866	21.92	V = 278300 Å^3
0.2946	21.32	W	202	0.2943	21.35	
0.3059	20.54	M	130	0.3057	20.55	
0.3404	18.46	VW	420	0.3404	18.46	
0.3608	17.41	W	510	0.3597	17.47	
			330	0.3629	17.31	
1.39	4.5	VS [12]	$h_{ch}+h_{ion}$			
1.745	3.60	W [28]	h_{π}			
Compound **Rh(L^{D1})$_4$Au(CN)$_2$** (20°C)						
0.1229	51.12	VS	11	0.1232	51.01	Col_{r1}
0.1457	43.13	S	20	0.1459	43.08	a = 86.1(5) Å
0.1985	31.65	M	02	0.1986	31.65	b = 63.2(9) Å
0.2464	25.50	S	22	0.2464	25.50	A = 5452 Å^2
0.2919	21.53	M	40	0.2917	21.54	(Z = 2)
0.3067	20.49	M	13	0.3066	20.49	
0.3705	16.96	VW	33	0.3696	17.00	
0.3771	16.66	VW	51	0.3779	16.62	
0.3974	15.81	VW	04	0.3971	15.82	
0.4704	13.36	VW	53	0.4708	13.34	
1.43	4.4	VS [13]	$h_{ch}+h_{ion}$			
1.775	3.54	W [25]	h_{π}			

q_{exp} (Å^{-1})	d_{exp} (Å)	I [x(Å)]	*hk*	q_{cal} (Å^{-1})	d_{cal} (Å)	Mesophase parameters
Compound **Rh(L^{D2})$_4$BF$_4$** (70°C)						
0.1138	55.23	VS	$1\bar{1}$	0.1135	55.38	Col_o
0.1206	52.11	S	11	0.1206	52.09	a = 84.7(7) Å
0.1480	42.45	M	20	0.1485	42.30	b = 69.5(4) Å
0.1803	34.86	M	02	0.1811	34.70	g = 93.5(8)°
0.2276	27.61	W	$2\bar{2}$	0.2269	27.69	A = 5883 Å^2
0.2431	25.85	S	22	0.2413	26.04	(Z = 2)
			31	0.2457	25.57	
0.2769	22.69	M	$1\bar{3}$	0.2771	22.68	
0.2980	21.08	W	40	0.2971	21.15	
0.3404	18.46	W	$3\bar{3}$	0.3404	18.46	
0.3612	17.40	VW	33	0.3619	17.36	
			04	0.3621	17.35	
0.3897	16.12	VW	51	0.3877	16.21	
			60	0.4456	14.10	
0.4473	14.05	VW	$5\bar{3}$	0.4462	14.08	
1.40	4.5	VS [12]	h_{ch}			
1.508	4.17	M [150]	h_{ion}			
1.743	3.60	W [50]	h_{π}			

q_{exp} (Å^{-1})	d_{exp} (Å)	I [x(Å)]	*hk*	q_{cal} (Å^{-1})	d_{cal} (Å)	Mesophase parameters
Compound **Rh(L^{D2})$_4$Au(CN)$_2$** (80°C)						
0.1136	55.31	VS	$1\bar{1}$	0.1137	55.27	Col_o
0.1228	51.18	S	11	0.1216	51.65	a = 83.7(6) Å
0.1502	41.83	M	20	0.1504	41.78	b = 69.5(2) Å
0.1808	34.76	M	02	0.1812	34.68	g = 93.9(4)°
0.2279	27.57	W	$2\bar{2}$	0.2274	27.63	A = 5810 Å^2
			22	0.2433	25.83	(Z = 2)
0.2472	25.42	S	31	0.2488	25.25	
0.2763	22.74	M	$1\bar{3}$	0.2769	22.69	
0.3022	20.79	W	40	0.3008	20.89	
			$4\bar{2}$	0.3403	18.46	
0.3414	18.41	W	$3\bar{3}$	0.3411	18.42	
			42	0.3616	17.37	
0.3626	17.33	VW	04	0.3624	17.34	
0.4541	13.84	VW	$1\bar{5}$	0.4540	13.84	
			$4\bar{4}$	0.4547	13.82	
0.4874	12.89	VW	44	0.4866	12.91	
1.39	4.5	VS [11]	h_{ch}			
1.499	4.19	M [150]	h_{ion}			
1.765	3.56	W [45]	h_π			

q_{exp}, d_{exp}, q_{cal}, d_{cal}: experimental and calculated scattering vectors and d-spacings from peak position; x (Å): correlation length from peak width using Scherrer equation with shape factor K = 0.9 (no indication: long-range periodicity from sharp reflection); I: intensity of reflection, signal intensity code: VS = very strong, S = strong, M = medium, W = weak, VW = very weak; (*hk*) are the Miller indices of the reflections; h_{ch} (Å): average lateral distances between molten chains; h_{ion} (Å): local-range periodicity of the ionic arrangement; h_p (Å): average piling distance along triphenylene columns; Col_r, Col_{r1}, Col_{r2}: rectangular columnar mesophases; Col_h; hexagonal columnar mesophase; Orth: orthorhombic mesophase; *a*, *b*, *A*, *Z*: columnar lattice parameters, lattice area and number of molecular stacks per lattice; *c*, *V*: lattice parameter in the direction of molecular piling and cell volume.

Small and wide-angle X-ray scattering (SAXS/WAXS) patterns of the complexes

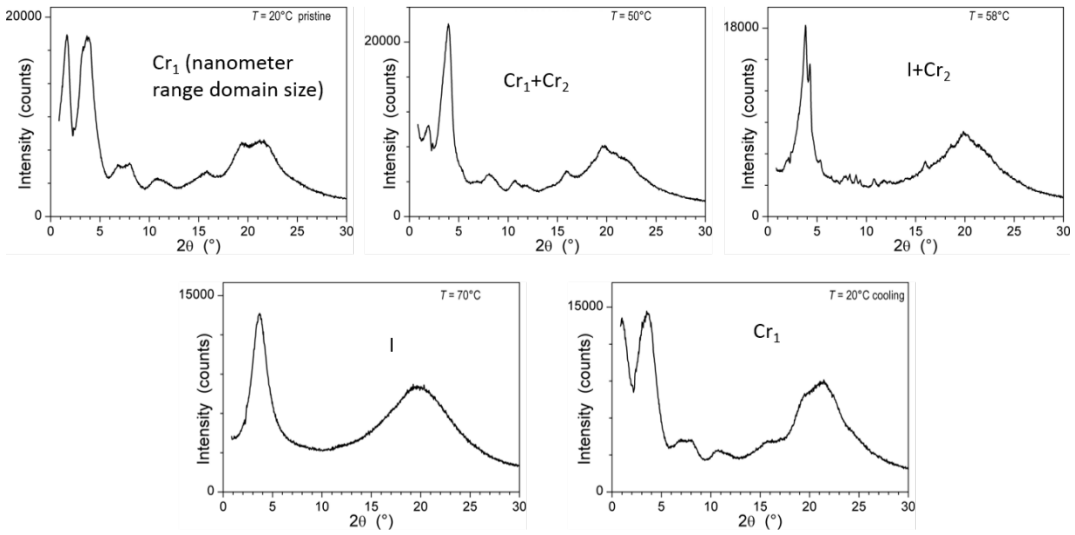

Figures ESI42. SAXS/WAXS patterns of ligand L^{D2}, at various temperatures, showing the co-existence of poorly developed crystalline phases.

Figures ESI43. Small- and wide-angle X-ray scattering (SAXS/WAXS) patterns (bottom and top graphs, respectively) of the pristine solid states (T = 20°C) of [Rh(**L**^{D1})$_4$]Cl, [Rh(**L**^{D1})$_4$]BF_4, [Rh(**L**^{D1})$_4$][Au(CN)$_2$], [Rh(**L**^{D2})$_4$]BF_4 and [Rh(**L**^{D2})$_4$][Au(CN)$_2$] (from left-to-right and top-to-bottom).

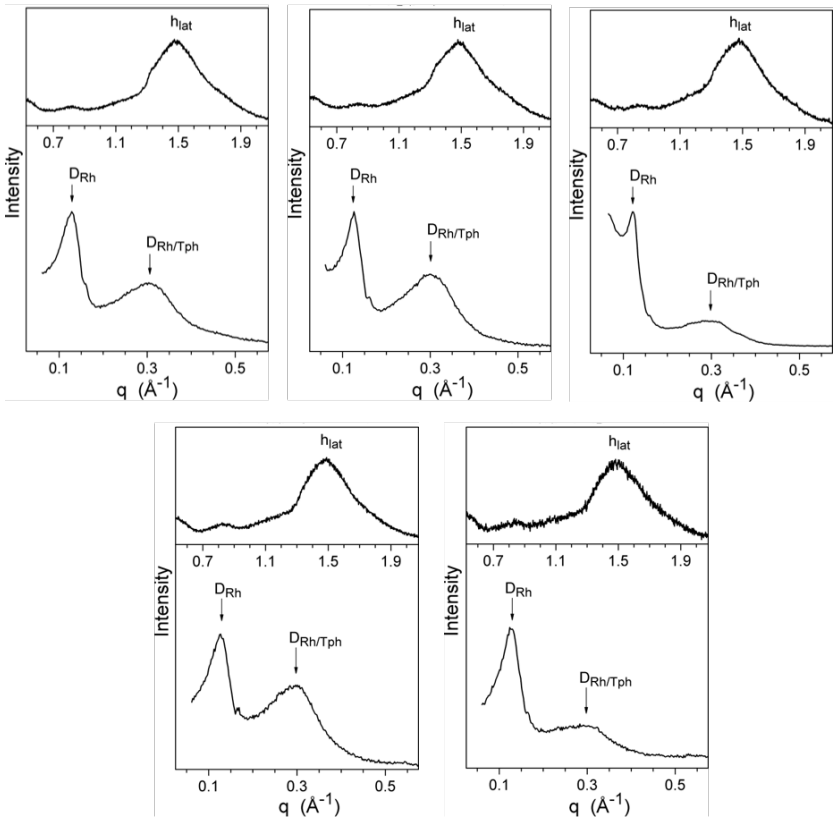

The compounds self-organize into multisegregated structures with self-assembled organometallic cores distinct from piled triphenylene mesogens and nanosegregated from alkyl tails and linkers. As shown by the presence of only broad signals, the structure is initially only defined at the local range, between few neighboring molecules. Furthermore, the scattering signature of triphenylene stacking h_π (expected at ca. 3.5 Å) is not separable from scattering contributions of other molecular segments h_{lat}, which indicates a rather irregular piling. The formation of the superlattice of intermingled domains is however demonstrated by two intense signals appearing in the small-angle region: a broad peak $D_{Rh/Tph}$, from the average spacing of triphenylenes or organometallic domains separated by chains, and a peak D_{Rh} from the average spacing of Rh complex domains.

Figures ESI44. SAXS/WAXS patterns on first heating in pre-developed mesophases of [Rh($\mathbf{L^{D1}}$)$_4$]Cl (T = 65°C), [Rh($\mathbf{L^{D1}}$)$_4$]BF$_4$ (T = 80°C), [Rh($\mathbf{L^{D1}}$)$_4$][Au(CN)$_2$] (T = 80°C), [Rh($\mathbf{L^{D2}}$)$_4$]BF$_4$ (T = 70°C) and [Rh($\mathbf{L^{D2}}$)$_4$][Au(CN)$_2$] (T = 80°C) (from left-to-right and top-to-bottom). With the fluidization, samples rearrange into mesomorphic structures, as revealed by the appearance of distinct scattering signals for the stacking of Tph (h_π) and for the packing of chains and ionic moieties (h_{ch}, h_{ion}), and by the structuration of the two small-angle scattering signals into reflections series of the superlattice arrangement. The structuration process of Rh($\mathbf{L^{D1}}$)$_4$A compounds was not finished at the temperature of patterns and required further heating to 120°C, contrarily to Rh($\mathbf{L^{D2}}$)$_4$A compounds already displaying a small-angle region resolved into sharp reflections.

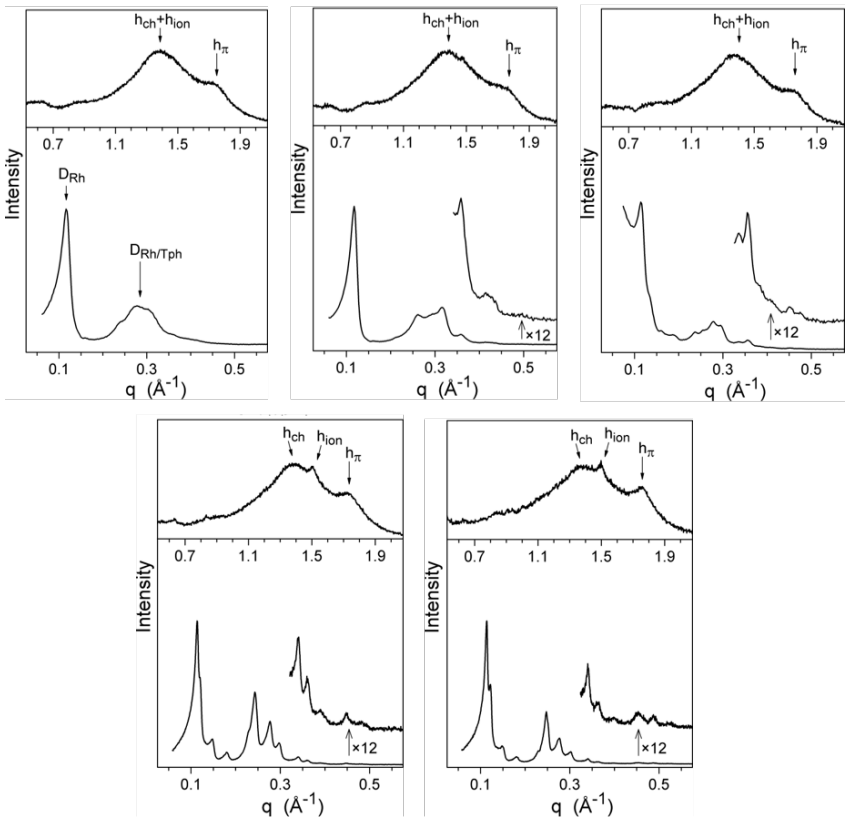

Figures ESI45. SAXS/WAXS patterns of the room temperature states (T = 20°C) obtained after pre-heating in the fluid mesophases (**Figures ESI44**) and cooling of [Rh($\mathbf{L^{D1}}$)$_4$]Cl, [Rh($\mathbf{L^{D1}}$)$_4$]BF$_4$, [Rh($\mathbf{L^{D1}}$)$_4$][Au(CN)$_2$], [Rh($\mathbf{L^{D2}}$)$_4$]BF$_4$ and [Rh($\mathbf{L^{D2}}$)$_4$][Au(CN)$_2$] (from left-to-right and top-to-bottom). The three Rh($\mathbf{L^{D1}}$)$_4$A compounds display a frozen columnar mesophase **Col$_r$**, characterized by sharp reflection series of a large-size two-dimensional rectangular *c*2*mm* lattice and by the scattering signals from π-stacking h_π and molten chain packing h_{ch}. In addition, Rh($\mathbf{L^{D1}}$)$_4$BF$_4$ presents a broad small-angle peak D coming from a local range periodicity and Rh($\mathbf{L^{D1}}$)$_4$Au(CN)$_4$, a small-angle scattering upturn due to structural disorder. Rh($\mathbf{L^{D2}}$)$_4$A compounds on the contrary lose the long-range order on cooling

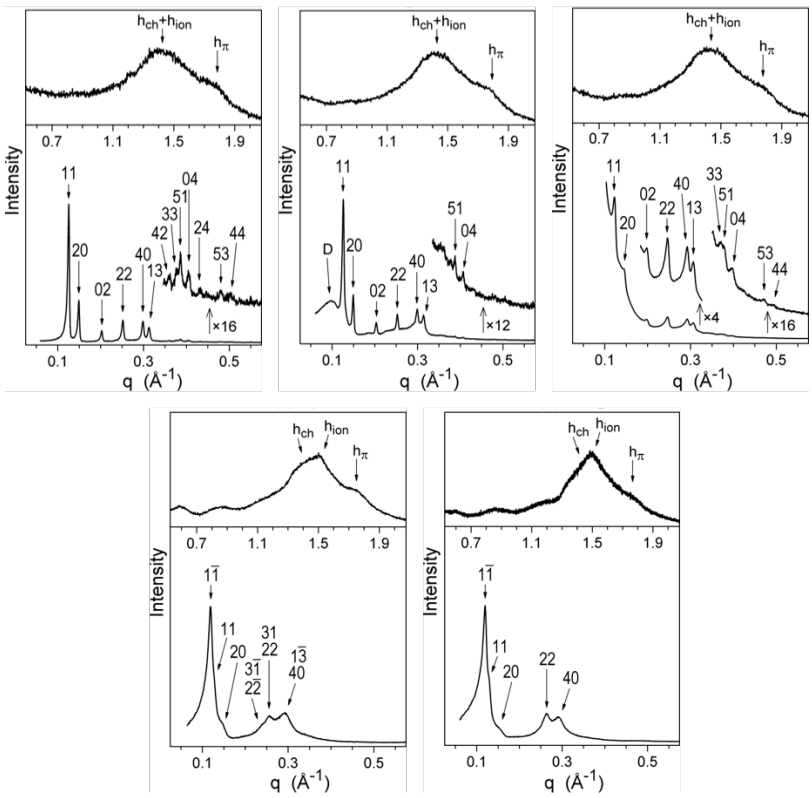

and give amorphous-like states keeping a residual columnar structure (Amo_{Col}) correlated over few molecules, as revealed by the broadened reflections in the small-angle region and by wide-angle scattering maximums.

Figures ESI46. GIWAXS patterns of thin films annealed at 75°C [Rh(L^{D1})$_4$Cl], 120°C [Rh(L^{D1})$_4$BF$_4$], 120°C [Rh(L^{D1})$_4$][Au(CN)$_2$], 70°C [Rh(L^{D2})$_4$BF$_4$] and 80°C [Rh(L^{D2})$_4$][Au(CN)$_2$] (from top-to-bottom); inset of expanded small-angle region with indexation labels on the left side of spots. All films display well-oriented columnar mesomorphic organizations, with [10] or [11] crystallographic direction aligned onto the film normal. Rh(**L^{D1}**)$_4$A films give large superlattices developed to long-range as in the bulk state, but the symmetry is lowered to oblique (**Col_o**). Bulk and film states of Rh(**L^{D2}**)$_4$A compounds display oblique superlattices (**Col_o**), but the detailed arrangements are different.

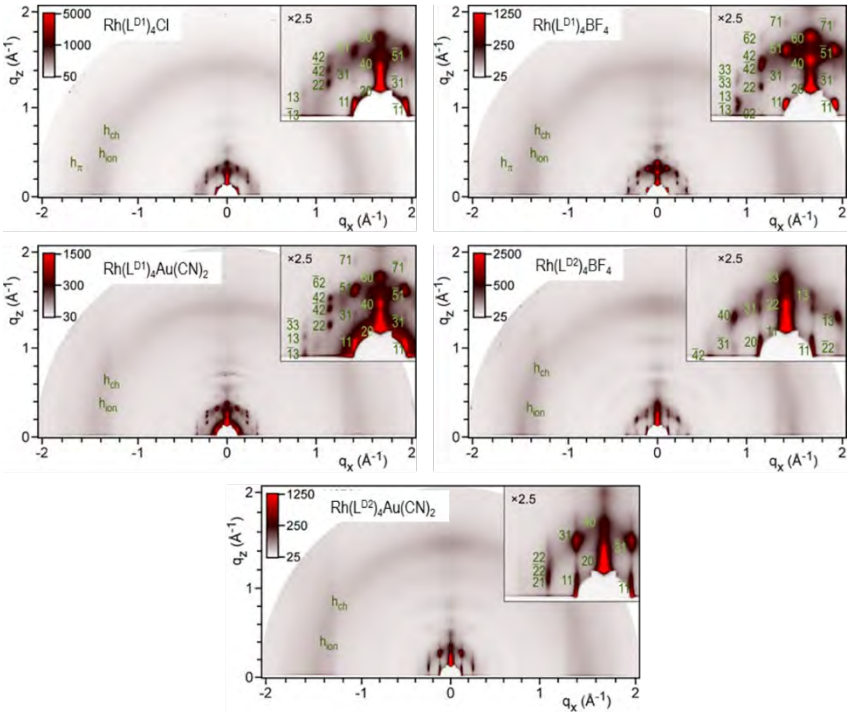

Figures ESI47. SAXS/WAXS patterns recorded in the isotropic liquid (T = 120°C) of [Rh(L^{D1})$_4$]Cl, [Rh(L^{D2})$_4$]BF$_4$ and [Rh(L^{D2})$_4$][Au(CN)$_2$] (from left-to-right), revealing the segregation of the different parts and the reminiscence of molecular clusters, meaning that the columnar superlattice-like organization is maintained at the local range between neighboring molecules.With the erasure of any regular structure, the wide-angle region has merged to unique maximum overlapping of all lateral distances between molecular segments. Simultaneously, the D_{Rh} and $D_{Rh/Tph}$ scattering peaks from pristine solid states reappear in the small-angle region, meaning that a columnar superlattice-like organization is maintained at the local range between neighboring molecules.

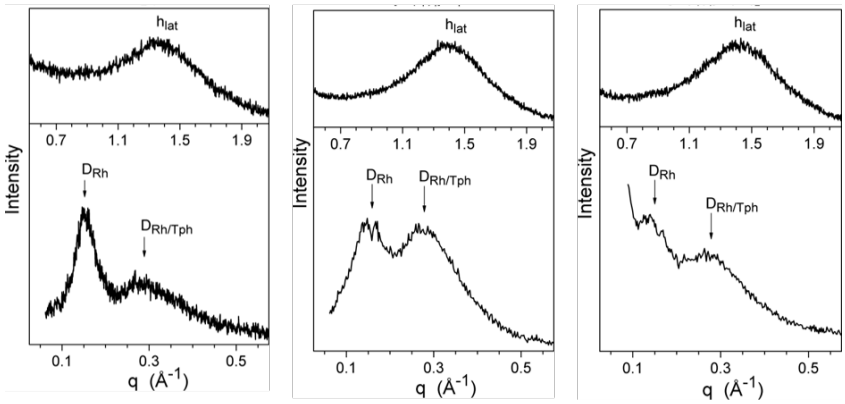

POLARIZED OPTICAL MICROSCOPY (POM)

(**10**) 1st cooling at 100 ˚C

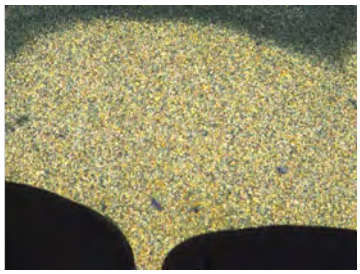

(**10**) 2nd cooling at 90 ˚C

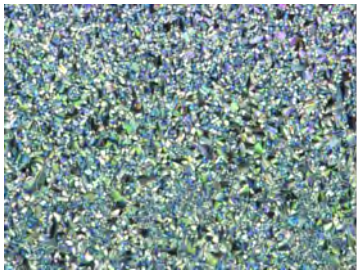

(**14**) 2nd cooling at 160 ˚C

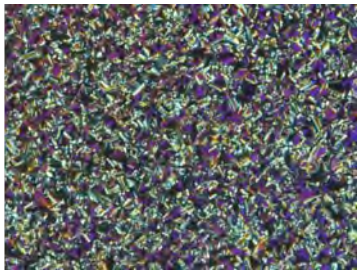

(**14**) 2nd cooling at 85 ˚C

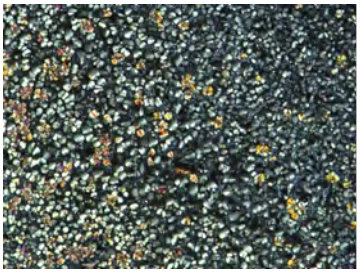

(**19**) 1st cooling at 120 ˚C

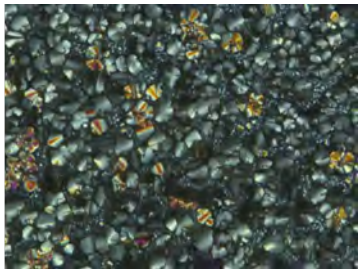

zoom

Figures ESI48. POM Microphotographs of **$[Rh(L^{D1})^4]A$ (A = Cl^- (10), BF_4^- (14), $[Au(CN)_2]^-$ (19))** complexes on cooling process at different temperatures.

$\mathbf{L^{D2}}$ 1st cooling at 35 ˚C

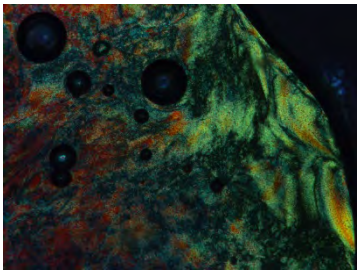

(**15**) 1st heating at 76 ˚C

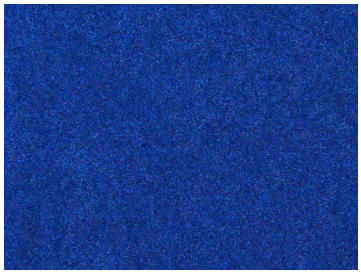

2nd cooling at 56 ˚C

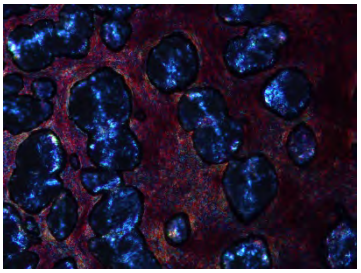

(**20**) 1st heating at 80 ˚C

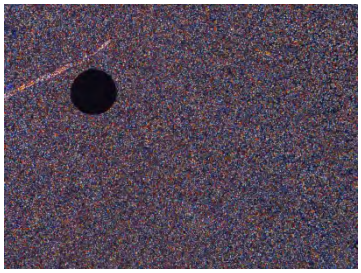

1st cooling at 95 ˚C

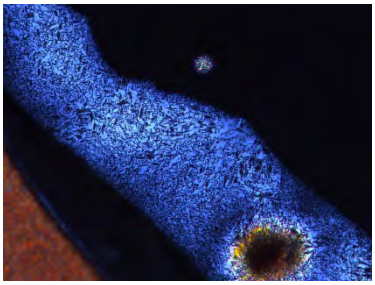

(**20**) 1st cooling at 92 ˚C

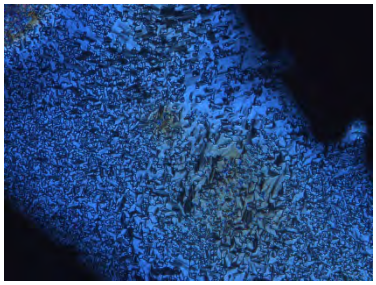

zoom 1st cooling at 30 ˚C

Figures ESI49. POM Microphotographs of **[Rh($\mathbf{L^{D2}}$)$_4$](A)** complexes (A = BF_4^- (**15**), $[Au(CN)_2]^-$ (**20**)) on cooling and heating process at different temperatures.

DIFFERENTIAL SCANNING CALORIMETRY (DSC)

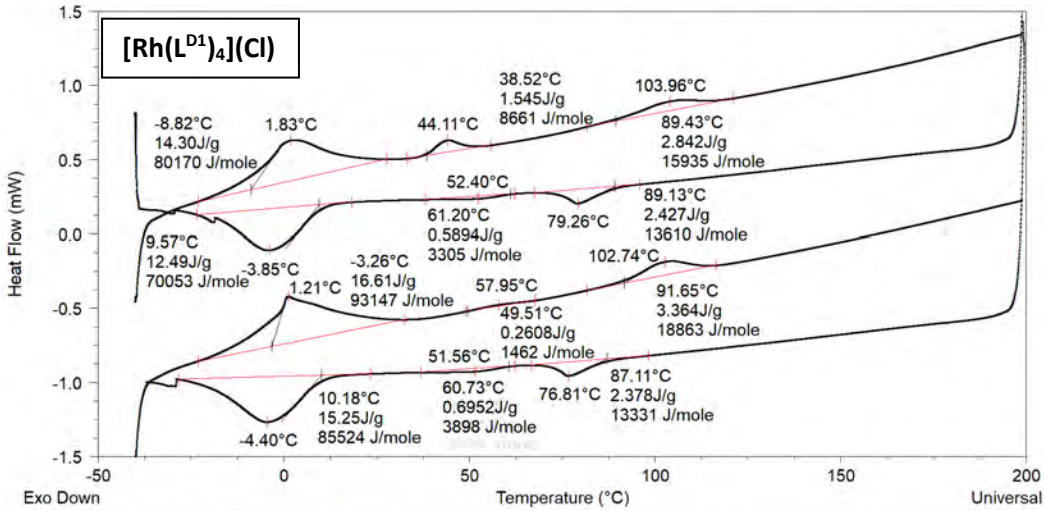

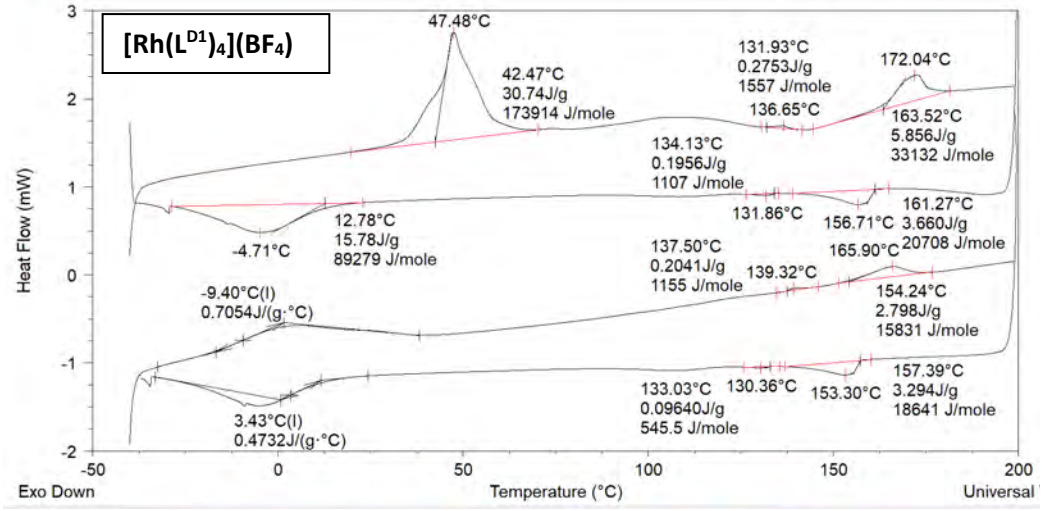

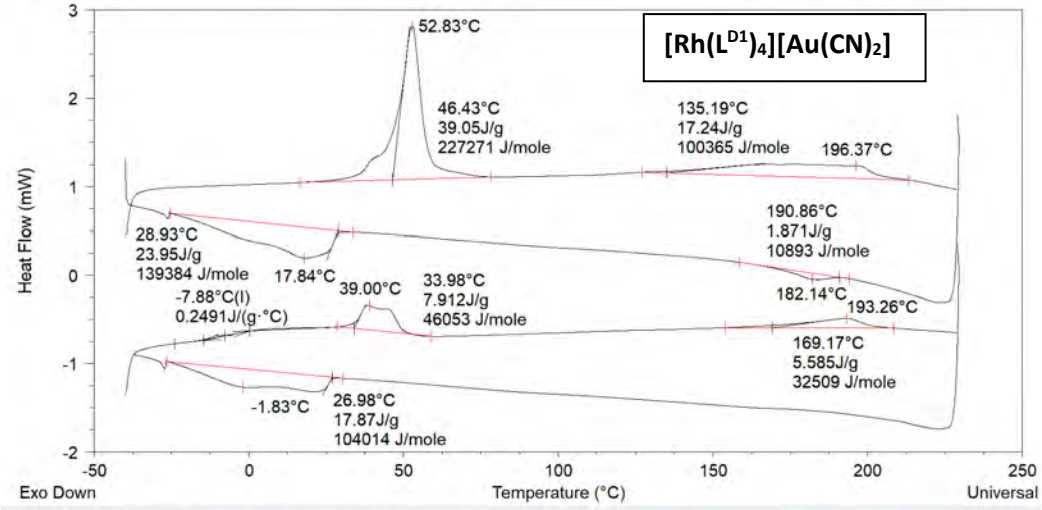

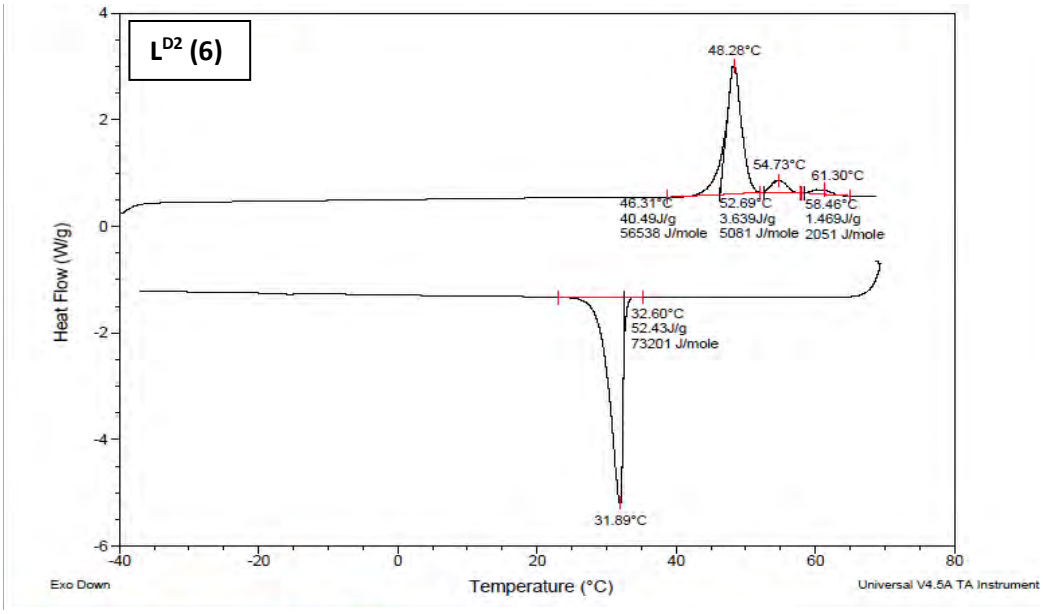
L^D2 (6)
48.28°C
54.73°C
61.30°C
46.31°C
40.49J/g
56538 J/mole
52.69°C
3.639J/g
5081 J/mole
58.46°C
1.469J/g
2051 J/mole
32.60°C
52.43J/g
73201 J/mole
31.89°C
Heat Flow (W/g)
Temperature (°C)
Exo Down
Universal V4.5A TA Instrument

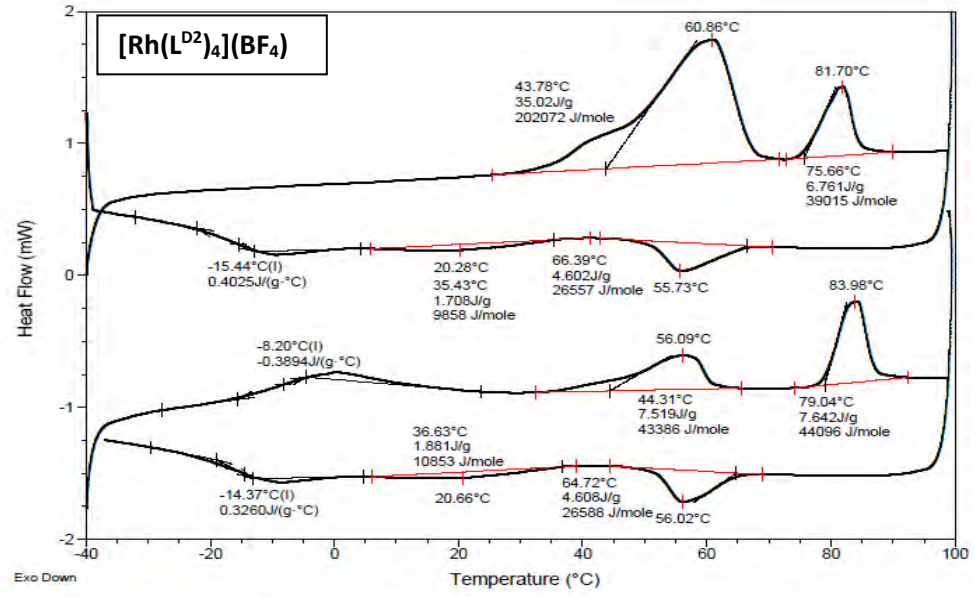
[Rh(L^D2)4](BF4)
60.86°C
43.78°C
35.02J/g
202072 J/mole
81.70°C
75.66°C
6.761J/g
39015 J/mole
-15.44°C(I)
0.4025J/(g·°C)
20.28°C
35.43°C
1.708J/g
9858 J/mole
66.39°C
4.602J/g
26557 J/mole
55.73°C
83.98°C
-8.20°C(I)
-0.3894J/(g·°C)
56.09°C
44.31°C
7.519J/g
43386 J/mole
79.04°C
7.642J/g
44096 J/mole
36.63°C
1.881J/g
10853 J/mole
-14.37°C(I)
0.3260J/(g·°C)
20.66°C
64.72°C
4.608J/g
26588 J/mole
56.02°C
Heat Flow (mW)
Temperature (°C)
Exo Down

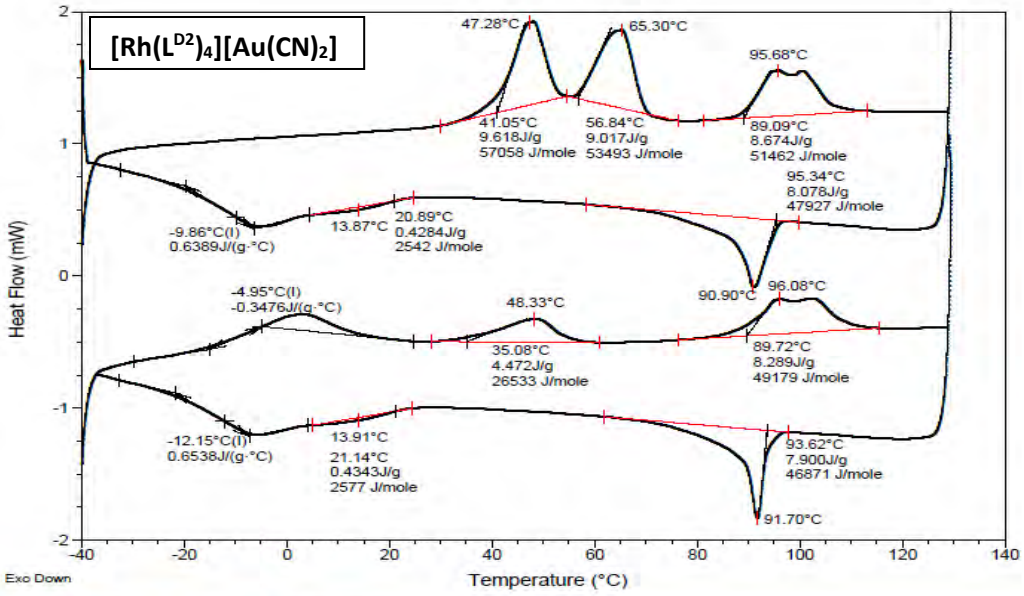

Figure ESI50. DSC thermograms (10 °C/min, endotherm up) of $[Rh(L^{D1})_4]Cl$ (**10**), $[Rh(L^{D1})_4]BF_4$ (**14**), $[Rh(L^{D1})_4][Au(CN)_2]$ (**19**), $[Rh(L^{D2})_4]BF_4$ (**15**), $[Rh(L^{D2})_4][Au(CN)_2]$ (**20**) (from top-to-bottom).

ELECTROCHEMICAL STUDIES

Cyclic Voltamograms

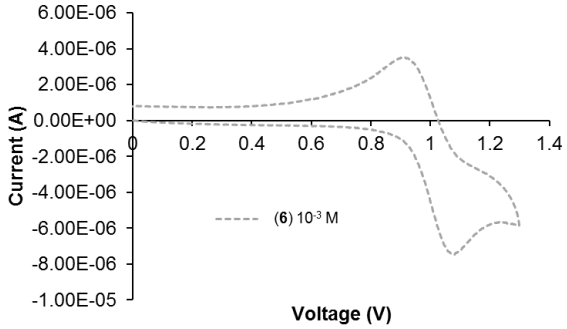

Figure ESI51. Cyclic voltamogram of **6, L^{D2} (10^{-3} M).**

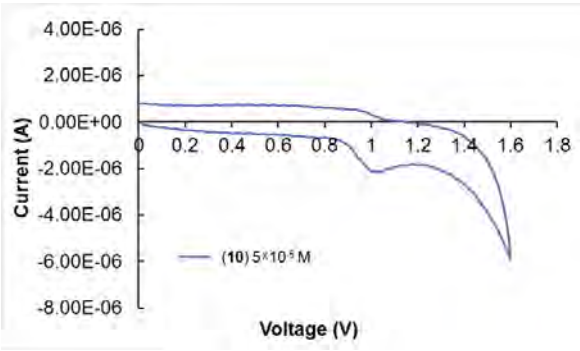

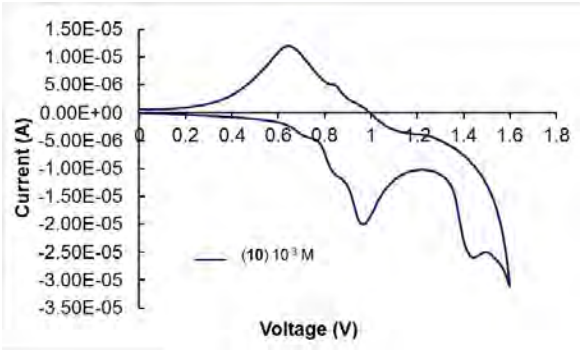

Figure ESI52. Cyclic voltamogram of **10 (5×10^{-5} M).** **Figure ESI53**. Cyclic voltamogram of **10 (10^{-3} M).**

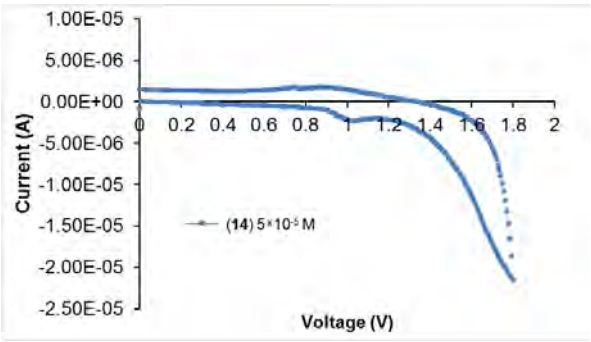

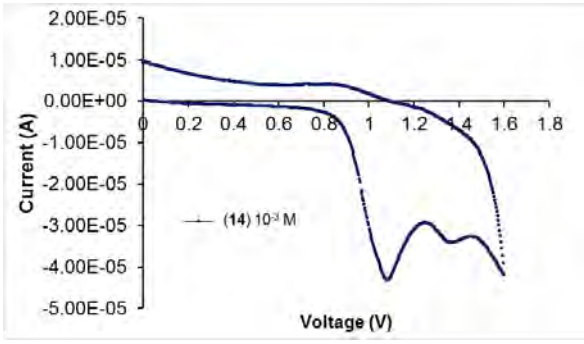

Figure ESI54. Cyclic voltamogram of **14 (5×10^{-5} M).** **Figure ESI55**. Cyclic voltamogram of **14 (10^{-3} M).**

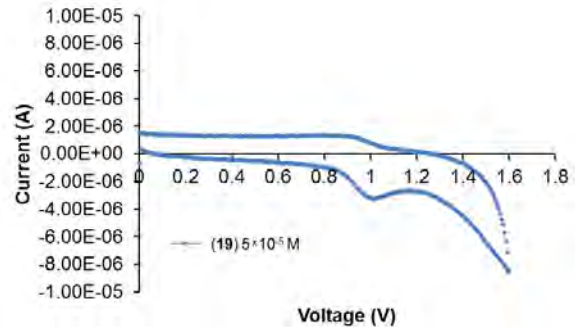

Fig. ESI56. Cyclic voltamogram of **19 (5 x10^{-5} M).**

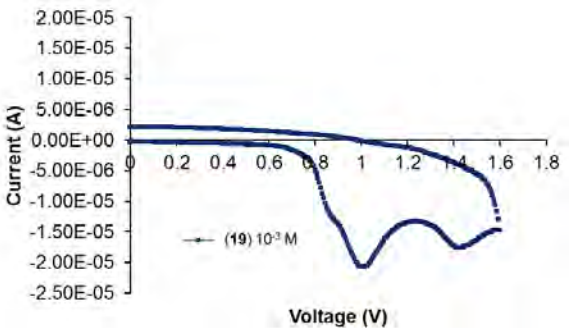

Fig. ESI57. Cyclic voltamogram of **19 (10^{-3} M).**

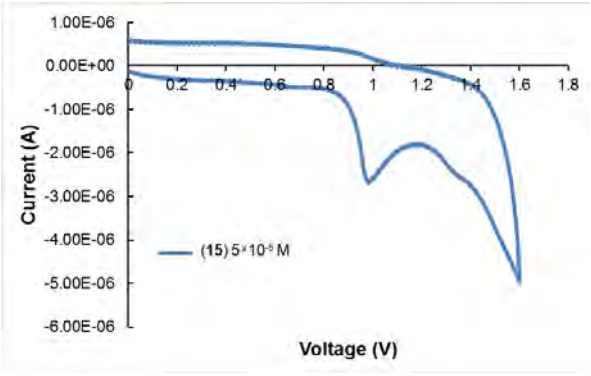

Fig. ESI58. Cyclic voltamogram of **15 (5 x10^{-5} M).**

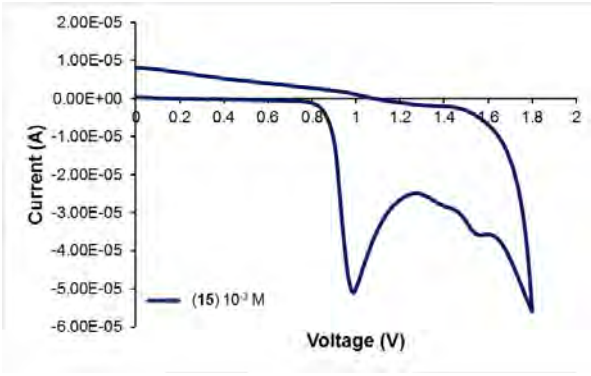

Fig. SI59. Cyclic voltamogram of **15 (10^{-3} M).**

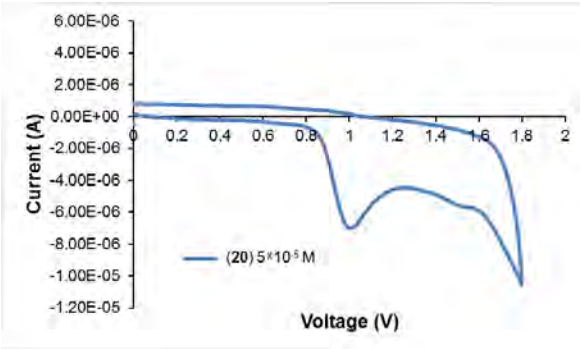

Fig. ESI60. Cyclic voltamogram of **20 (5 x10^{-5} M).**

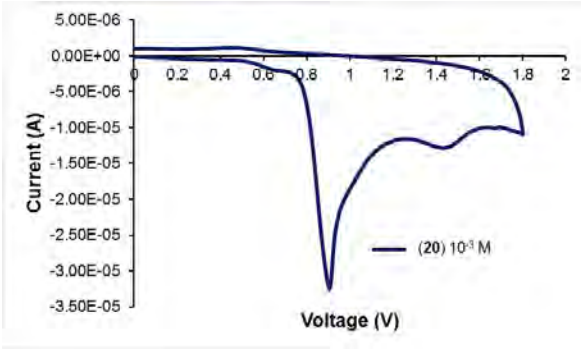

Fig. ESI61. Cyclic voltamogram of **20 (10^{-3} M).**

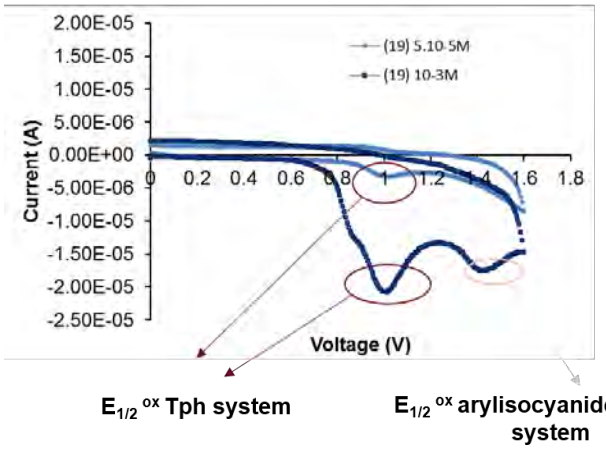

Figure ESI62. Cyclic voltammograms of **19** at different molarities.

Table ESI6. Electrochemical Parameters (HOMO and LUMO Energy Levels)

Compound	$E_{1/2}^{ox}$/V[a]	E_{HOMO}/eV[b]	E_{LUMO}/eV[c]	Optical gap E_g/eV[d]
$[Rh(L^{D1})_4]A$				
L^{D1}	0.99*	-5.33	-1.97	3.36
10 **$[Rh(L^{D1})_4](Cl)$**	0.91 1.60	-5.26[e] -5.95[f]	-1.67 -3.25[g] -4.12[h]	3.59 2.7 1.83 (λ_{onset} = 680 nm)
14 **$[Rh(L^{D1})_4](BF_4)$**	1.05 1.35	-5.40[e] -5.70[f]	-1.82 -3.01[g] -3.87[h]	3.58 2.69 1.83 (λ_{onset} = 680nm)
19 **$[Rh(L^{D1})_4][Au(CN)_2]$**	0.98 1.42	-5.33[e] -5.77[f]	-1.75 -3.08[g] -3.94[h]	3.58 2.69 1.83 (λ_{onset} = 680nm)
$[Rh(L^{D2})_4]A$				
6 **L^{D2}**	1.08	-5.42	-1.83	3.59
15 **$[Rh(L^{D2})_4](BF_4)$**	0.89 1.27	-5.24[e] -5.92[f]	-1.68 -3.22[g] -3.44[h]	3.56 2.7 2.48 (λ_{onset} = 500 nm)
20 **$[Rh(L^{D2})_4][Au(CN)_2]$**	1.01 1.44	-5.36[e] -5.79[f]	-1.79 -3.08[g] -3.31[h]	3.57 2.71 2.48 (λ_{onset} = 500 nm)

[a] V vs calomel electrode with a platinum working electrode in dichloromethane. [b] E_{HOMO} (eV) = $-[E_{1/2}^{ox}(V) - E_{1/2}^{ox}$ fc(V)] − 4.8 (eV) ($E^{1/2}_{ox}$ Fc is the averaged oxidation potential of the system ferrocene/ferrocenium (Fc) versus the calomel electrode).[11] [c] LUMO (eV) potentials were calculated from the optical gaps observed in the absorption spectra and the HOMO potentials obtained with CV. [d] Optical gap calculated from E_g = 1242/λonset, where λonset is the onset of the band of the absorption spectra that appears at highest wavelength. [e] E_{HOMO} (eV) calculated from the irreversible oxidation potential peak for the triphenylene group.[12] [f] E_{HOMO} (eV) calculated from the irreversible oxidation potential peak for the arylisocyanide-Rh^I · Rh^I system. [g] E_{LUMO} obtained directly from the onset of the band of the absorption spectra that appears at highest wavelength at 10^{-5} M for the arylisocyanide-Rh^I · Rh^I system. [h] E_{LUMO} (eV) calculated for a value of λonset (theoretical value) corresponding to the green and red colors observed for the compounds. * Reversible process.

HOLE MOBILITY MEASUREMENTS (SCLC Measurements)

The Space-Charge Limited Current (SCLC) method was used to measure the charge mobility of complexes **10**, **14**, **19**, **15** and **20**. The SCLC technique consists in measuring the electric current that flows through a sample placed between two electrodes as a function of the applied voltage. When applying low voltages, the current follows Ohm's law, while when applying higher voltages it can be limited by a space charge field so that the voltage dependence will no longer be linear, but will become quadratic. In this case, neglecting the effect of the traps, the dependence of the current on the voltage will be described by the Mott-Gurney law:

$$i = \frac{9}{8}\varepsilon_r\varepsilon_0\mu\frac{A\,V^2}{d^3} \qquad (1)$$

where i is the current, ε_r is the relative dielectric constant of the material, ε_0 is the permittivity of free space, μ is the mobility of charges, V is the applied voltage, A is the area and d is the thickness of the device.

A typical example of J /V curve for complex **15** is shown in Figure SI63

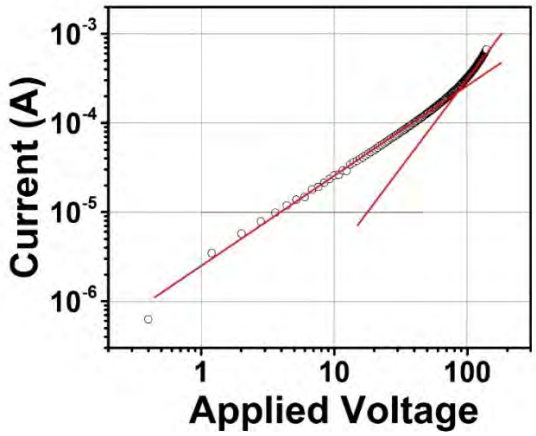

Figure ESI63. Current as function of the applied voltage for a sample of complex **15**. The red lines represent ideal linear and quadratic dependences.

Mobility values can be calculated starting from equation (1) only if the electrode that injects the charges forms an ohmic contact with the compound, in such a way as to act as an infinite reserve of charges. Usually, in order to obtain an ohmic contact, in the case of p-conductors, the difference between the energy of the HOMO level of the material (LUMO in the case of n-conductors) and the work function of the electrode must not be larger than 0.3-0.4 eV. In the case of the complexes measured we have used gold electrodes, which allowed to measure the mobility despite the difference in energy between the HOMO of the complexes and the work function of the electrode is a little higher than the values above mentioned.

Samples were prepared by superimposing one glass with three 1.2 mm wide gold electrodes with another glass with five 0.5 mm wide ITO electrodes, obtaining 15 independent overlapping areas. Gold electrodes were prepared by thermal deposition on glasses at a base pressure of 10^{-6} mbar, while ITO electrodes are prepared by photolithography, starting from commercial fully covered ITO glasses (VisionTek 12 Ω/sq). The gold electrodes are labelled with letters (a, b, c) while the ITO ones with numbers (from 1 to 5). The substrates were glued together with an epoxy glue, controlling the thickness by 5 μm glass spacers. The thickness actually obtained was measured by interferometry and varied between 8 μm and 10 μm. In figure SI64 the geometry the resulting cells is schematically illustrated.

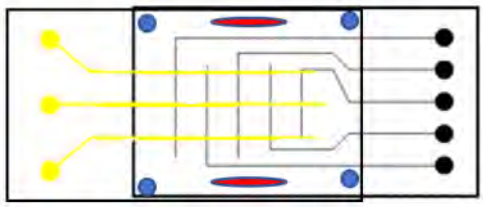

Figure ESI64. Illustration of a typical cell used for SCLC measurements. The yellow lines represent gold electrodes, the gray ones the ITO electrodes, blue circles are spacers, while with red the epoxy glue is indicated.

The cells thus obtained were then filled by capillarity with the complexes to be analyzed in the isotropic phase. Afterwards, samples were subjected to a thermal treatment to induce the formation of homogeneously oriented domains: first the samples were heated to the isotropic phase, then they were cooled to a temperature 0.5 °C higher than the transition from isotropic to liquid crystal, keeping this temperature for 5 hours; the temperature was then decreased by 0.2 °C, keeping the new temperature for another 5 hours. The cycle of lowering by 0.2 °C and maintaining the temperature for 5 hours was repeated several times, until a temperature of 3°C lower than the isotropic - liquid crystal transition was reached. At that point the samples were cooled down to room temperature at 0.05 °C/min. The J/V curves were obtained by using either a Keithley 2636B, or a Keithley 6517A source meter. The dielectric constant of the different complexes was derived from capacity measurements performed on an HP 4284A Precision LCR Meter.

---

[1] D. Perrin. D.; Armarego, W. l. F. *Purification of Laboratory Chemicals*, 3rd ed., Pergamon Press, Oxford, UK, **1988**.

[2] G. Giordano, G.; Crabtree, R. H; Heintz, R. M.; Forster, D.; Morris, D. E. Di-μ-Chloro-Bis(η4-1,5-Cyclooctadiene)-Dirhodium(I). *Inorg. Synth*., 1990, **28**, 88–90.

[3] Schenck, T. G.; Downes, J. M.; Milne, C. R. C.; Mackenzie, P. B.; Boucher, H.; Whelan, J.; Bosnich, B. Bimetallic reactivity. Synthesis of bimetallic complexes containing a bis(phosphino)pyrazole ligand. *Inorg. Chem*., **1985**, *24*, 2334–2337.

[4] Ugi, I.; Meyr, R. Isonitrile, I. Darstellung von Isonitrilen aus monosubstituierten Formamiden durch Wasserabspaltung. *Chem. Ver.*, **1960**, *93*, 239-248. b) Weber, W. P.; Gowel, G. W.; Ugi, I. Phase Transfer Catalysis in the Hofmann Carbylamine Reaction. *Angew. Chem., Int. Ed. Engl.*, **1972**, *11*, 530-531.

[5] Tritto, E.; Chico, R.; Ortega, J.; Folcia, C. L. Folcia, Etxebarria, J.; Coco, S.; Espinet, P. Synergistic π–π and Pt–Pt interactions in luminescent hybrid inorganic/organic dual columnar liquid crystals. *J. Mater. Chem. C.*, **2015**, *3*, 9385–9392.

[6] CrysAlisPro Software system, version 1.171.33.51, **2009**, Oxford Diffraction Ltd, Oxford, UK.

[7] Dolomanov, O. V.; Bourhis, L. J.; Gildea, R. J.; Howard, J. A. K.; Puschmann, H. OLEX2: a complete structure solution, refinement and analysis program. *J. Appl. Cryst.* **2009**, *42*, 339–341.

[8] Bourhis, L. J.; Dolomanov, O. V.; Gildea, R. J.; Howard, J. A. K.; Puschmann, H. The anatomy of a comprehensive constrained, restrained refinement program for the modern computing environment–Olex2 dissected. *Acta Cryst.* **2015**, *A71*, 59–75.

[9] Sheldrick, G. M. Crystal structure refinement with SHELXL. *Acta Cryst.* **2015**, *C71*, 3–8.

[10] Q. Liu, M. Xie, X. Chang, Q. Gao, Y. Chen and W. Lu, *Chem. Commun.*, 2018, **54**, 12844

[11] (a) Ahmida, M. M.; Eichhorn, S. H. Measurements and predic-tion of electronic properties of discotic triphenylenes and phthalo-cyanines. *ECTS Trans*., **2010**, *25*, 1−10; (b) Mahoney, S. J.; Ahmida, M. M.; Kayal, H.; Fox N.; Shimizucand, Y.; Eichhor, S. H.; Synthesis, mesomorphism and electronic properties of nonaflate and cyano-substituted pentyloxy and 3-methylbutyloxy triphenylenes. *J. Mater. Chem.*, **2009**, *19*, 9221–9232.

[12] Chico, R.; de Domingo, E.; Domínguez, C.; Donnio, B.; Heinrich, B.; Termine, R.; Golemme, A.; Coco, S.; Espinet, P. High One-Dimensional Charge Mobility in Semiconducting Columnar Mesophases of Isocyano-Triphenylene Metal Complexes. *Chem. Mater*. **2017**, *29*, 7587−7595.